



High-Strength Steel Tower for Wind Turbines (HISTWIN_Plus)

Background Document

Long version

Project Coordinator: Prof. Milan Veljkovic (TULUL)

Luleå Tekniska Universitet* Luleå University of Technology,
Universitetsområdet, Porsön, SE-97187 Luleå, Sweden

+

Authors: see attached list

Funded by

Research Programme of the Research Fund for Coal and Steel

Grant Agreement Number: *RFS2-CT-2014-00023*

LIST OF AUTHORS

Milan Veljkovic, Christine Heistermann, Marko Pavlovic

Luleå Tekniska Universitet
Universitetsområdet, Porsön
SE-97187 Luleå, Sweden

Markus Feldmann, Daniel Pak, Carl Richter

Rheinisch-Westfälische Technische Hochschule Aachen
Templergraben 55
DE-52062 Aachen, Germany

Carlos Rebelo, Paulo Pinto, Rui Matos

Universidade de Coimbra
Paco das Escolas
PT-3001-451 Coimbra, Portugal

Charalampos Baniotopoulos, Michaela Gkantou

University of Birmingham
Edgbaston,
B15 2TT Birmingham, United Kingdom

Veronique Dehan

Convention Européenne de la Construction Métallique ASBL
Avenue des Ombrages 32/20
BE-1200 Brussels, Belgium

Gregor Nüsse

Forschungsvereinigung Stahlanwendung EV
Sohnstr. 65
DE-40237 Düsseldorf, Germany

Table of contents

| | | |
|----------|---|-----------|
| 1 | INTRODUCTION | 6 |
| 1.1 | A CASE STUDY EXAMPLE, TOWER GEOMETRY..... | 7 |
| 2 | STRUCTURAL SAFETY AND LOADS..... | 8 |
| 2.1 | INTRODUCTION | 8 |
| 2.2 | BASIC PHYSICS CONCEPTS OF WIND ENERGY CONVERSION | 8 |
| 2.2.1 | <i>Extracting energy from the wind</i> | <i>8</i> |
| 2.2.2 | <i>Wind energy converters types.....</i> | <i>11</i> |
| 2.2.3 | <i>Rotor aerodynamics: parameters influencing the performance of horizontal axis wind turbines</i> <i>13</i> | |
| | <i>Tip speed ratio</i> | <i>14</i> |
| | <i>Rotor power coefficient.....</i> | <i>14</i> |
| | <i>Number of Blades in HAWT.....</i> | <i>15</i> |
| | <i>Rotor (Torque) Power coefficient</i> | <i>15</i> |
| | <i>Pitch/Stall Regulation</i> | <i>16</i> |
| 2.3 | CURRENT SOLUTIONS FOR HAWT SUPPORTING STRUCTURES | 17 |
| 2.4 | SAFETY CHECK FRAMEWORK OF HAWT COMPONENTS..... | 19 |
| 2.4.1 | <i>Certification and International standards</i> | <i>19</i> |
| 2.4.2 | <i>Safety classes</i> | <i>20</i> |
| 2.4.3 | <i>External conditions and wind turbine classes</i> | <i>21</i> |
| 2.4.4 | <i>Load types on HAWT supporting structure</i> | <i>21</i> |
| 2.4.5 | <i>Design criteria for HAWT tower</i> | <i>22</i> |
| 2.4.6 | <i>Reliability considerations and safety factors.....</i> | <i>23</i> |
| 2.4.7 | <i>Influence of dynamic characteristics of tower and foundation.....</i> | <i>25</i> |
| 2.5 | WIND LOADS | 27 |
| 2.5.1 | <i>Wind load assumptions and models in IEC61400</i> | <i>27</i> |
| 2.5.2 | <i>Extreme loads</i> | <i>28</i> |
| 2.5.3 | <i>Fatigue loads</i> | <i>32</i> |
| 2.6 | EARTHQUAKE LOADS | 36 |
| 2.6.1 | <i>General requirements in IEC 61400.....</i> | <i>36</i> |
| 2.6.2 | <i>General requirements in Eurocode 8 parts 1 and 6.....</i> | <i>36</i> |
| 2.7 | SOFTWARE ASHES - CALCULATION OF EIGENMODES | 39 |
| 2.7.1 | <i>Definition of input data.....</i> | <i>39</i> |
| 2.7.2 | <i>ASHES Procedure.....</i> | <i>40</i> |
| 3 | STABILITY | 43 |
| 3.1 | GENERAL..... | 43 |
| 3.2 | THEORETICAL BACKGROUND | 43 |
| 3.3 | DESIGN PROCEDURE FOR SHELL STRUCTURES | 45 |

| | | |
|----------|---|-----------|
| 3.4 | FLOWCHART | 48 |
| 3.5 | NUMERICAL EXAMPLE | 48 |
| 4 | FATIGUE | 51 |
| 4.1 | INTRODUCTION | 51 |
| 4.1.1 | <i>Stages of fatigue damage</i> | 51 |
| 4.1.2 | <i>Main factors influencing fatigue damage</i> | 52 |
| 4.2 | FATIGUE SAFETY ASSESSMENT IN CODES | 54 |
| 4.2.1 | <i>Basis of structural design</i> | 54 |
| 4.2.2 | <i>Eurocode 3 part 1-9</i> | 55 |
| 4.2.3 | <i>Fatigue verification formats</i> | 57 |
| 4.2.4 | <i>Example: Tubular steel tower</i> | 59 |
| 4.2.5 | <i>Fatigue design loads for connections</i> | 62 |
| 4.2.5.1 | Fatigue design for flange connection | 63 |
| 4.2.5.1 | Fatigue design | 67 |
| 5 | CONNECTIONS | 71 |
| 5.1 | GENERAL | 71 |
| 5.2 | FLANGE CONNECTION | 71 |
| 5.2.1 | <i>Theoretical background</i> | 72 |
| 5.2.1.1 | Bolt forces | 72 |
| 5.2.1.2 | Influence of flange imperfections on bolt forces | 73 |
| 5.2.1.3 | Ultimate limit state | 74 |
| 5.3 | FRICTION CONNECTION | 76 |
| 5.3.1 | <i>Theoretical background</i> | 77 |
| 5.3.2 | <i>Flowchart (Excel-Tool)</i> | 81 |
| 5.4 | NUMERICAL EXAMPLES | 82 |
| 5.4.1 | <i>Flange connection</i> | 82 |
| 5.4.1.1 | Flange geometry | 83 |
| 5.4.1.2 | Ultimate Limit State | 84 |
| 5.4.2 | <i>Friction connection</i> | 86 |
| 5.4.2.1 | Geometry of friction connection | 86 |
| 5.4.2.2 | Ultimate limit state | 87 |
| 6 | DOOR OPENING | 90 |
| 6.1 | STABILITY | 91 |
| 6.1.1 | <i>MNA/LBA approach</i> | 91 |
| 6.1.2 | <i>GMNIA approach</i> | 91 |
| 7 | FOUNDATIONS | 96 |
| 7.1 | FINITE ELEMENT STRUCTURAL FOUNDATION MODELS | 98 |
| 7.1.1 | <i>Modelling of the foundation in case of partially prestressed anchors</i> | 98 |
| 7.1.2 | <i>Modelling of the foundation in case of embedding the tower to the concrete</i> | 99 |

| | | |
|-----------|--|------------|
| 7.2 | DESIGN OF SHALLOW FOUNDATIONS | 100 |
| 7.3 | NUMERICAL EXAMPLE OF THE FOUNDATION FOR THE MM92 EVOLUTION – 80 M WIND TURBINE | 102 |
| 7.3.1 | <i>Introduction</i> | 102 |
| 7.3.2 | <i>Codes and regulations</i> | 102 |
| 7.3.3 | <i>Loads</i> | 103 |
| 7.3.3.1 | Coordinate system..... | 103 |
| 7.3.3.2 | Dead loads | 104 |
| 7.3.3.3 | Wind loads..... | 104 |
| 7.3.3.4 | Seismic loads | 105 |
| 7.3.4 | <i>Ground conditions</i> | 106 |
| 7.3.5 | <i>Geometry</i> | 107 |
| 7.3.6 | <i>Safety verification – Geotechnical design</i> | 108 |
| 7.3.6.1 | Verification of the ground gap | 108 |
| 7.3.6.2 | Verification of the uncompressed area..... | 108 |
| 7.3.6.3 | Soil bearing pressures for circular bases | 108 |
| 7.3.6.4 | Results | 109 |
| 7.3.6.5 | Parametric study of the geometry | 109 |
| 7.3.6.6 | Geotechnical design according to Eurocode 7 | 110 |
| 7.3.6.6.1 | <i>Load combinations</i> | 110 |
| 7.3.6.6.2 | <i>Equilibrium Limit State</i> | 110 |
| 7.3.7 | <i>Safety verification - Structural design</i> | 114 |
| 7.3.7.1 | Loads | 114 |
| 7.3.7.2 | Materials | 115 |
| 7.3.7.3 | Structural model..... | 116 |
| 7.3.7.4 | Bending reinforcement..... | 118 |
| 7.3.7.5 | Shear reinforcement..... | 122 |
| 7.3.7.6 | Serviceability limit states..... | 124 |
| 7.3.8 | <i>Connection of the anchor steel ring to the foundation slab</i> | 125 |
| 7.3.8.1 | Geometric data | 125 |
| 7.3.8.2 | Material data | 127 |
| 7.3.8.3 | Design of the anchor reinforcement | 127 |
| 7.3.9 | <i>Quantities</i> | 133 |
| 7.3.10 | <i>Conclusions</i> | 133 |
| 7.4 | CONNECTION OF THE FOUNDATION WITH PARTIALLY PRESTRESSED ANCHORS..... | 134 |
| 7.5 | OTHER TYPES OF FOUNDATIONS | 136 |
| 8 | ACRONYMS AND ABBREVIATIONS..... | 137 |
| 9 | REFERENCES | 138 |

1 INTRODUCTION

Energy from renewable resources is of increasing demand worldwide. Wind energy produced onshore is one of these resources. In order to increase its competitiveness a European research project, called “High-strength tower in steel for wind turbines (HISTWIN)” [1], was carried out focussing on the joint between two tower segments and the possibility to use higher strength steel. The research was conducted in cooperation of Luleå University of Technology (Sweden), RWTH-Aachen University (Germany), Germanischer Lloyd Industrial Services GmbH (Germany), Aristotle University of Thessaloniki (Greece), Martifer Energia – Equipamentos para energia, S.A. (Portugal) and University of Coimbra (Portugal).

In order to increase the number of steel tubular towers, the tower design has to become more transparent and automatic. Ambitions of this document is to guide throughout the design process and to help designers by considering specific issues. It consists of explanations on state-of-the-art solutions, suggestions for its improvements and gives numerical examples to simplify the designers’ work throughout the design process.

Design loads, stability of the towers, fatigue resistance, connection details and door openings in the tower are considered. Finally, the latest research results on tower foundations are presented.

1.1 A case study example, tower geometry

The calculation examples are made for an existing MM92 tower, which consists of three sections assembled with two intermediate L-flange connections. The geometry is given in Figure 1.1.

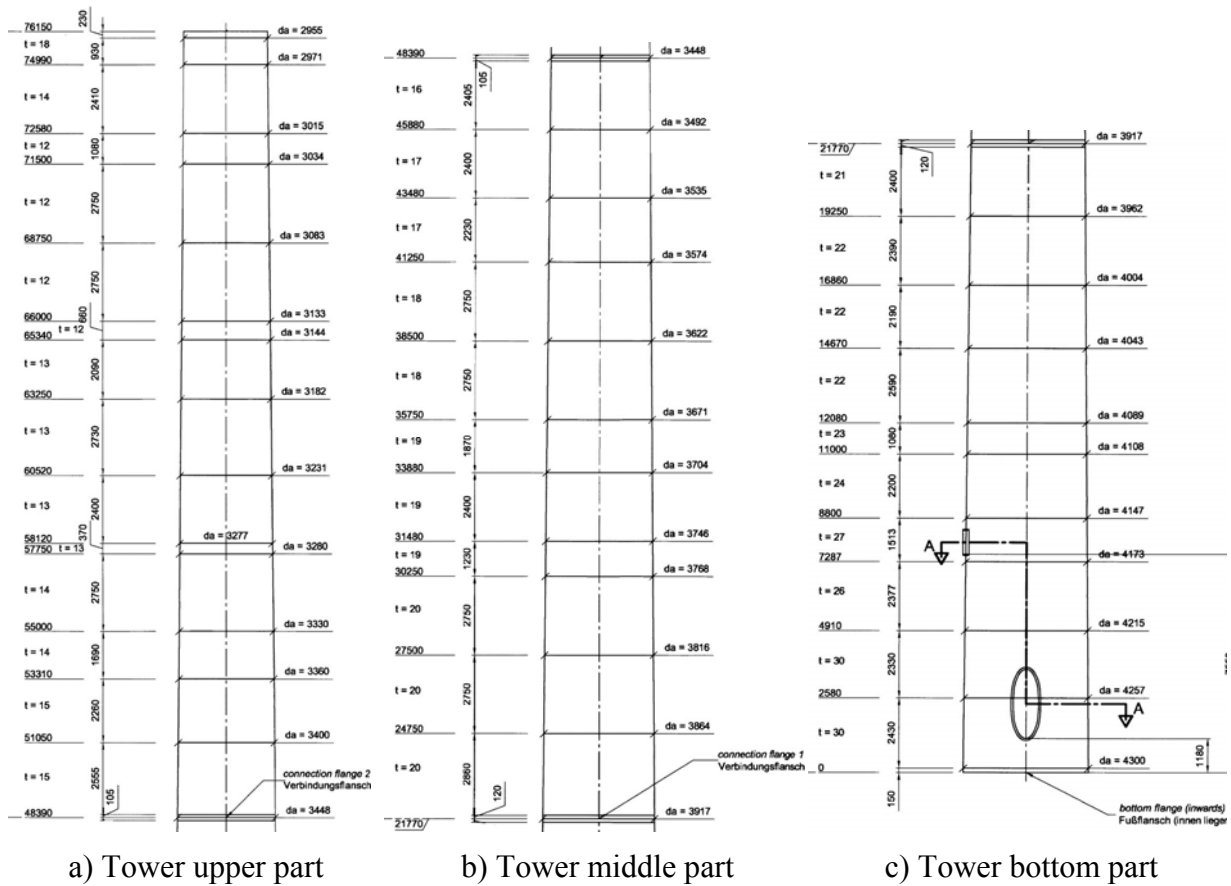


Figure 1.1: Tower geometry

2 STRUCTURAL SAFETY AND LOADS

2.1 Introduction

The behaviour and structural design of support structures for multi-megawatt wind turbines, especially steel tubular towers and foundations is a main topic of the dissemination workshops developed within the project HISTWIN+. This chapter aims at giving basic information on structural safety concepts and loading related to wind turbines supporting structures and is directed to structural engineers that need basic understanding of the multi-megawatt wind turbine components and operation and of the different type of loads acting on the tower and foundation. The contents give information on following topics:

- basic physics concepts of wind energy converters;
- standards and Guidelines for wind turbine design certification;
- basic load analysis and safety strategy for Wind Towers based on partial safety factors;
- design loads, including background of the approximation of external loads to design values of the cross-section forces of the tower, including the foundation;
- calculation of wind loading using dedicated software and application to a numerical example;
- calculation of seismic loading based on Eurocode 8 including a numerical example;
- calculation of cyclic load spectra for fatigue analysis and practical methods for fatigue load definition including a numerical example

2.2 Basic physics concepts of wind energy conversion

2.2.1 Extracting energy from the wind

In order to transform the entire kinetic energy contained in the air stream (Figure 2.1) the wind velocity should be reduced to zero when passing the energy converter. Reduced velocity, however, means at the same time a widening of the cross-section, as the same mass flow must pass through it. There would be a 'stack' of the air mass when this approaches the converter, which is physically impossible. Therefore, there must be a Theoretical Maximum for the energy that can be converted from wind.

The extraction of mechanical energy from a stream of moving air with the help of a disk-shaped, rotating wind energy converter follows the principle stated by Albert Betz in the 20's of 20th century. Betz's Elementary Momentum Theory follows elementary physical laws, that is, the mechanical energy extractable from an air stream passing through a given cross-sectional area is restricted to a certain fixed proportion of the energy or power contained in the air stream.

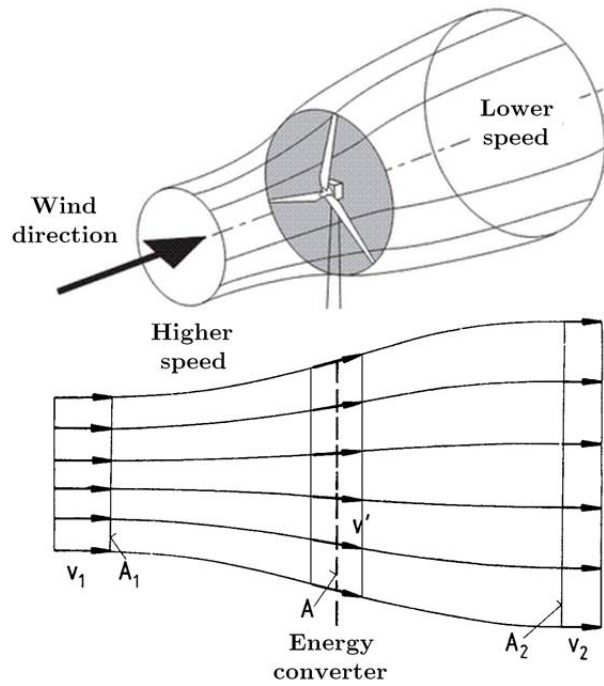


Figure 2.1: Extracting energy from wind with a rotor disc (adapted from [1])

The kinetic energy of an air mass m moving at a velocity v can be expressed as:

$$E = \frac{1}{2} m \cdot v^2 \text{ (Nm)} \quad (1)$$

Considering a certain cross-sectional area A , through which the air passes at a velocity v , the volume V flowing through during a certain time unit, the so-called volume flow, is:

$$V = v \cdot A \text{ (m}^3\text{/s)} \quad (2)$$

and the air mass flow, when using the air density ρ is:

$$m = \rho \cdot v \cdot A \text{ (kg/s)} \quad (3)$$

The equations expressing the kinetic energy of the moving air and the mass flow yield the amount of energy passing through cross-section A per unit time. This energy is physically identical to the power P :

$$P = \frac{1}{2} \cdot \rho \cdot v^3 \cdot A \text{ (W)} \quad (4)$$

Considering that v_1 is the free-stream velocity, i.e. the wind velocity before the converter and v_2 is the flow velocity after crossing the converter, the mechanical energy which the disk-shaped converter extracts from the airflow corresponds to the power difference of the air stream before and after the converter.

The calculation of the energy converted from wind, equivalent to the power of the converter uses two basic principles: the conservation of mass and the conservation of momentum. The Continuity Equation corresponding to maintaining the mass flow (see Figure 2.1) is:

$$\rho \cdot v_1 \cdot A_1 = \rho \cdot v_2 \cdot A_2 \quad (5)$$

and the power of the converter is given by the difference of energy before and after the converter:

$$\begin{aligned} P &= \frac{1}{2} \cdot \rho \cdot v_1^3 \cdot A_1 - \frac{1}{2} \cdot \rho \cdot v_2^3 \cdot A_2 \\ P &= \frac{1}{2} \cdot \rho \cdot v_1 \cdot A_1 \cdot (v_1^2 - v_2^2) \\ P &= \frac{1}{2} \cdot m \cdot (v_1^2 - v_2^2) \end{aligned} \quad (6)$$

The mechanical power of the converter obeys the Law of Conservation of Momentum, that is, the force exerted on the converter $F = m \cdot (v_1 - v_2)$ corresponding to the slowdown of the wind when crossing the converter is counteracted by the same force of the converter on the air. This thrust ‘pushes’ the air mass present in the plane of flow of the converter at velocity v' . The power required for this is given by:

$$P = F \cdot v' = m \cdot (v_1 - v_2) \cdot v' \quad (7)$$

and therefore:

$$v' = \frac{v_1 + v_2}{2} \quad (8)$$

$$P = \frac{1}{4} \cdot \rho \cdot A \cdot (v_1^2 - v_2^2) \cdot (v_1 + v_2) \quad (9)$$

The ratio between the mechanical power extracted by the converter and that of the undisturbed air stream is called the “power coefficient” c_p .

$$\begin{aligned} c_p &= \frac{P}{P_0} = \frac{\text{mechanical power output of the converter}}{\text{power of the free – air stream}} \\ &= \frac{\frac{1}{4} \cdot \rho \cdot A \cdot (v_1^2 - v_2^2) \cdot (v_1 + v_2)}{\frac{1}{2} \cdot \rho \cdot A \cdot v_1^3} \end{aligned} \quad (10)$$

$$c_p = \frac{P}{P_0} = \frac{1}{2} \left| 1 - \left(\frac{v_2}{v_1} \right)^2 \right| \left| 1 + \left(\frac{v_2}{v_1} \right) \right|$$

The maximum “ideal power coefficient” c_p is obtained for $v_2/v_1 = 1/3$.

$$c_p = \frac{16}{27} = 0,593 \quad (11)$$

$$v' = \frac{2}{3} v_1 ; v_2 = \frac{1}{3} v_1 \quad (12)$$

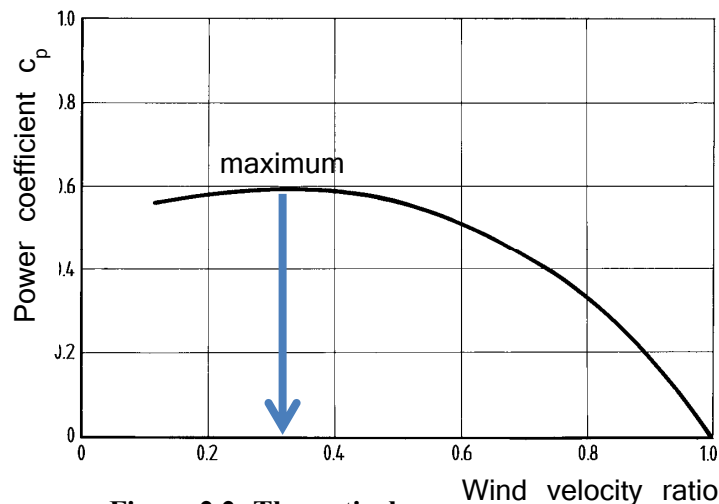


Figure 2.2: Theoretical power coefficient c_p

The essential findings derived from the momentum theory can be summarised as follows:

- The mechanical power which can be extracted from a free-stream airflow by an energy converter increases with the third power of the wind velocity.
- The power increases linearly with the cross-sectional area of the converter traversed; it thus increases with the square of its diameter.
- Even with an ideal airflow and lossless conversion, the ratio of extractable mechanical work to the power contained in the wind is limited to a value of 0,593. Hence, only about 60% of the wind energy of a certain cross-section can be converted into mechanical power.
- When the ideal power coefficient achieves its maximum value $c_p = 0,593$, the wind velocity in the plane of flow of the converter amounts to two thirds of the undisturbed wind velocity and is reduced to one third behind the converter.

However, the power which can be achieved under real conditions cannot be independent of the characteristics of the energy converter.

2.2.2 Wind energy converters types

The actual power of the converters depends on which aerodynamic forces are utilised for producing mechanical power. All bodies exposed to an airflow experience an aerodynamic force the components of which are defined as:

- Aerodynamic drag in the direction of flow, and
- Aerodynamic lift at a right angle to the direction of flow.

In devices using the aerodynamic drag forces ("sail" in Figure 2.3) the air impinges on the surface with velocity v_w and the surface moves with velocity v . The aerodynamic drag D develops the power given by $P=D(v_w-v)=Dv_r$.

The aerodynamic drag coefficient c_D defines the efficiency of the area A of the drag device. Considering the law of conservation of momentum equations for the power of the converter can be derived as follows. The conservation of momentum:

$$P = F \cdot v' = m \cdot (v_1 - v_2) \cdot v' \quad (13)$$

becomes:

$$P = m \cdot (v_1 - v_2) \cdot \frac{1}{2} (v_1 + v_2) \quad (14)$$

when including the flow velocity v' derived before. Therefore, when identifying velocities and using the common aerodynamic drag coefficient c_D , the power is given by:

$$P = (\rho \cdot v_r \cdot c_D \cdot A) \cdot (v_w - v_r) \cdot \frac{1}{2} (v_w + v_r) \quad (15)$$

and the drag force D is identified:

$$P = \left[\frac{1}{2} \cdot \rho \cdot c_D \cdot A \cdot (v_w - v_r)^2 \right] \cdot v_r = D \cdot v_r \quad (16)$$

If power is expressed again in terms of the power contained in the free-stream airflow, the following power coefficient is obtained:

$$c_p = \frac{P}{P_0} = \frac{\frac{\rho}{2} \cdot c_D \cdot A \cdot (v_w - v_r)^2 \cdot v_r}{\frac{\rho}{2} \cdot v_w^3 \cdot A} \quad (17)$$

It can be shown that c_p reaches a maximum value with a velocity ratio of $v/v_w = 1/3$. The maximum value is then $c_{p_{max}} = \frac{4}{27} \cdot c_D$. Considering that the aerodynamic drag coefficient will not reach values above about 1.3, the maximum power coefficient should be about $c_{p_{max}} \approx 0,2$, which is much lesser than the theoretical maximum of about 0.6.

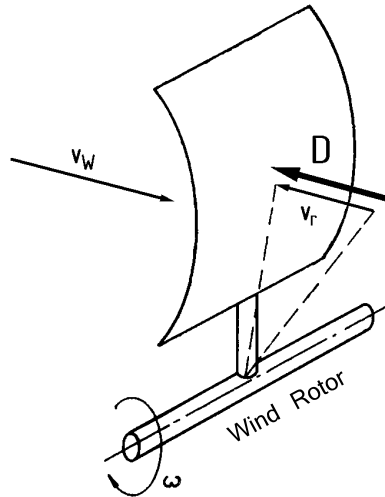


Figure 2.3: “Sail” uses aerodynamic drag forces (adapted from [1])

Aerodynamic lift at a right angle to the direction of flow is an alternative to drag forces. All modern wind rotor types are designed for utilising this effect and the type best suited for this purpose is the propeller type with a horizontal rotational axis. The wind velocity v_w is

combined with the peripheral velocity u of the airfoil (rotor blade). Together with the airfoil chord the resultant free-stream velocity v_r forms the aerodynamic angle of attack.

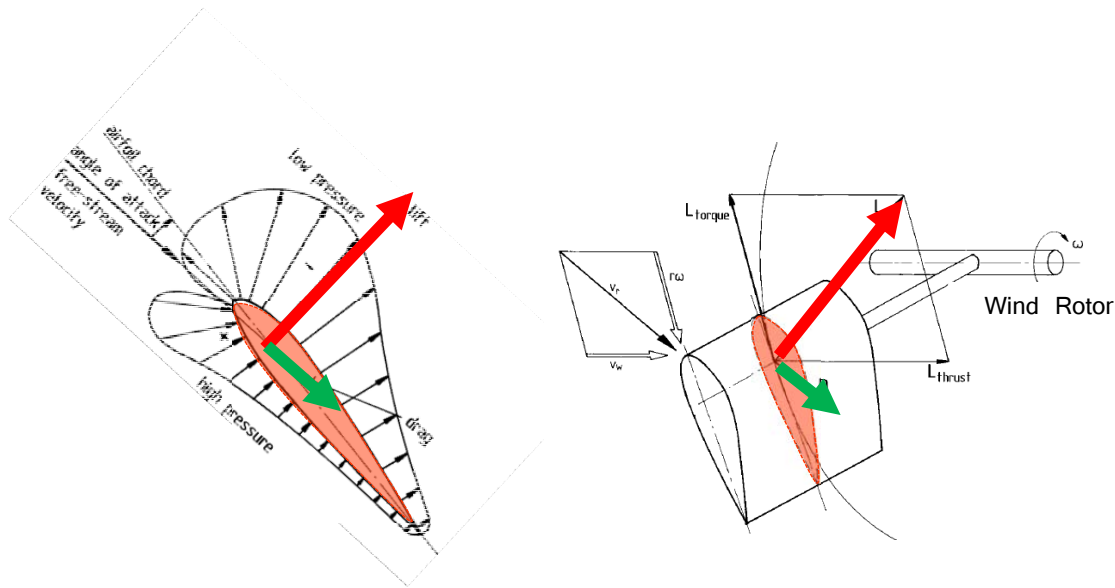


Figure 2.4: “Airfoil” uses aerodynamic lift combined with drag (adapted from [1])

The aerodynamic force created (Figure 2.4) is resolved into a component in the direction of the free-stream velocity, the drag D , and a component perpendicular to the freestream velocity, the lift L . Modern airfoils developed for aircraft wings and which also found application in wind rotors, have an extremely favourable lift-to-drag ratio (E). This ratio can reach values of up to 200.

The lift force L , in turn, can be resolved into a component L_{torque} in the plane of rotation of the rotor and a second component perpendicular to its plane of rotation L_{thrust} . L_{torque} constitutes the driving torque of the rotor and L_{thrust} is responsible for the rotor thrust and must be resisted by the supporting structure, tower and foundation.

The blade element theory provides the distribution of aerodynamic forces over the length of the blade (Figure 2.5). This is usually divided into two components: one in the plane of rotation of the rotor, the tangential force distribution, and one at right angles to it, the thrust distribution. Integrating the tangential force distribution over the rotor radius provides the driving torque of the rotor and, with the rotational speed of the rotor, the rotor power, respectively. Integrating the thrust distribution yields the total rotor thrust to the tower.

2.2.3 Rotor aerodynamics: parameters influencing the performance of horizontal axis wind turbines

Betz's simple momentum theory is based on the modelling of a two-dimensional flow through the actuator disc. In reality, however, the rotating converter will additionally impose a rotating motion to the rotor wake. To maintain the angular momentum, the spin in the wake must be opposite to the torque of the rotor. The energy contained in this spin reduces the useful proportion of the total energy content of the air stream and consequently the extractable mechanical energy. Therefore, the efficiency of horizontal axis wind turbines (HAWT) is influenced by the movement of the blades.

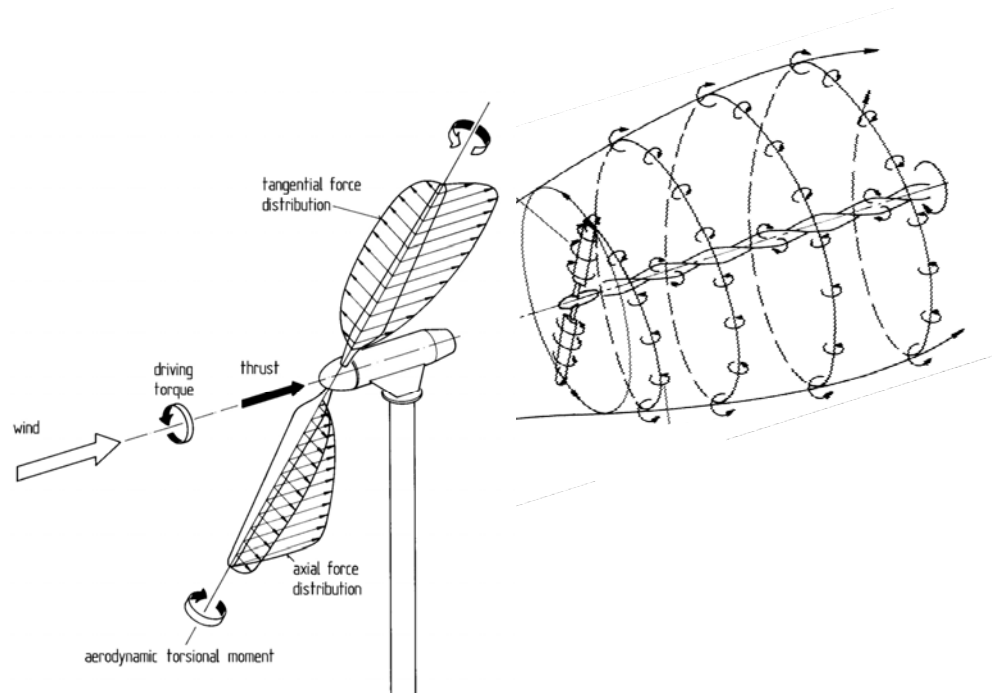


Figure 2.5: Two-blade rotor: forces and downwind developed wakes (adapted from [1])

Tip speed ratio

The tangential velocity of the rotor blades is commonly referenced to the tangential velocity of the rotor blade tip. The ratio of the rotor blade tip to the velocity of the undisturbed axial airflow, the wind velocity v_w is called the tip speed ratio, TSR or λ . This ratio is frequently used instead of the wind speed as shown in the graphic for the rotor power coefficient of different types of turbines in Figure 2.6.

A rotor that rotates slowly will allow the wind to pass unperturbed through the gaps between the blades. A rotor rotating rapidly will appear as a solid wall to the wind. On the other hand, when a rotor blade passes through the air stream it leaves a turbulent wake in its path. If the next blade in the rotating rotor arrives at the wake when the air is still turbulent, it will not be able to extract power from the wind efficiently, and will be subjected to increasing vibration. Therefore, wind turbines must be designed to operate at their optimal TSR in order to extract as much power as possible from the wind stream.

In general a high TSR is a desirable feature since it results in a high shaft rotational speed that is needed for the efficient operation of an electrical generator. However, rotor blade tips rotating at a speed larger than 80 m/s will be subject to erosion of the leading edges from their impact with dust or sand particles in the air; they will be also prone to noise generation and vibration and will have reduced rotor efficiency due to drag and tip losses.

Rotor power coefficient

The rotor power depends on the combination of the wind velocity components originated by the rotating motion of the blades and the (un)disturbed air stream. Using the rotor power coefficient c_{PR} the rotor power P_R can be calculated as a function of the wind speed:

$$P_R = C_{PR} \cdot \frac{\rho}{2} \cdot v_w^3 \cdot A \quad (18)$$

Whereas the historical wind wheels, which essentially only operated with aerodynamic drag, only achieved power coefficients of about 0,3, at the most, modern rotors achieve power coefficients of almost 0,5 which clearly demonstrate the superiority of the principle of using aerodynamic lift (see Figure 2.6a).

Number of Blades in HAWT

Blades are an important component of the WT from economical point of view. Therefore, the number of blades plays important role in market competitiveness of the turbine. Analysing Figure 2.6b it is obvious that HAWT with a lower number of blades (economic advantage) show lower performance (disadvantage). They also rotate faster (increasing TSR) with consequence of increase of abrasion and of dynamic problems.

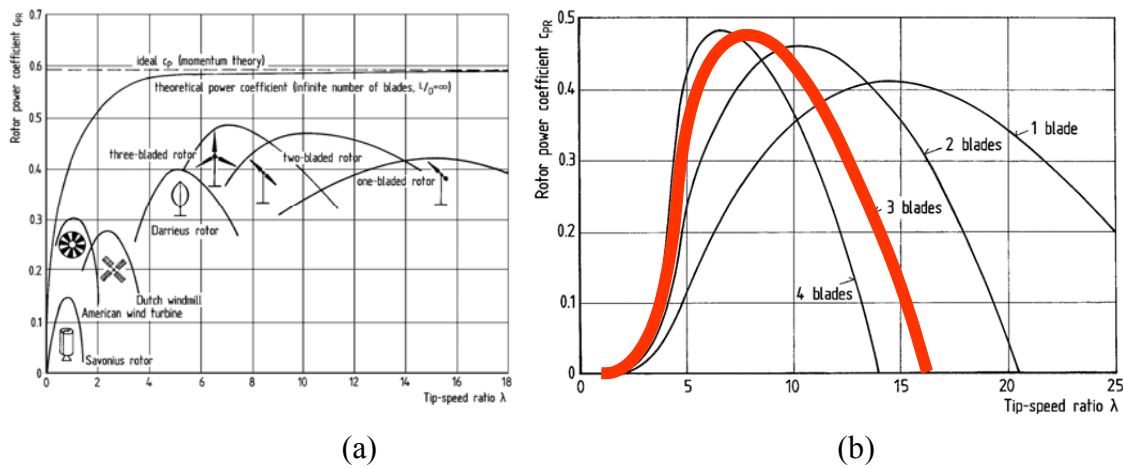


Figure 2.6: Rotor power coefficient depending on type of WT and TSR (a) and on number of blades for HAWT (b) [1]

Rotor (Torque) Power coefficient

Apart from the rotor power, there are other parameters which are of significance in characterizing rotor performance.

The most important of these is the behaviour of the torque. Analogously to the power, the rotor torque can also be calculated by using a so-called torque coefficient and the rotor radius R as the reference parameter:

$$M = c_Q \cdot \frac{\rho}{2} \cdot v_w^2 \cdot A \cdot R \quad (19)$$

The torque can be calculated by dividing power by the rotational speed. Therefore, a simple relationship between power and torque coefficient can be obtained¹:

¹ By definition, a moment of 1 Nm applied through a full revolution requires 2π Jouls of energy (power); $P = M \omega$

$$c_{PR} = \lambda \cdot c_Q \quad (20)$$

The rotor power curves and the torque curves are the characteristic features of each rotor configuration. Knowledge of these curve are important to maximize the generated electric power. Starting torque is very important when trying to minimize the need for external electric power of current wind turbines to start operating at low wind speed.

The main parameters dominating the c_{PR} are related to the number and aerodynamic form of the blades. The precise shape of this curve is difficult to predict as it depends on several factors: air density, humidity, temperature, wind speed and tip speed.

Once the power coefficient curve is found, it is possible to propose optimal operation points for the turbine that are fed to a controller for the electric generator.

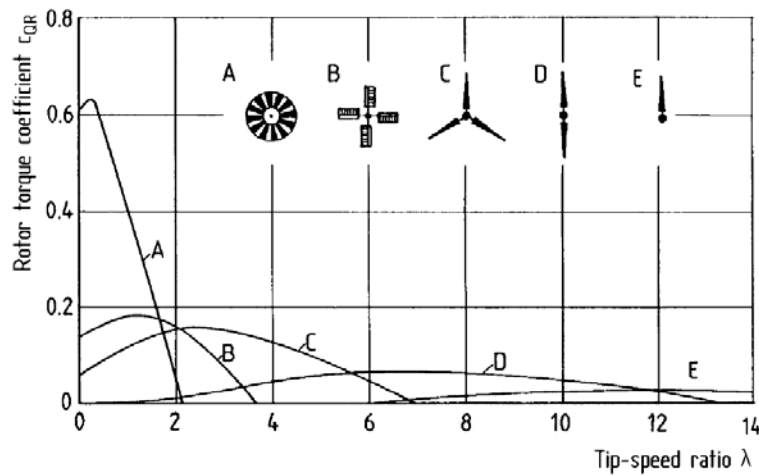


Figure 2.7: Rotor torque coefficient vs TSR depending on number of blades for HAWT [1]

Pitch/Stall Regulation

At high wind speeds, the power captured from the wind by the rotor far exceeds the limits set by the design strength of the rotor structure. There is also the problem of maintaining rotor speed at a constant value or within predetermined limits. Speed limitation becomes a question of survival when, for example during a grid outage, the generator torque is suddenly lost. In such a case, rotor speed would increase extremely rapidly and would certainly lead to the destruction of the turbine unless countermeasures were taken immediately.

The rotor of a wind turbine must, therefore, have an aerodynamically effective means for limiting its power and its rotational speed or to stop the rotation using only aerodynamic brakes. This is achieved by means of the regulation of the pitch angle of the blades, that is, the angle between the airfoil (blade) chord and the plane of rotation (Figure 2.8)

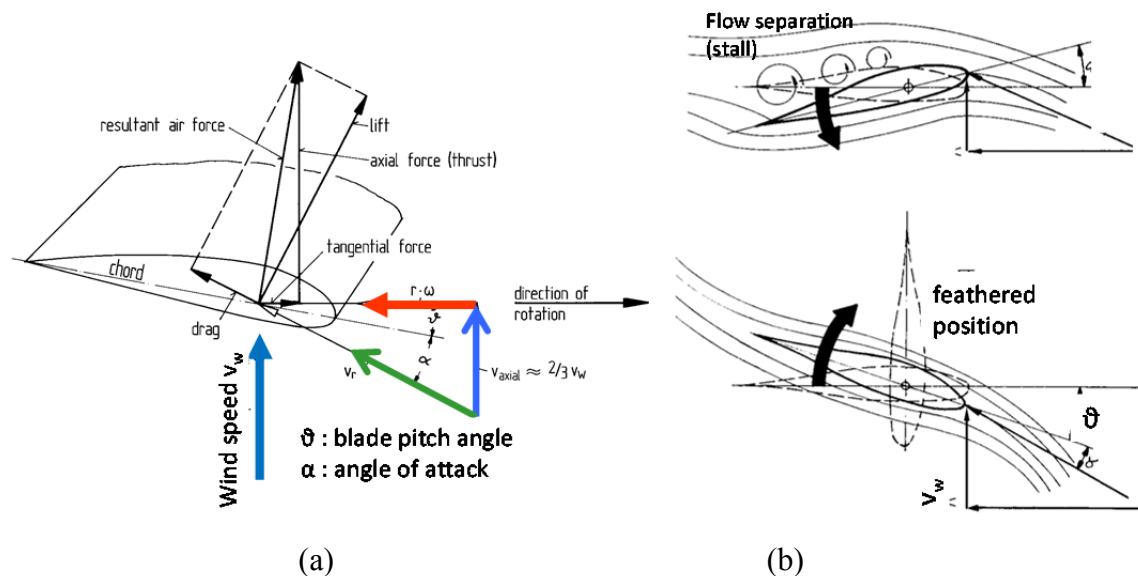


Figure 2.8: Aerodynamic control of rotation speed (a) angle definition; (b) Pitch regulation and stall effect [1]

2.3 Current solutions for HAWT supporting structures

The most common structural forms of onshore wind turbines at present are supported on tubular steel towers, pre-stressed tubular concrete towers or hybrid tubular steel-concrete towers (Figure 2.9). Future opportunities for growth in wind energy exploitation onshore are contingent on an increase in the height of towers to support larger turbines. For steel construction, that increase leads to tubular towers with a larger diameter which cannot be transported on public roads. Therefore, the main limitation for tubular pre-fabricated towers (transportation) can be overcome only by extra work on site, comprising the assembly of full diameter sections from smaller pieces. This approach can be adopted for both concrete (Figure 2.9b) and steel towers (Figure 2.9c and Figure 2.9d) using prefabricated modules that are assembled on site. However, the use of concrete and hybrid concrete-steel towers (Figure 2.9a), has gained advantage over all steel towers, mainly due to the lack of competitive steel solutions.

Tubular construction has the advantage of being familiar and is now highly optimized for steel towers with diameters suitable for transport on public roads. Steel producers all over the world have invested in equipment to fabricate tubes for wind towers. Other advantages, such as the possibility of preinstalling all the internal equipment of the tower, have meant that tubular steel towers became the standard solution in the market. However, most of these advantages are eroded when the modular tower has to be assembled on site due to transportation size constraints. An alternative to steel tubular construction is steel lattice structures. This is also familiar technology for a range of tower types, such as for energy transmission lines. They were also widely used to support wind turbines in the early days of wind energy exploitation, mainly in the USA. More recently, in 2006 in Germany, a 160 m high steel lattice tower was built, with a rotor of 90 m diameter and a capacity of 2,5 MW (Figure 2.10b).

The advantages of lattice towers are well known: straightforward design and detailing (simple member and connection design and modelling, easy detailing of members and connections); good dynamic behaviour (ideal for wind turbines); economy of fabrication (lattice towers are cheaper than tubular towers due to the price of the plates, ease of fabrication and ease of

protection against corrosion by galvanizing); economy of transportation (lattice angle sections are easier and lighter to transport when compared to tubular structures); simpler erection procedures (flexible scheduling with possibility of parallel working, different erection techniques are feasible); and ecological advantages (highly transparent structure, optimum ecological balance due to galvanizing and small concrete foundations required).



Figure 2.9: Tubular towers: a) Nordex steel tower 120 m; b) modular concrete INNEO tower; c) Siemens polygonal shaped steel tower; d) Modular tower using friction connection developed in HISTWIN project

Figure 2.10a shows a comparison of investment costs, relative to annual energy output, needed to commission wind turbine towers based on different structural solutions for a 3 MW turbine and for hub heights between 75 and 175 meters. The cost increase above 150 m is mainly due to the assembly procedure, which uses external lifting towers instead of cranes. Therefore, the optimum height may be increased if more economical lifting technology is available. Nevertheless, there is a consensus in the technical community that lattice towers are a very competitive solution for heights above 120 meters.

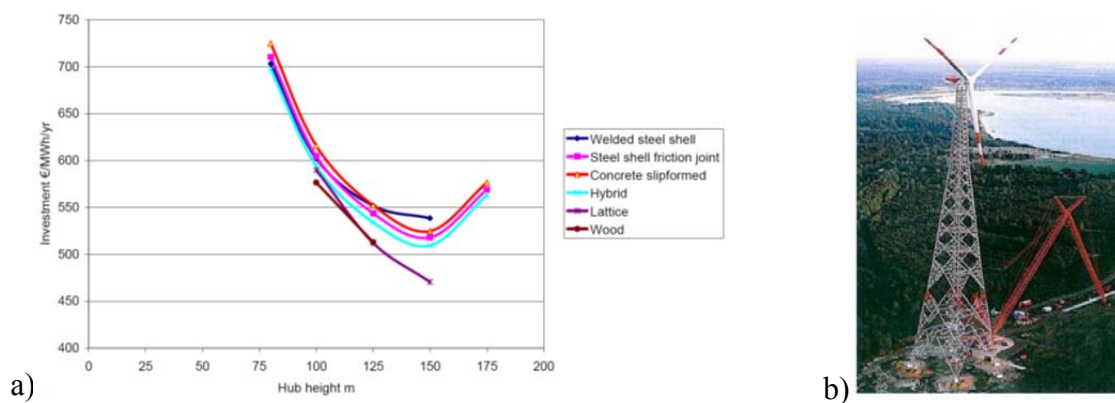


Figure 2.10: a) summary of the relative cost of tower alternatives for 3 MW wind turbines [2]; b) Fuhrländer Lattice tower with 160 m hub height

Some of the disadvantages of lattice towers, (e.g. the complexity of using conventional square truss tower made of L-sections), have been overcome in recent commercial proposals for new types of cross-section [3]. Also, the assembly and erection of the new generation of lattice towers is being improved by the use of new low-maintenance fasteners, which were successfully tested in HISTWIN project (RFSR-CT-2006-00031) [4]. The main advantages of those types of fasteners are the lower rate of pretension loss when compared to normal bolts and the fact that they do not require maintenance such as retightening.

2.4 Safety check framework of HAWT components

2.4.1 Certification and International standards

Production and commercialization of Wind Turbines is based on product certification, i.e. all components including support structure are parts of a complete set for which a certification document is issued, usually by insurance companies.

According to the European standard EN 45020 [5], certification is the confirmation of compliance of a product or a service with defined requirements (e.g. guidelines, codes and standards). In the field of wind energy the focus is the complete wind turbines or components such as rotor blades, gearboxes or towers. The scope consists of the examination of structural integrity, safety and compliance with these requirements [5].

Certification companies (GL, DNV, BV, UL, etc) have developed their own guidelines for certification [6], [7] based on international [8], [9], [10] or national standards [11].

Wind Turbine Type Certification requires conformity with regulations and/or guidelines in following items:

- Design Evaluation
 - Safety concept and evaluation of loads
 - Evaluation of safety system and design of components (e.g. support structure)
- Type Testing

- Manufacturing Evaluation
- Foundation Design Evaluation (optional)
- Type Characteristic Measurement (optional)
- Structural Reliability framework in IEC 61400-1 [8] and EN1990 [12]

IEC 61400 outlines minimum design requirements and specifies essential design requirements to ensure the engineering integrity of onshore wind turbines. It is concerned with all subsystems of wind turbines such as control and protection mechanisms, internal electrical systems, mechanical systems and support structures. Compliance with this standard does not relieve from the responsibility of observing other applicable regulations, such as those applied to the supporting structure (tower and foundation) concerning the structural safety, the actions and the relevant design rules.

EN 1990 describes the principles and requirements for safety, serviceability and durability of structures. It is based on the limit state concept used in conjunction with a partial factor method. It may be used, when relevant, as a guidance document for the design of structures outside the scope of the Eurocodes EN 1991 to EN 1999, for:

- assessing other actions and their combinations;
- modelling material and structural behavior;
- assessing numerical values of the reliability format.

The basic requirement stated in the standard is that a structure shall be designed and executed in such a way that it will, during its intended life, with appropriate degrees of reliability and in an economical way, sustain all actions and influences likely to occur during execution and use and remain fit for the use for which it is required.

To ensure the appropriate level of safety and reliability, environmental actions (wind and others e.g. earthquake, ice, impacts...), electrical conditions and soil parameters shall be taken into account in the design of WT.

2.4.2 Safety classes

According to IEC61400-1 [8] wind turbines shall be designed according to one of the following two safety classes:

- The normal safety class which applies when a failure results in the risk of personal injury or economic and social consequences;
- The special safety class which applies when the safety requirements are determined by local regulations and/or the safety requirements are agreed between the manufacturer and the customer.

Partial safety factors for a wind turbine of the normal safety class are specified in IEC61400. Partial safety factors for wind turbines of the special safety class require prior agreement between the manufacturer and the customer.

2.4.3 External conditions and wind turbine classes

IEC 61400-1 [8] defines two categories of external conditions for which the WT safety must be checked (Figure 2.11). Category 'Normal' includes the frequent situations during the service life of the WT. Category 'Extreme' external conditions represent rare external design situations. Category definition influence the load values, the safety factors and the load combinations to be considered in the analysis and design.

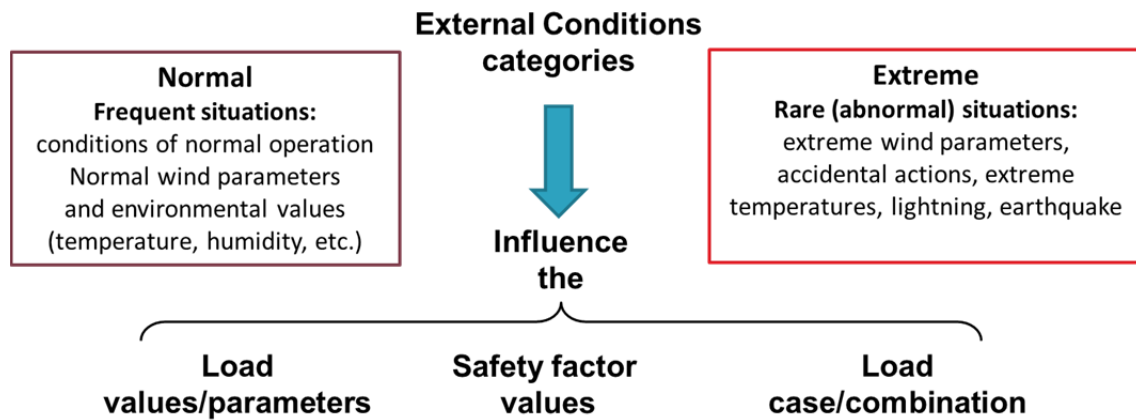


Figure 2.11: External conditions to be considered in the safety check of WT components

The external conditions to be considered for design are dependent on the intended site or site type for a wind turbine installation. In order to be able to pre-qualify WT to be installed in different sites, WT classes are defined in terms of wind speed and turbulence parameters as shown in Table 2.1 where v_{ref} is the reference wind speed defined as the extreme 10 min average wind speed at the hub-height with a 50 year return period, considering air density $1,225 \text{ kg/m}^3$ and I_{ref} is the reference turbulence intensity defined as expected value of hub-height turbulence intensity (coefficient of variation of wind speed) at a 10 min average wind speed of 15 m/s.

Table 2.1: Wind Turbine Classes according to IEC61400-1 [8]

| | Wind Turbine Class | | |
|--|--------------------|------|------|
| | I | II | III |
| V_{ref} | 50 | 42,5 | 37,5 |
| I_{ref} for type A (high turbulence) | 0,16 | | |
| I_{ref} for type B (medium turbulence) | 0,14 | | |
| I_{ref} for type C (low turbulence) | 0,12 | | |

2.4.4 Load types on HAWT supporting structure

Due to the nature of wind, the loads are highly variable in time; (aero-)dynamic forces are much more difficult to handle than static forces. The air is of low density, therefore the surface required for capturing energy must be large and the dimensions of the rotor and the tower height must increase.

Large structures tend to be flexible and the changing loads thus create a complex aeroelastic interplay which induces vibrations and resonances and can produce high dynamic load components.

Majority of loads supported by the tower/foundation are induced by the rotor. Loads, both static and static and dynamic transmitted from the nacelle to the tower can be divided into following types:

- Aerodynamic
- Gravitational
- Inertial
- Operational (fault)

According to GL guidelines [6] the loads to be considered for the design calculations include:

1. Inertial and gravitational loads, both static and dynamic resulting from vibration, rotation, gravity and seismic activity;
2. Aerodynamic loads, both static and dynamic, which are caused by the airflow and its interaction with the stationary and moving parts of wind turbines. These loads are dependent upon the rotational speed of the rotor, the average wind speed across the rotor plane, the turbulence intensity, the density of the air, and the aerodynamic shapes of the wind turbine components and their interactive effects, including the aeroelastic effects.
3. Operational loads, which result from the operation and control of wind turbines. They shall be assigned to several categories. These are the control of rotor speed and the torque control by pitching of blades or other aerodynamic devices. Other operational loads are the mechanical braking and transient loads arising during the starting and stopping of the rotor, connection and disconnection of the generator, and yaw movements.
4. Other loads, such as wake loads, impact loads, ice loads may occur and shall be included where appropriate depending on the installation site.

2.4.5 Design criteria for HAWT tower

Due to the nature of wind, the loads are highly variable in time; (aero) dynamic forces are much more difficult to handle than static forces.

The air is of low density; therefore the surface required for capturing energy must be large and the dimensions of the rotor and the tower height must increase.

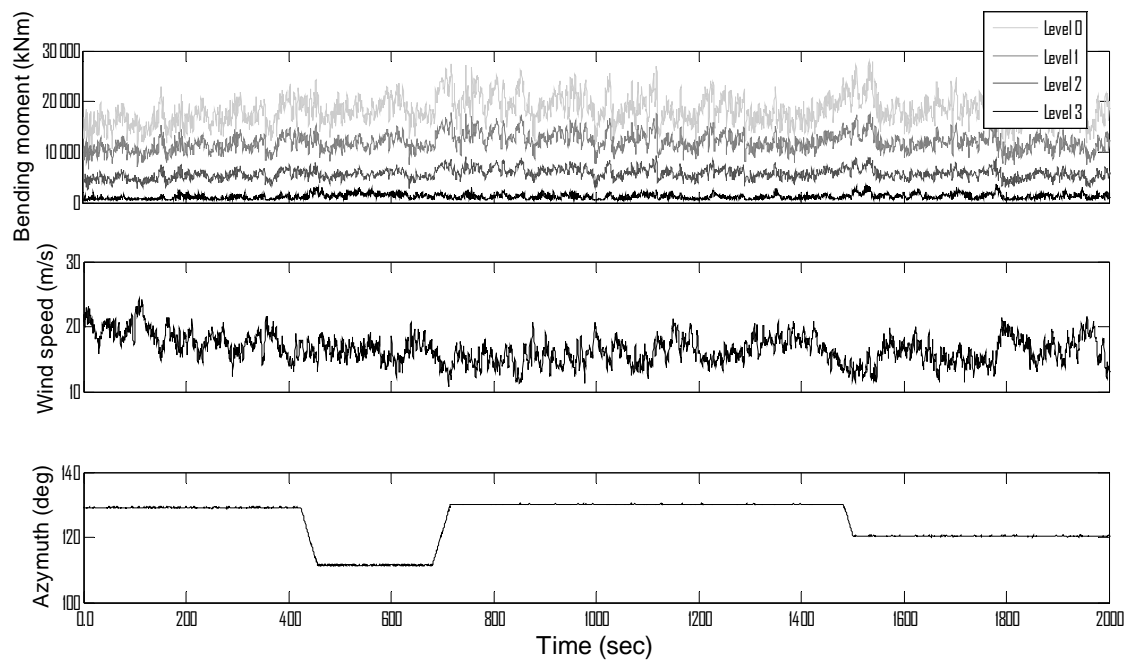


Figure 2.12: Cross section bending moments time histories at different levels of a 80m wind tower and corresponding wind velocity and azimuth of the nacelle

Large structures tend to be flexible and the changing loads thus create a complex aeroelastic interplay which induces vibrations and resonances and can produce high dynamic load components.

The structural design of a wind turbine supporting structure must provide adequate strength and stiffness:

- to withstand extreme loads from the highest wind speeds which may occur; Ultimate Limit States (U) concerning strength and stability must be checked;
- to guarantee fatigue strength/life of all components including support structure; Fatigue Strength Limit States (F) must be checked
- to provide adequate dynamic behaviour and control of deflections by avoiding resonance situations through well balanced natural frequencies in relation to rotation frequency ranges; the vibrational behaviour of a wind turbine can be kept under control only when the stiffness and mass parameters of all its components are carefully matched; Maximum Deflection of blades and tower must be checked so that no contact can occur between the blades and the tower; also, resonance between rotor frequencies and tower eigenfrequencies must be avoided.

2.4.6 Reliability considerations and safety factors

The design of the supporting structures needs the application of different standards. Usually, the IEC 61400-1 [8] is used to define load case sets and national standards (e.g. DIN, DNV) or CEN (Eurocodes) standards are used to assess resistances. The general principles of structural

reliability preconized by the Eurocodes [12] are in agreement with ISO 2394 [9] which is also the reliability reference assumed by the IEC 61400-1 [8] standard for the structural analysis of wind turbines. In most countries the referred building codes are mandatory when design calculations are to be submitted for approval by local authorities, which is usually the case of wind towers foundation design. Furthermore, the procedure is also allowed by the IEC standard given that the reliability level is not lower than the one imposed by this standard, which is controlled by the safety factors applied to loads and resistances.

The design of the foundations is performed according to the concept presented above using the rules prescribed in Eurocode 7 [13] for geotechnical design, in Eurocode 8 [14] for seismic design, in Eurocode 2 [15] for reinforced concrete design and in Eurocode 3 [16] for steel design. Fatigue may be the critical limit state for the design of the tower and foundation.

The partial factors on actions (γ_F) used for the structural design are defined in IEC 61400-1 [8] and are presented in GL guidelines [6] operationalize the use of load safety factors. If the loads of different causes can be determined independently of each other, the partial safety factors for the loads shall have the minimum values given in Table 2.3. Partial safety factor for the loads in the analysis of the fatigue strength (F) shall amount to $\gamma_F = 1,0$ for all design situations. Partial safety factors for the loads in the analysis of the serviceability limit state (SLS) of $\gamma_F = 1,0$ shall be used for all load components.

Table 2.2. The partial factors on materials (γ_M) for resistance and fatigue analysis are those given in Eurocodes 2 [15] and 3 [17].

GL guidelines [6] operationalize the use of load safety factors. If the loads of different causes can be determined independently of each other, the partial safety factors for the loads shall have the minimum values given in Table 2.3. Partial safety factor for the loads in the analysis of the fatigue strength (F) shall amount to $\gamma_F = 1,0$ for all design situations. Partial safety factors for the loads in the analysis of the serviceability limit state (SLS) of $\gamma_F = 1,0$ shall be used for all load components.

Table 2.2: Partial factors on actions (γ_F) ([8])

| Unfavourable loads | | | Favourable loads | Fatigue |
|--------------------------|-----------------|-------------------------------|-----------------------|---------|
| Type of design situation | | | All design situations | |
| Normal (N) | Abnormal (A) | Transport and erection (T) | | |
| 1.35 | 1.1 | 1.5 | 0.9 | 1.0 |

According to IEC61400 the combined partial safety factors for loads, materials and consequences of failure where recognized design codes are available shall not be less than those specified in IEC standard.

Table 2.3: Partial factors on actions (γ_F) ([6])

| Source of loading | Unfavourable loads | | | Favourable loads |
|---|---|---------------|-----------------------------|-----------------------|
| | Type of design situation (see Tables 4.3.1 and 4.3.2) | | | All design situations |
| | N Normal and extreme | A Abnormal | T Transport and erection | |
| Aerodynamic | 1.35 | 1.1 | 1.5 | 0.9 |
| Operational | 1.35 | 1.1 | 1.5 | 0.9 |
| Gravity | 1.1/1.35* | 1.1 | 1.25 | 0.9 |
| Other inertial forces | 1.25 | 1.1 | 1.3 | 0.9 |
| Heat influence | 1.35 | - | - | - |
| * in the event of the masses not being determined by weighing | | | | |

2.4.7 Influence of dynamic characteristics of tower and foundation

The vibrational behaviour of a wind turbine can be kept under control only when the stiffness and mass parameters of all its components are carefully matched. The most important design requirement concerning vibrations of the turbine as a whole is to prevent the exciting rotor forces from resonating with the natural tower bending frequencies. To provide adequate dynamic behaviour and control of deflections resonance situations shall be avoided through well balanced natural frequencies in relation to rotation frequency ranges. When this is not possible, additional measures to control vibration during operation must be implemented (e.g. monitoring vibrations, special devices to control vibrations such as tuned mass dampers).

The natural frequencies of the tower must include tower head mass and soil-structure interaction.

The exciting forces of the rotor have basically two sources:

- “mass imbalances” of moving parts, mainly the rotor with blades
- “aerodynamic imbalances” that result from the asymmetrical air flow against the rotor, mostly the tower shadow effect and the vertical wind shear

The second type of forces is the critical one, since it cannot be avoided or minimized through precise manufacturing.

The first frequency of excitation is usually called 1 P (per revolution) and corresponds to the rotor angular speed. It is the only one present in one-bladed turbines and it is the basic frequency of excitation for all other turbines. Higher harmonics appear for multi-blade turbines as 2 P , 3 P , etc.

The tower’s first natural bending frequency must not coincide with the critical exciting forces. Furthermore, care must be taken to ensure that a certain distance from the remaining multiples of the rotor frequency is maintained, depending on structural as well as aerodynamic damping. A safety distance of 0,25 P from the dominant frequency of excitation and of 0,15 P to 0,20 P from the less critical ones is a good guide value.

Designation "stiff" or "soft" tower corresponds to the position of the tower's first frequency relative to the dominant excitation frequency of the rotor (see Figure 2.13). Stiff towers are only possible in short steel towers. Current steel wind turbine towers with heights between 60 and 120 meters are soft towers.

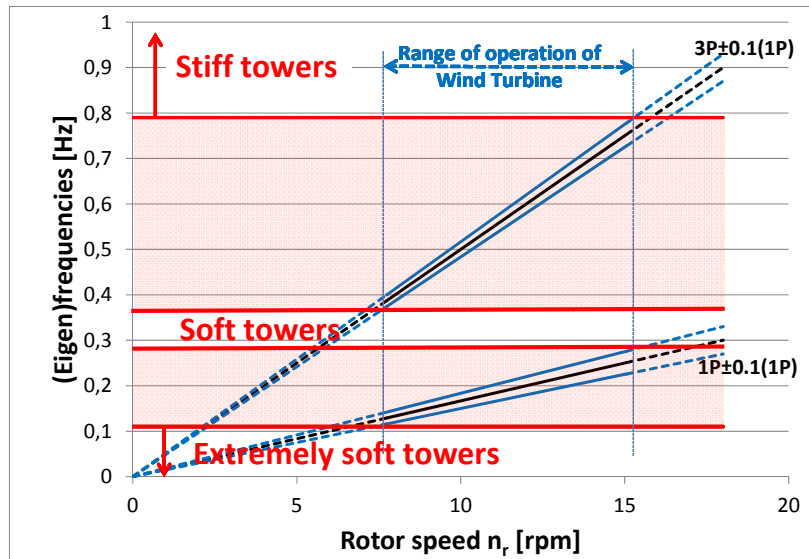


Figure 2.13: Campbell diagram relating rotor speed and eigenfrequencies of the tower

Natural frequencies depend not only on the tower structure but also on stiffness of the foundation and on the soil-structure interaction. Minimum rotational stiffness of foundation implies a minimum subgrade reaction modulus that must be checked using adequate site tests like SPT, cross-hole or seismic refraction tests.

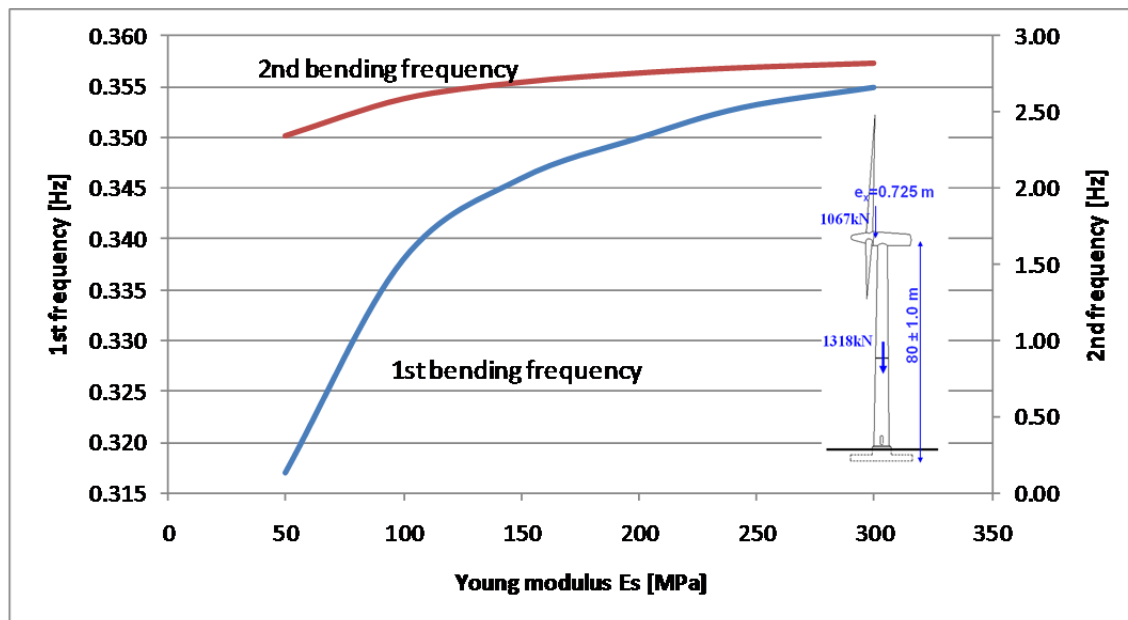


Figure 2.14: Influence of subgrade reaction modulus in the 1st and 2nd eigenfrequencies of a 80 meters high wind tower

2.5 Wind loads

2.5.1 Wind load assumptions and models in IEC61400

The wind loads on the rotor blades during steady and symmetrical flows are determined by the effective wind speed varying from the blade root to the tip and by the geometrical shape of the rotor blades. Pitch controlled rotors limit power capture to the rated power point at about 12 m/s wind speed; rotor thrust is maximum at this point dropping off for increasing wind speed

For design purposes, the life of a wind turbine is represented by a set of design situations covering the most significant conditions that the wind turbine may experience. The load cases are determined from the combination of operational modes or other design situations with the external conditions giving three main design load cases:

- normal operation and appropriate normal or extreme wind conditions
- fault situations and appropriate wind conditions
- transportation, installation and maintenance and appropriate wind conditions

Wind model assumptions are stated for two situations, normal and extreme. Wind condition "Normal" occur frequently in the course of a year. Wind condition "Extreme" include wind shear events, as well as peak wind speeds due to storms and rapid changes in wind speed and direction. Normal external conditions are assigned a recurrence period of 1 year, whereas extreme external conditions are assigned a recurrence period of 50 years as a rule.

The combination of the design situations with pertinent safety factors is operationalized in IEC61400 using 22 Design Load Cases (DLC) schematized in Table 2.4. The load cases used for performing Ultimate Limit State (U) analyses are 15 and those requiring Fatigue Limit State (F) analyses are 7. Only some of them are usually relevant for assessing the structural safety of the support structure.

Table 2.4: Design Load Cases and Type of Analysis (IEC61400-1)

| DLC | Situation | Type of Analysis | Safety Factor |
|------------|---|-------------------------|----------------------|
| 1.x | power production | U or F | N |
| 2.x | power production plus occurrence of fault | U or F | N or A |
| 3.x | start up of wind turbine | U or F | N |
| 4.x | normal shut down | U or F | N |
| 5.x | emergency shut down | U or F | N |
| 6.x | parked wind turbine | U or F | N or A |
| 7.x | parked wind turbine and fault conditions | U | N or A |
| 8.x | transport, assembly, maintenance and repair | U | N or A or T |

The complete load document delivered by fabricators of wind turbines to certification bodies for WT type certification includes information about the wind turbine specifications, environmental conditions, coordinate system, load simulation details and boundary conditions,

as well as load tables all relevant components like support structure rotor blades and machinery parts. Furthermore, extreme loads are usually provided with and without safety factors

Considering tubular wind towers the relevant load cases are those that deliver maximum effects (e.g. cross-section forces) along the tower height when the ultimate limit states are envisaged. This is not necessarily connected with only one load case, since along the tower maximum effects can be achieved with different load cases in different heights. However, the load case that delivers maximum shear force at the top of the tower will be usually design driving for the bending moment along the tower, except perhaps for the upper part of the tower where the load case delivering maximum bending moment will be controlling the design. For fatigue check general conclusion about the design driving load case is usually not possible. Therefore, information about load fatigue spectra for each section has to be provided based on the 7 load cases.

Dynamic simulations utilizing a structural dynamics model are usually used to calculate wind turbine loads. To address the problem of extrapolation to 20 years of fatigue loads and extreme loads designers typically use the models to simulate loading conditions over a range of operational and extreme wind speeds. Fault states are also simulated. The total period of load data shall be long enough to ensure statistical reliability of the estimate of the characteristic load. At least six 10-min stochastic realizations shall be required for each mean, hub-height wind speed used in the simulations.

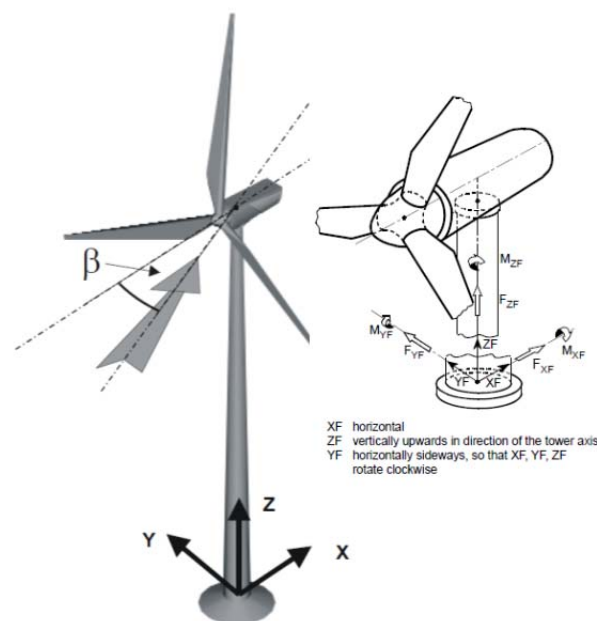


Figure 2.15: Coordinate system used to define loading and wind direction

2.5.2 Extreme loads

The results of the extreme load evaluations, including the partial safety factors, are presented in tabular form for the positions investigated (e.g. blade sections, blade root, rotor shaft, yaw system, tower etc.). This shall contain a brief description of the load case with statement of the partial safety factors applied. The following presentation format is recommended: the extreme

values (maxima and minima) of the corresponding load component are located on the diagonal; the simultaneous loads of the other load components are given in the rows.

For the extreme loads in the tower coordinate system, a column is added to the table for the wind speed and wind direction belonging to the extreme load situation. The sign of the wind direction shall be indicated in a sketch or stated in accordance with the coordinate systems (see Figure 2.15).

Example of extreme loads for a 80 metres high wind turbine tower are shown in Table 2.5 to Table 2.9 for cross sections at bottom and top of the tower and for intermediate cross-sections, above the door opening and in an intermediate ring flange connection.

Table 2.5: Example of extreme loads at tower bottom

| section | FxTS01 | FyTS01 | FzTS01 | Fr01 | MxTS01 | MyTS01 | MzTS01 | Mr01 | VcupHC | VdirHC | safety |
|---------|---------------|---------------|----------------|--------------|-----------------|-----------------|----------------|----------------|--------|--------|--------|
| 0 | kN | kN | kN | kN | kNm | kNm | kNm | kNm | m/s | deg | factor |
| MAX: | 725.2 | 37.6 | -3266.2 | 726.2 | -743.6 | 54973.6 | 1125.3 | 54978.8 | 16.5 | -7.9 | 1.35 |
| MIN: | -873.2 | 27.6 | -3174.7 | 873.6 | 521.1 | -67796.3 | -1363.1 | 67798.3 | 9.0 | -0.1 | 1.35 |
| MAX: | 177.6 | 958.3 | -2495.2 | 974.6 | -64868.7 | 10167.4 | -1043.1 | 65660.7 | 55.8 | -59.2 | 1.10 |
| MIN: | -217.4 | -933.0 | -2602.6 | 958.0 | 64537.7 | -14579.7 | 1339.3 | 66164.0 | 56.4 | 120.7 | 1.10 |
| MAX: | 188.3 | -495.9 | -2220.2 | 530.4 | 35316.9 | 6203.4 | 24573.0 | 35857.5 | 57.8 | 4.4 | 1.10 |
| MIN: | 56.9 | -249.6 | -3507.7 | 256.1 | 18529.1 | -234.7 | 590.7 | 18531.0 | 37.5 | 14.7 | 1.50 |
| MAX: | 177.6 | 958.3 | -2495.2 | 974.6 | -64868.1 | 10167.4 | -1043.1 | 65660.7 | 55.8 | -59.2 | 1.10 |
| MIN: | 0.1 | -0.1 | -3205.9 | 0.2 | 18.5 | -962.5 | -70.0 | 962.8 | 0.8 | -63.5 | 1.35 |
| MAX: | -217.4 | -933.0 | -2602.6 | 958.0 | 64537.7 | -14579.7 | 1339.3 | 66164.0 | 56.4 | 120.7 | 1.10 |
| MIN: | 177.6 | 958.3 | -2495.2 | 974.6 | -64368.7 | 10167.4 | -1043.1 | 65660.7 | 55.8 | -59.2 | 1.10 |
| MAX: | 722.2 | 64.7 | -3266.6 | 725.1 | -1668.7 | 55329.4 | 1130.3 | 55354.4 | 16.5 | -7.9 | 1.35 |
| MIN: | -873.2 | 27.6 | -3174.7 | 873.6 | 521.1 | -67796.3 | -1363.1 | 67798.3 | 9.0 | -0.1 | 1.35 |
| MAX: | 462.4 | -178.8 | -2695.1 | 495.8 | 15718.7 | 32538.1 | 5556.6 | 36135.5 | 24.0 | -7.5 | 1.10 |
| MIN: | -262.0 | 85.9 | -3010.3 | 275.8 | -6287.4 | -25287.7 | -6476.2 | 26056.9 | 32.9 | -8.5 | 1.35 |
| MAX: | -873.2 | 27.6 | -3174.7 | 873.6 | 521.1 | -67796.3 | -1363.1 | 67798.3 | 9.0 | -0.1 | 1.35 |
| MIN: | 17.1 | 4.8 | -2629.3 | 17.8 | -3.4 | -0.3 | -132.5 | 3.4 | 14.0 | -8.0 | 1.10 |

Table 2.6: Example of extreme loads at Level 6.99 m from bottom (above door opening)

| section | FxTS05 | FyTS05 | FzTS05 | Fr05 | MxTS05 | MyTS05 | MzTS05 | Mr05 | VcupHC | VdirHC | safety |
|---------|---------------|---------------|----------------|--------------|-----------------|-----------------|----------------|----------------|--------|--------|--------|
| 6.99 | kN | kN | kN | kN | kNm | kNm | kNm | kNm | m/s | deg | factor |
| MAX: | 727.8 | 12.1 | -2964.4 | 727.9 | 151.3 | 50056.4 | 1368.3 | 50056.0 | 16.4 | -7.9 | 1.35 |
| MIN: | -878.1 | 28.1 | -2873.3 | 878.6 | 715.3 | -61674.6 | -1364.5 | 61678.8 | 9.0 | -0.1 | 1.35 |
| MAX: | 171.9 | 950.8 | -2249.6 | 966.2 | -58192.1 | 8944.2 | -1043.2 | 58875.5 | 55.8 | -59.2 | 1.10 |
| MIN: | -211.9 | -926.0 | -2357.0 | 950.0 | 58036.2 | -13077.3 | 1340.3 | 59491.3 | 56.4 | 120.7 | 1.10 |
| MAX: | 175.6 | -495.5 | -1974.6 | 525.7 | 31849.8 | 4928.1 | 2458.2 | 32229.1 | 57.8 | 4.4 | 1.10 |
| MIN: | 50.1 | -248.5 | -3172.8 | 253.5 | 16787.0 | -610.3 | 591.1 | 16798.5 | 37.5 | 14.7 | 1.50 |
| MAX: | 171.9 | 950.8 | -2249.6 | 966.2 | -58192.1 | 8944.2 | -1043.2 | 58875.5 | 55.8 | -59.2 | 1.10 |
| MIN: | 0.0 | 0.0 | -2838.0 | 0.0 | -440.0 | -2069.7 | -521.6 | 2116.0 | 21.9 | 0.0 | 1.35 |
| MAX: | -211.9 | -926.0 | -2357.0 | 950.0 | 58036.2 | -13077.3 | 1340.3 | 59491.0 | 56.4 | 120.7 | 1.10 |
| MIN: | 171.9 | 950.8 | -2249.6 | 966.2 | -58192.1 | 8944.2 | -1043.2 | 58875.5 | 55.8 | -59.2 | 1.10 |
| MAX: | 725.0 | 64.0 | -2965.2 | 727.8 | -1218.1 | 50270.9 | 1131.7 | 50286.0 | 16.5 | -7.9 | 1.35 |
| MIN: | -878.1 | 28.1 | -2873.3 | 878.6 | 715.3 | -61674.6 | -1364.5 | 61678.8 | 9.0 | -1.0 | 1.35 |
| MAX: | 462.2 | -180.2 | -2449.5 | 496.0 | 14464.0 | 29305.1 | 5557.8 | 32680.1 | 24.0 | -7.5 | 1.10 |
| MIN: | -269.5 | 85.9 | -2708.8 | 282.9 | -5686.9 | -23431.2 | -6476.3 | 24111.2 | 32.9 | -8.5 | 1.35 |
| MAX: | -878.1 | 28.1 | -2873.3 | 878.6 | 715.3 | -61674.6 | -1364.5 | 61678.8 | 9.0 | -0.1 | 1.35 |
| MIN: | 30.5 | 63.3 | -2895.3 | 70.3 | -1.0 | 2.7 | -360.8 | 3.1 | 9.0 | -8.0 | 1.35 |

Table 2.7: Example of extreme loads at level immediately below second connection (level 21.46m from bottom)

| section | FxTS13 | FyTS13 | FzTS13 | Fr13 | MxTS13 | MyTS13 | MzTS13 | Mr13 | VcupHC | VdirHC | safety |
|---------|---------------|---------------|----------------|--------------|-----------------|-----------------|----------------|----------------|--------|--------|--------|
| 21.46 | kN | kN | kN | kN | kNm | kNm | kNm | kNm | m/s | deg | factor |
| MAX: | 731.4 | 9.8 | -2541.6 | 731.5 | 312.3 | 39485.5 | 1369.1 | 39487.0 | 16.4 | -7.9 | 1.35 |
| MIN: | -885.8 | 26.7 | -2450.5 | 886.2 | 1121.0 | -48892.1 | -1367.7 | 48904.9 | 9.0 | -0.1 | 1.35 |
| MAX: | 154.3 | 919.0 | -1905.0 | 931.9 | -44623.5 | 6577.1 | -1048.3 | 45105.5 | 55.8 | -59.2 | 1.10 |
| MIN: | -195.2 | -898.8 | -2012.4 | 919.7 | 44805.0 | -10124.5 | 1337.0 | 45934.4 | 56.4 | 120.7 | 1.10 |
| MAX: | 136.9 | -485.9 | -1630.0 | 504.8 | 24721.7 | 2652.1 | 2466.0 | 24863.3 | 57.8 | 4.4 | 1.10 |
| MIN: | 31.1 | -243.9 | -2703.0 | 245.9 | 13220.2 | -1199.7 | 592.5 | 13274.7 | 37.5 | 14.7 | 1.50 |
| MAX: | 154.3 | 919.0 | -1905.0 | 931.9 | -44623.5 | 6577.1 | -1048.3 | 45105.5 | 55.8 | -59.2 | 1.10 |
| MIN: | 0.2 | 0.0 | -2475.7 | 0.2 | 2648.9 | -1057.8 | -96.2 | 2852.4 | 11.0 | 0.0 | 1.35 |
| MAX: | -196.9 | -896.6 | -2011.4 | 918.0 | 44808.8 | -10166.8 | 1357.6 | 45947.7 | 56.9 | 120.3 | 1.10 |
| MIN: | 159.3 | 888.7 | -1907.4 | 902.8 | -44715.8 | 6560.5 | -1116.2 | 45194.5 | 56.9 | -59.9 | 1.10 |
| MAX: | 730.3 | 58.8 | -2542.3 | 732.7 | 119.5 | 39733.3 | 1134.4 | 39734.5 | 16.5 | -7.9 | 1.35 |
| MIN: | -885.8 | 26.7 | -2450.5 | 886.2 | 1121.0 | -48892.1 | -1367.7 | 48904.9 | 9.0 | -0.1 | 1.35 |
| MAX: | 457.2 | -182.6 | -2105.0 | 492.3 | 11833.8 | 22639.4 | 5559.3 | 25545.7 | 24.0 | -7.5 | 1.10 |
| MIN: | -291.2 | 851.0 | -2286.0 | 303.4 | -4446.9 | -19377.2 | -6477.3 | 19881.1 | 32.9 | -8.5 | 1.35 |
| MAX: | -885.8 | 26.7 | -2450.5 | 886.2 | 1121.0 | -48892.1 | -1367.7 | 48904.9 | 9.0 | -0.1 | 1.35 |
| MIN: | 25.6 | -2.9 | -2464.3 | 25.8 | -5.6 | -2.8 | 67.1 | 6.2 | 11.0 | 8.0 | 1.35 |

Table 2.8: Example of extreme loads at level immediately below third connection (level 48.08m from bottom)

| section | FxTS13 | FyTS13 | FzTS13 | Fr13 | MxTS13 | MyTS13 | MzTS13 | Mr13 | VcupHC | VdirHC | safety |
|---------|---------------|---------------|----------------|--------------|-----------------|-----------------|----------------|----------------|--------|--------|--------|
| 48.08 | kN | kN | kN | kN | kNm | kNm | kNm | kNm | m/s | deg | factor |
| MAX: | 724.7 | 39.9 | -1941.9 | 725.8 | 1021.8 | 20308.9 | 1137.0 | 20334.5 | 16.5 | -7.9 | 1.35 |
| MIN: | -865.9 | 5.2 | -1850.1 | 865.9 | 1603.6 | -25436.2 | -1373.5 | 25486.7 | 9.0 | -0.1 | 1.35 |
| MAX: | 114.1 | 811.4 | -1416.1 | 819.4 | -22096.7 | 2858.0 | -1162.0 | 22280.8 | 57.5 | -60.3 | 1.10 |
| MIN: | -157.9 | -812.2 | -1522.2 | 827.4 | 21954.4 | -5436.2 | 1340.2 | 22617.4 | 56.9 | 120.3 | 1.10 |
| MAX: | 55.7 | -436.5 | -1140.8 | 440.0 | 12349.4 | 95.8 | 2490.7 | 12349.8 | 57.8 | 4.4 | 1.10 |
| MIN: | 0.8 | -239.0 | -2035.9 | 239.0 | 6806.5 | -1580.4 | 596.0 | 6987.5 | 37.5 | 14.7 | 1.50 |
| MAX: | -865.8 | 16.9 | -1848.5 | 866.0 | 1933.7 | -25350.0 | -1406.5 | 25423.3 | 9.0 | -0.1 | 1.35 |
| MIN: | 0.1 | -0.1 | -1872.4 | 0.1 | -63.6 | -970.2 | 14.5 | 972.1 | 8.0 | 0.0 | 1.35 |
| MAX: | -157.9 | -812.2 | -1522.2 | 827.4 | 21954.4 | -5436.2 | 1340.2 | 22617.4 | 56.9 | 120.3 | 1.10 |
| MIN: | 114.1 | 811.4 | -1416.1 | 819.4 | -22096.7 | 2858.0 | -1162.0 | 22280.8 | 57.5 | -60.3 | 1.10 |
| MAX: | 724.7 | 39.9 | -1941.9 | 725.8 | 1021.8 | 20308.9 | 1137.0 | 20334.5 | 16.5 | -7.9 | 1.35 |
| MIN: | -865.9 | 5.2 | -1850.1 | 865.9 | 1603.6 | -25436.2 | -1373.5 | 25486.7 | 9.0 | -0.1 | 1.35 |
| MAX: | 424.4 | -177.2 | -1615.8 | 459.9 | 7001.0 | 10818.9 | 5558.8 | 12886.6 | 24.0 | -7.5 | 1.10 |
| MIN: | -332.3 | 77.0 | -1685.6 | 341.1 | -2273.4 | -11053.2 | -6480.0 | 11284.6 | 32.9 | -8.5 | 1.35 |
| MAX: | -865.9 | 5.2 | -1850.1 | 865.9 | 1603.6 | -25436.2 | -1373.5 | 25486.7 | 9.0 | -0.1 | 1.35 |
| MIN: | 31.3 | 2.5 | -1880.5 | 31.4 | -0.7 | -0.7 | -12.1 | 1.0 | 2.6 | 11.4 | 1.35 |

Table 2.9: Example of extreme loads at tower top

| section | FxTS45 | FyTS45 | FzTS45 | Fr45 | MxTS45 | MyTS45 | MzTS45 | Mr45 | VcupHC | VdirHC | safety |
|---------|---------------|---------------|----------------|--------------|----------------|----------------|----------------|---------------|--------|--------|--------|
| 75.64 | kN | kN | kN | kN | kNm | kNm | kNm | kNm | m/s | deg | factor |
| MAX: | 697.9 | 18.4 | -1549.7 | 698.1 | 1629.5 | 639.8 | 1248.0 | 1750.6 | 16.5 | -7.9 | 1.35 |
| MIN: | -808.3 | -9.2 | -1457.3 | 808.4 | 1480.7 | -2248.3 | -1378.9 | 2692.0 | 9.0 | -0.1 | 1.35 |
| MAX: | -1.9 | 691.2 | -1295.7 | 691.2 | -1296.7 | 1257.9 | -2451.0 | 1806.5 | 47.8 | -17.3 | 1.35 |
| MIN: | -102.5 | -682.9 | -1202.2 | 690.5 | 1216.9 | -1803.8 | 1334.4 | 2175.9 | 56.9 | 120.3 | 1.10 |
| MAX: | -37.4 | -383.1 | -820.8 | 384.9 | 1089.3 | -177.3 | 2506.9 | 1103.7 | 57.8 | 4.4 | 1.10 |
| MIN: | -37.7 | -221.5 | -1599.5 | 224.7 | 408.2 | -1098.5 | 599.3 | 1172.0 | 37.5 | 14.7 | 1.50 |
| MAX: | -808.3 | -9.2 | -1457.3 | 808.4 | 1480.7 | -2248.3 | -1378.9 | 2692.0 | 9.0 | -0.1 | 1.35 |
| MIN: | 0.0 | 0.1 | -1094.4 | 0.1 | 109.4 | -347.2 | 50.4 | 364.0 | 31.0 | 14.9 | 1.10 |
| MAX: | 75.3 | 6.2 | -1488.3 | 75.6 | 3549.5 | -89.7 | -103.1 | 3550.6 | 11.0 | 8.0 | 1.35 |
| MIN: | 37.9 | 264.4 | -1042.9 | 267.1 | -2963.7 | 182.0 | -289.4 | 2969.3 | 40.5 | -11.6 | 1.10 |
| MAX: | -155.7 | -151.3 | -1364.4 | 217.1 | 408.0 | 6130.9 | -817.1 | 6144.5 | 35.9 | 8.0 | 1.35 |
| MIN: | -115.1 | 103.5 | -1471.7 | 154.8 | 206.7 | -7054.7 | -2115.1 | 7057.7 | 26.0 | -65.5 | 1.35 |
| MAX: | 369.7 | -158.0 | -1295.8 | 402.1 | 2334.0 | -179.8 | 5562.5 | 2341.0 | 24.0 | -7.5 | 1.10 |
| MIN: | -356.2 | 72.7 | -1292.8 | 363.5 | -240.2 | -1481.9 | -6480.8 | 1501.3 | 32.9 | -8.5 | 1.35 |
| MAX: | -115.1 | 103.5 | -1471.7 | 154.8 | 206.7 | -7054.7 | -2115.1 | 7057.7 | 26.0 | -65.5 | 1.35 |
| MIN: | 139.9 | -29.1 | -1034.4 | 142.9 | -0.1 | 0.0 | -636.0 | 0.1 | 40.3 | -3.1 | 1.10 |

2.5.3 Fatigue loads

The load simulation in the time domain provides time series of the relevant load effect, be it a cross section force or a stress in some point of the structure. The results for the support structure (tower and foundation) are time series for different load cases and for all load components.

The time series are the most accurate means of delivering loads for fatigue analysis, but they are complex to handle. The time series include the information about the load range and its level as well as how often and when an event occurs. The time phase between different load components is kept and can be taken into account in the calculations.

In order to use data from irregular load histories for practical fatigue design, the cycles must be extracted. There are several methods to extract cycles but the best ones recognize the hysteresis effects by combining the cycles between the highest peak and lowest valley in the time series. The most commonly used methods are range-mean-pair and rainflow.

To derive the values needed for fatigue analysis the cycle count of the time series must be performed. The resulting number of cycles and load ranges, producing damage, have to be weighted according to the number of occurrences of the individual time series during the wind turbines lifetime.

For some components where load amplitude is required e.g. if nonlinear load functions are involved like in fiber reinforced plastic components (blades), the fatigue calculations demand information about load range and mean value. In that case, the information given by the time series calculated for each of the design load cases pertinent for fatigue calculations is condensed, by means of a range-mean-pair count to a Marcov Matrix containing the number of cycles for each pair of values defined by the range value and the mean value of the pertinent load effect. Marcov matrices are easier to handle due to its table form. A fatigue calculation can be performed using the Palmgren-Miner approach, but there is still a large amount of data to be handled, especially when more load components have to be taken into account.

The fatigue design of components like the steel tower or the reinforced concrete foundation only need information about the range value and respective number of cycles, which can be easily obtained using well established algorithms for rainflow counting. The result is the Whöler curve or S/N curve relating the load range and the number of cycles. Such a curve obtained from measurements in an instrumented wind tower is shown in the Figure 2.16 in a log-log scale.

In this way, each of the design load cases requiring fatigue design (F) is simulated producing a set of time series. For instance, DLC 1.1 embodies the requirements for loads resulting from atmospheric turbulence during power production, that is, for wind speeds at hub height v_{hub} between v_{in} and v_{out} . Therefore turbulent wind must be considered in the simulation and the discretization of the wind speed intervals within the wind speed range must be specified, e.g 2 m/s [6]. However, since we are dealing with a situation of power production, related turbine operations must be also considered. For instance, in the fatigue load calculation [6] imposes the consideration of 700 generator switching operations (high speed /low speed and vice versa), 300 changes in the mean wind speeds from v_{in} to v_{rated} and back to v_{in} , 50 changes in the mean wind speeds from v_{rated} to v_{out} and back to v_{rated} . All these values are considered per year of life.

Other DLCs require other type of events, such as normal start-up and shut-down, grid failure, failure in the control system, and others. The set of time series from all DLCs and from all

events defined in each DLC constitutes the complete time series to be used in fatigue design after rainflow counting.

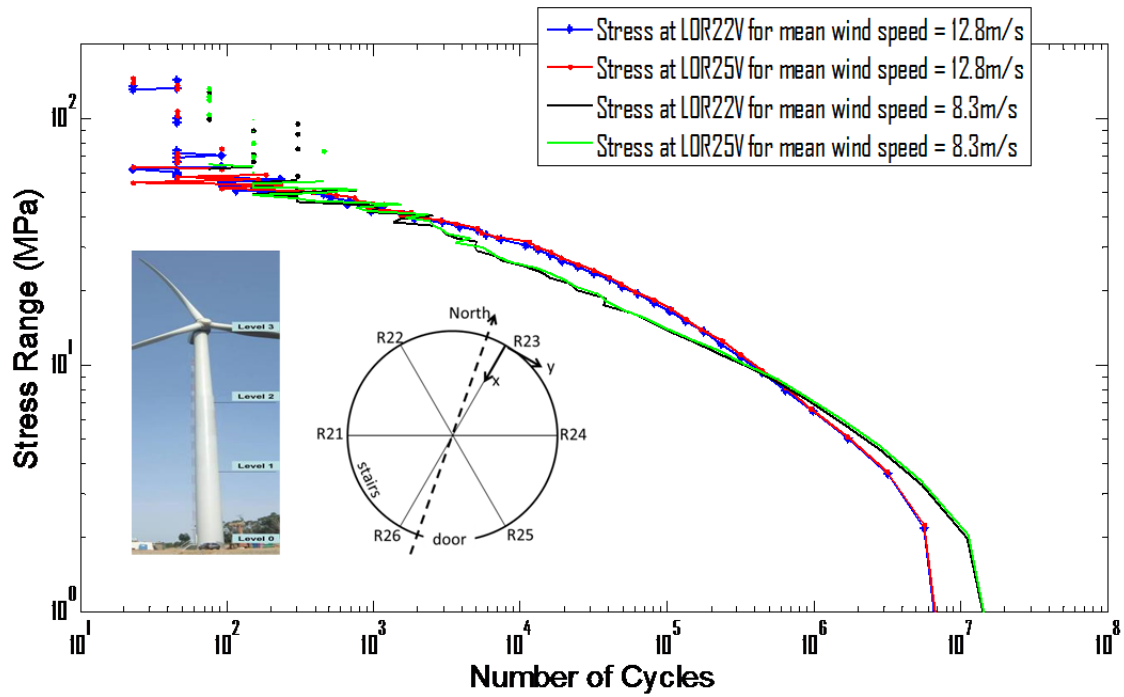


Figure 2.16: S-N spectrum from measurements

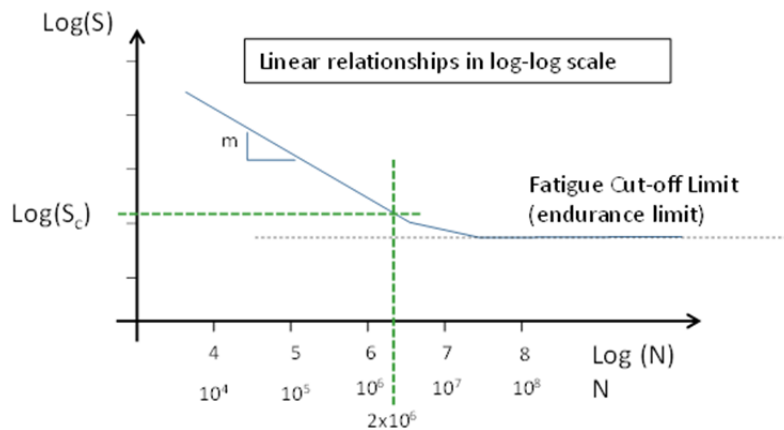


Figure 2.17: S-N curve for steel structures

A further simplification in the provided fatigue loading information is achieved when using damage equivalent loads (DEL) instead of fatigue spectra. Definition of DEL is the equivalent load (or load effect) with constant amplitude that would produce the same damage in the structure as the damage induced by the original time series of the same load (or load effect). The conversion is based on the formula

$$\Delta\sigma_{E,ref} = \left(\sum_i \frac{n_i \Delta\sigma_i^m}{N_{ref}} \right)^{\frac{1}{m}} \quad (21)$$

Where m is the Wöhler slope adopted to define the DEL (see Figure 2.18), n_i is the number of cycles corresponding to load range $\Delta\sigma_i$ in the original time history and N_{ref} is the reference number of cycles for which the reference DEL ($\Delta\sigma_{E,ref}$) is calculated.

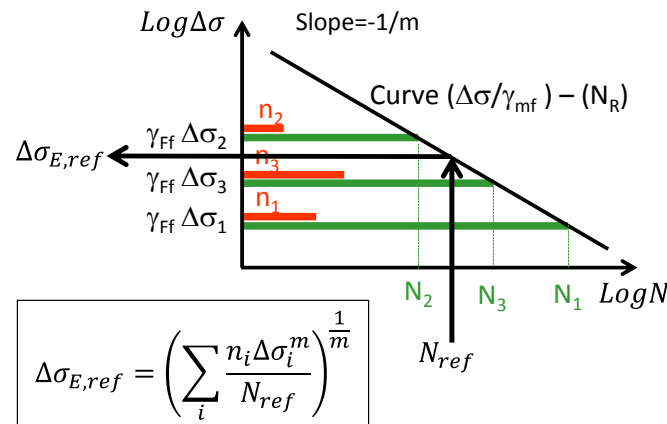


Figure 2.18: Calculation of Damage Equivalent Load $\Delta\sigma_{E,ref}$ for a given N_{ref} and slope m

A typical S/N-curve for steel structures has two different Wöhler slopes, $m = 3$ and $m=5$. In general, the DEL will include load cycles acting in the range of both Wöhler slopes and therefore the standard Wöhler slope cannot be used. An S/N-curve with a constant Wöhler slope has to be defined so that all load cycles can be recalculated on the same basis. For steel, it is state of the art to use a Wöhler slope of $m = 4$, that is connected to the standard S/N-curve at $N_{ref} = 2 \times 10^6$.

The results of the fatigue loads are usually presented in a set of damage equivalent fatigue load tables for different tower section heights. The damage equivalent loads (DEL) given in the load tables can be handled like a static load case in combination with the reference number of cycles (e.g. $N_{ref} = 2 \times 10^8$) and a constant Wöhler slope m . For a certain type of structural material only one slope is usually of interest (e.g. for steel structures $m = 4$ is relevant).

Example of dalage equivalent load effects for a 80 metres high wind turbine tower are shown in Table 2.10 for cross sections at bottom and top of the tower and for intermediate cross-sections, above the door opening and in an intermediate ring flange connection.

Table 2.10: Example of damage equivalent load effects

| section 0 | Nref: 2.0E+08 Tower Base | | | | | |
|------------------|--------------------------|--------------|--------------|---------------|---------------|---------------|
| | FxTS01 kN | FyTS01 kN | FZTS01 kN | MxTS01 kNm | MyTS01 kNm | MzTS01 kNm |
| m | | | | | | |
| 3 | 92.2 | 47.9 | 26.4 | 3239.6 | 5057.2 | 1104.0 |
| 4 | 102.6 | 67.8 | 28.9 | 4774.0 | 6204.1 | 1228.7 |
| 5 | 115.5 | 91.0 | 32.7 | 6443.5 | 7353.9 | 1383.6 |
| section 6.99 | Nref: 2.0E+08 | | | | | |
| | FxTS05 kN | FyTS05 kN | FZTS05 kN | MxTS05 kNm | MyTS05 kNm | MzTS05 kNm |
| m | | | | | | |
| 3 | 91.5 | 47.9 | 26.4 | 2981.6 | 4492.0 | 1104.1 |
| 4 | 102.2 | 67.9 | 28.9 | 4309.4 | 5548.3 | 1228.7 |
| 5 | 115.2 | 91.2 | 32.7 | 5813.7 | 6600.4 | 1383.6 |
| section 21.46 | Nref: 2.0E+08 | | | | | |
| | FxTS13 kN | FyTS13 kN | FZTS13 kN | MxTS13 kNm | MyTS13 kNm | MzTS13 kNm |
| m | | | | | | |
| 3 | 85.0 | 46.4 | 26.4 | 2270.8 | 3376.7 | 1104.1 |
| 4 | 96.6 | 66.9 | 28.9 | 3361.6 | 4267.4 | 1228.8 |
| 5 | 110.5 | 90.2 | 32.7 | 4526.7 | 5109.7 | 1383.7 |
| section 48.08 | Nref: 2.0E+08 | | | | | |
| | FxTS29 kN | FyTS29 kN | FZTS29 kN | MxTS29 kNm | MyTS29 kNm | MzTS29 kNm |
| m | | | | | | |
| 3 | 65.7 | 41.1 | 26.4 | 1179.1 | 1910.0 | 1104.2 |
| 4 | 81.2 | 60.8 | 28.9 | 1725.6 | 2379.4 | 1228.8 |
| 5 | 96.3 | 81.9 | 32.7 | 2321.3 | 2824.4 | 1383.8 |
| section 75.64 | Nref: 2.0E+08 Tower Top | | | | | |
| | FxTS45 kN | FyTS45 kN | FZTS45 kN | MxTS45 kNm | MyTS45 kNm | MzTS45 kNm |
| m | | | | | | |
| 3 | 65.4 | 37.8 | 26.4 | 235.3 | 1065.2 | 1104.4 |
| 4 | 80.5 | 55.1 | 28.9 | 312.9 | 1206.5 | 1229.1 |
| 5 | 95.4 | 74.4 | 32.7 | 393.3 | 1378.4 | 1384.1 |

2.6 Earthquake loads

2.6.1 General requirements in IEC 61400

In Europe structures in seismic regions shall be designed and constructed according to Eurocode 8 part 1 in such a way that the following requirements are met, each with an adequate degree of reliability:

- No-collapse requirement - The design seismic action is expressed in terms of the reference seismic action associated with a reference return period of 475 years.
- Damage limitation requirement

There are no earthquake resistance requirements for standard class turbines. Assessment of earthquake conditions according to IEC61400-1 §11.6 and respective Annex C is only required if the construction site has seismic risk. The engineering integrity shall be demonstrated for locations where the seismic load cases are critical when assessed using the following parameters:

- The ground acceleration shall be evaluated for a 475-year recurrence period;
- The earthquake loading shall be superposed with operational loading;
- The partial safety factor for load for all load components shall be 1,0;
- The number of tower natural vibration modes represents at least 85 % of the total mass of the tower and turbine;
- The evaluation of the resistance of the structure may assume elastic response only (behaviour factor $q=1$)

A conservative simplified approach to the calculation and the combination of loads on the tower may be used according to IEC61400-1 Annex C. The procedure includes the following steps:

- Evaluate or estimate the site and soil conditions required by the relevant local standard;
- Use the normalised design response spectrum and the seismic hazard-zoning factor to establish the acceleration at the first tower bending natural frequency assuming a damping of 1 % of critical damping;
- Calculate the load for a system subject to the above acceleration in which the total rotor, nacelle and 50 % of the tower mass is concentrated at the tower head;
- Add the result to the characteristic loads calculated for an emergency stop at rated wind speed, e.g. Load case 5.1 with $v_{hub} = v_{rated}$;
- Compare the result against the design loads or the design resistance for the wind turbine

If the tower can sustain the resulting combined loading, no further investigation is needed. Otherwise, a thorough investigation shall be carried out using Eurocode 8 [14].

2.6.2 General requirements in Eurocode 8 parts 1 and 6

Fundamental requirements for seismic resistant structures are addressed in Eurocode 8 part 1 [14]. The no-collapse requirement applies, in order to protect the safety of people, nearby

buildings and adjacent facilities. The structure shall be designed and constructed to withstand the design seismic action defined without local or global collapse, thus retaining its structural integrity and a residual load bearing capacity after the seismic events.

The **design seismic action** is expressed in terms of:

- the reference seismic action associated with a reference probability of exceedance, $PNCR$, in 50 years or a reference return period, $TNCR$; The recommended values are $PNCR = 10\%$ and $TNCR = 475 \text{ years}$ which agree with those imposed by IEC61400-1
- the importance factor γ_I to take into account reliability differentiation; for wind towers $\gamma_I = 1,0$ may be assumed
- The hazard is described in terms of a single parameter, i.e. the value of the reference peak ground acceleration on type A ground, a_{gR} .
- The peak ground acceleration on any type of ground is $S \cdot a_{gR}$ where S is the soil parameter (five standard soil types are considered – A ... E – stiff ... soft)
- The elastic response spectrum is the basic representation of the seismic action.

The elastic response spectrum in terms of acceleration is defined for the horizontal translational components for the vertical translational component and for the rotational components. The design response spectrum is defined using the behaviour factor $q=1$ (Figure 2.19).

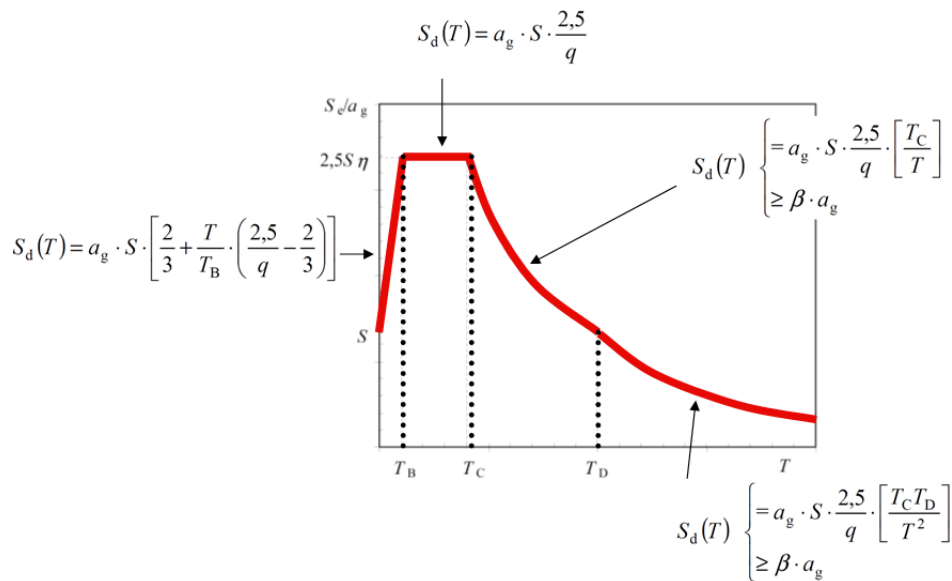


Figure 2.19: Design Response Spectrum

Eurocode 8 part 6 [18] establishes requirements, criteria, and rules for the design of tall slender structures.

For towers, masts and chimneys, depending on the cross section of the members, design based on elastic behaviour until the Ultimate Limit State is appropriate. In addition to the translational components of the earthquake motion, the rotational component of the ground motion should be taken into account for tall structures in regions of high seismicity. The recommended conditions are defined for structures taller than 80 m in regions where the

product $a_g S$ exceeds 0,25g. In this case the rotational component of the seismic action in tower base is defined in proportion of the horizontal acceleration response spectrum using following relations:

$$\begin{aligned} R_x^\theta(T) &= 1,7 \cdot \pi \cdot S_e(T) / v_s \cdot T \\ R_y^\theta(T) &= 1,7 \cdot \pi \cdot S_e(T) / v_s \cdot T \\ R_z^\theta(T) &= 2,0 \cdot \pi \cdot S_e(T) / v_s \cdot T \end{aligned} \quad (22)$$

Where $R_x^\theta, R_y^\theta, R_z^\theta$ are the rotation response spectra around x, y and z axes, in rad/s^2 , $S_e(T)$ is the elastic response spectra for the horizontal components at the site in ms^2 , T is the period in seconds and v_s is the average S-wave velocity, in m/s, of the top 30 m of the ground profile. The value corresponding to low amplitude vibrations, i.e., to shear deformations of the order of 10^{-6} , may be used. S-wave velocity $v_s = \sqrt{G/\rho}$ can be obtained from Table 2.11.

Table 2.11: Shear wave velocity according to soil classification

| Ground type | Shear wave velocity v_s (m/s) |
|-------------|---------------------------------|
| A | 800 |
| B | 580 |
| C | 270 |
| D | 150 |

Towers are often sensitive to the long-period content of the ground motion. Soft soils (e.g. ground type D) or peculiar topographic conditions might provide unusually large amplification of the long-period content of the ground motion and also a large contribution of the rotational movement at tower bottom. The example shown in the Figure 2.20 refers to a Wind Tower with first natural period $T_1=3$ s; and height of 80m. The comparison is made between soil types A and D. For soil type D the increase of the horizontal accelerations due to rotation at base is 38% while for soil type A the increase is only 2%.

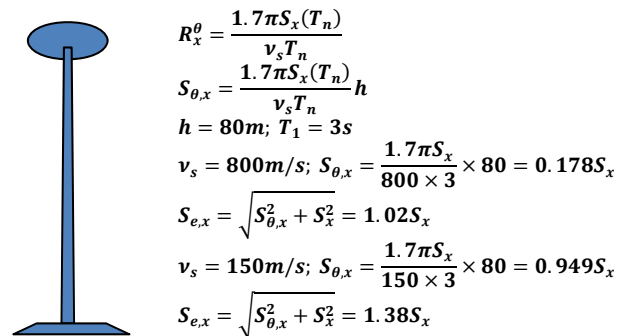


Figure 2.20: Effect of rotational accelerations in different types of soil

2.7 Software ASHES - Calculation of Eigenmodes

2.7.1 Definition of input data

Calculation of eigenmodes in ASHES [19] using histwin example tower REPOWER MM92

Data for tower: File histwin.txt

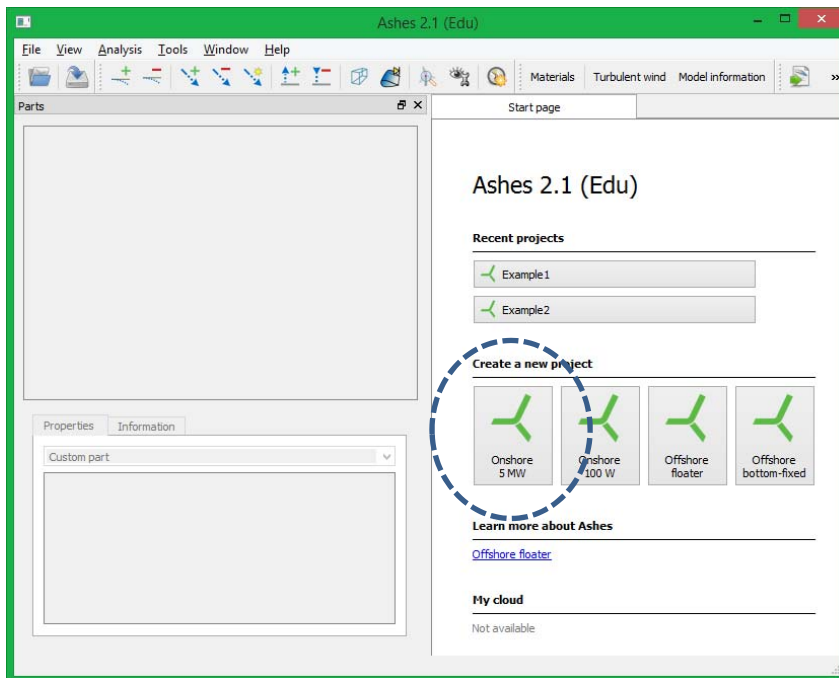
| global height z [mm] | outer diameter [mm] | thickness [mm] | point mass [kg] | tapered [0/1] |
|----------------------|---------------------|----------------|-----------------|---------------|
| 0 | 4300 | 30 | 0 | 1 |
| 382 | 4300 | 30 | 0 | 1 |
| 622 | 4300 | 30 | 0 | 1 |
| 2000 | 4276 | 30 | 0 | 1 |
| 3082 | 4257 | 30 | 0 | 1 |
| 5412 | 4215 | 30 | 0 | 1 |
| 5802 | 4208 | 26 | 0 | 1 |
| 7789 | 4173 | 26 | 0 | 1 |
| 9302 | 4147 | 27 | 0 | 1 |
| 11502 | 4108 | 24 | 0 | 1 |
| 12582 | 4089 | 23 | 0 | 1 |
| 15172 | 4043 | 22 | 0 | 1 |
| 17362 | 4004 | 22 | 0 | 1 |
| 17972 | 3993 | 22 | 0 | 1 |
| 19752 | 3962 | 22 | 0 | 1 |
| 22182 | 3917 | 21 | 0 | 1 |
| 22362 | 3917 | 20 | 0 | 1 |
| 25252 | 3864 | 20 | 0 | 1 |
| 28002 | 3816 | 20 | 0 | 1 |
| 30752 | 3768 | 20 | 0 | 1 |
| 31982 | 3746 | 19 | 0 | 1 |
| 34382 | 3704 | 19 | 0 | 1 |
| 36252 | 3671 | 19 | 0 | 1 |
| 39002 | 3622 | 18 | 0 | 1 |
| 41752 | 3574 | 18 | 0 | 1 |
| 43982 | 3535 | 17 | 0 | 1 |
| 44592 | 3524 | 17 | 0 | 1 |
| 46382 | 3492 | 17 | 0 | 1 |
| 48817 | 3448 | 16 | 0 | 1 |
| 48967 | 3448 | 15 | 0 | 1 |
| 51552 | 3400 | 15 | 0 | 1 |
| 53812 | 3360 | 15 | 0 | 1 |
| 55502 | 3330 | 14 | 0 | 1 |
| 58252 | 3280 | 14 | 0 | 1 |
| 58622 | 3277 | 13 | 0 | 1 |
| 61022 | 3231 | 13 | 0 | 1 |
| 63752 | 3182 | 13 | 0 | 1 |
| 65842 | 3144 | 13 | 0 | 1 |
| 66502 | 3133 | 12 | 0 | 1 |
| 69252 | 3083 | 12 | 0 | 1 |
| 71152 | 3049 | 12 | 0 | 1 |
| 72002 | 3034 | 12 | 0 | 1 |
| 73082 | 3015 | 12 | 0 | 1 |
| 75492 | 2971 | 14 | 0 | 1 |
| 75640 | 2955 | 18 | 0 | 1 |

Data for Nacelle: Mass= 53220 kg

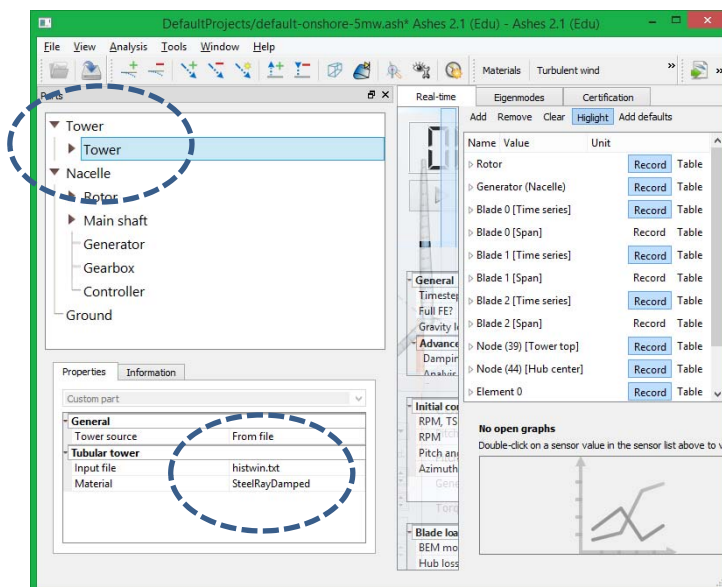
Data for Rotor: Hub Mass= 56780 kg; Rotor inertia= 0

2.7.2 ASHES Procedure

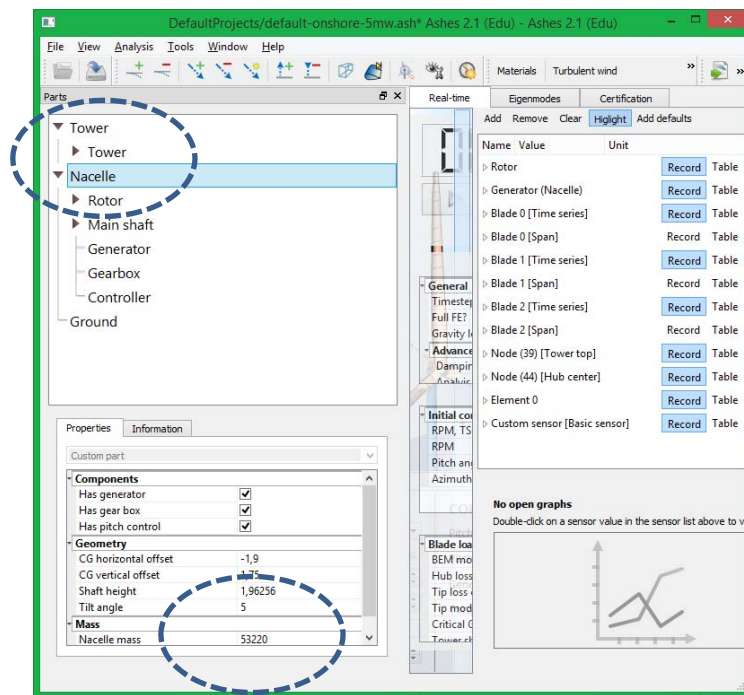
1. Start ASHES and chose <create new project> <onshore 5MW>



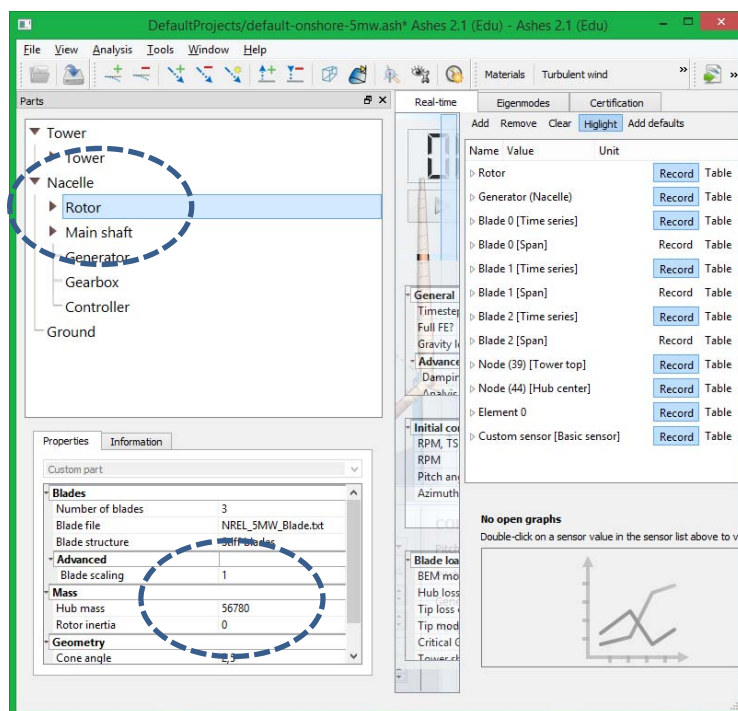
Select <TOWER><TOWER> <input file> (histwin.txt)



Select <NACELLE><NACELLE mass> 53220



Select <ROTOR><ROTOR INERTIA> 0



<EIGENMODE><RFRESH><SOLVE>

The screenshot displays the HISTWIN_Plus software interface. The title bar indicates the project is 'DefaultProjects/default-onshore-5mw.ash* Ashes 2.1 (Edu) - Ashes 2.1 (Edu)'. The main menu includes File, View, Analysis, Tools, Window, and Help. The toolbar contains various icons for file operations and analysis. The 'Parts' panel on the left shows a hierarchical tree of the wind turbine components: Tower, Nacelle, Rotor, Main shaft, Generator, Gearbox, and Controller. The 'Properties' panel below it shows settings for the selected part, including 'Number of blades' (3), 'Blade file' (NREL_5MW_Blade.txt), 'Blade structure' (Stiff blades), 'Advanced' settings (Blade scaling: 1), 'Mass' settings (Hub mass: 56780, Rotor inertia: 0), and 'Geometry' settings (Cone angle: 2,5). The 'Eigenmodes' tab is active, showing a 3D model of the wind turbine. The 'Eigenmodes' panel includes a 'Refresh model' button, a 'Solve' button, and input fields for 'Modes to find' (25), 'Search range [Hz]' (0 to 50), and 'Search resolution [Hz]' (0.01). The 'Results' section displays a table of eigenmodes with columns for Mode, Frequency [Hz], and Period [s].

| | Mode | Frequency [Hz] | Period [s] |
|---|------|----------------|------------|
| 1 | 0 | 0.365332 | 2.73724 |
| 2 | 1 | 0.366187 | 2.73084 |
| 3 | 2 | 2.72626 | 0.366803 |
| 4 | 3 | 2.76051 | 0.362252 |
| 5 | 4 | 3.32201 | 0.301022 |
| 6 | 5 | 6.04463 | 0.165436 |
| 7 | 6 | 9.24736 | 0.108139 |
| 8 | 7 | 10.0532 | 0.099471 |
| 9 | 8 | 13.2889 | 0.0752507 |

3 STABILITY

3.1 General

Thin walled shell and plate elements subjected to in-plane loading are sensitive against local buckling due to compression stress and/or shear stress. Buckling is influenced by many parameters such as:

- the component's geometry
- the material properties
- the boundary- and bearing-conditions
- imperfections
- residual stresses

Dependent on the degree of consideration of the mentioned parameters and their interaction, various buckling theories can be derived which differ in their complexity and accuracy. These theories range between extremes as highly idealised bifurcation theories and labour intensive non-linear ultimate loading theory which take into account residual stresses and imperfections of the structure.

To derive a realistic estimation of the failure load from a simple calculation of the idealised structure is the goal of numerous engineering approaches. A typical procedure of such approaches is to calculate the structural and material resistance for the perfect system and to determine the slenderness of the structure with these theoretical values. Subsequently a slenderness dependent reduction factor is defined by the use of buckling curves which are mostly of empirical or semi-empirical origin.

Design check of shell structures is defined by the Eurocode 3, Part 1-6 [42]. Several ultimate limit states are distinguished: plastic limit state (LS1), cyclic plasticity limit state (LS2), buckling limit state (LS3) and fatigue limit state (LS4).

There are three different approaches for verification of local buckling resistance: Stress limitation; materially nonlinear analysis (MNA) in conjunction with linear bifurcation analysis (LBA); and geometrically and materially nonlinear analysis with imperfections included (GMNIA).

Generally, the stress limitation approach and the MNA/LBA approach are suitable for verification of the shell, while the MNA/LBA and GMNIA approaches are suitable for verification of door openings.

3.2 Theoretical background

Buckling of plates is characterized by favourable influence of spatiality. Therefore, the post-buckling resistance of the plate structure allows use of the effective width design concept, which is given in EN1995-1-5. This is not the case for shell structures as there is an unfavourable influence of spatiality, see Figure 3.1.

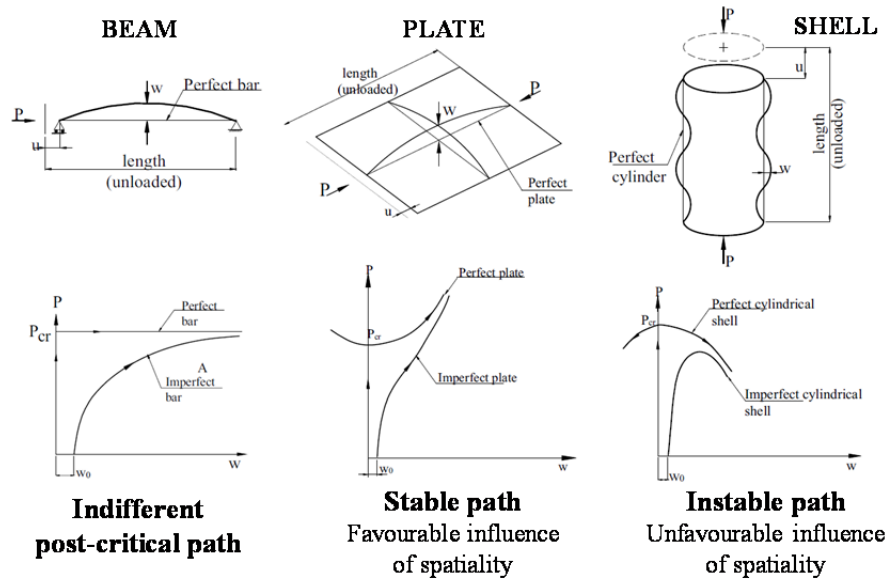


Figure 3.1: Post-buckling behaviour of different structures.

Both the plate and shell structures can be verified by reducing the sectional yield strength to the buckling stress resistance of the structural element. The main difference between EN 1993-1-5 and EN 1993-1-6, for design of shell and plate structures, respectively, is given by the applied buckling curves. Contrary to the buckling curves of EN 1993-1-5 the reduction curves given in EN 1993-1-6 are dependent on the geometry properties of the structures, namely the dimension-ratio t/R . As shell buckling is closer to column buckling than to plate buckling, the applied reduction is much stricter than it is for flat plates. In fact for most t/R -ratios the shell buckling curves (SBC) are even below the column buckling curves (CBC), cp. also Figure 3.2. Due to this fact no column-like buckling behaviour has to be checked for shell elements.

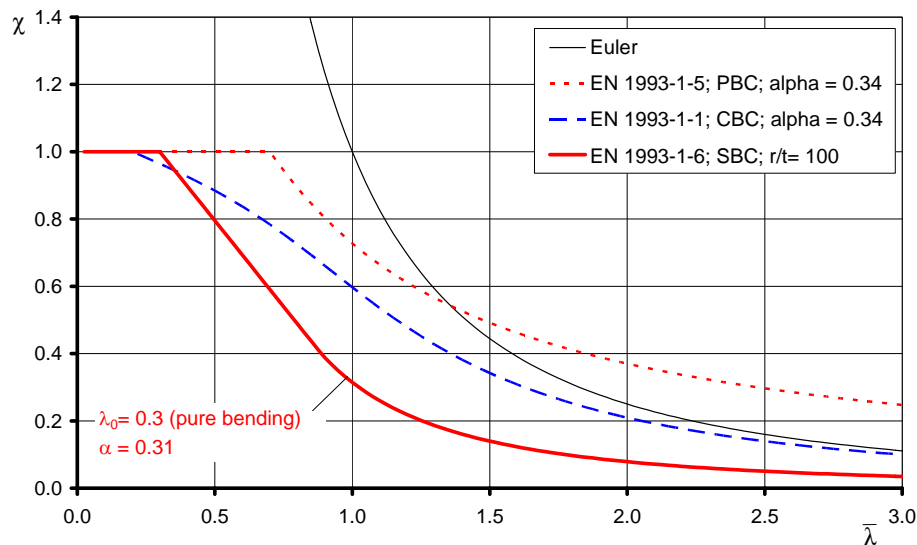


Figure 3.2: Comparison between different buckling curves (BC)

3.3 Design procedure for shell structures

To verify the buckling limit state, the following methods may be used according to EN 1993-1-6:

- Reduced Stress Method (described below), whereas the two main input parameters (buckling- and squash-load) may be determined by the use of:
 - a) a simplified hand-calculation based on analytically solutions (given in the Annex of EN 1993-1-6,
 - b) a global FEA in forms of a Materially Non-linear Analysis (MNA) and Linear-elastic Bifurcation Analysis (LBA).
- Design by global numerical Geometrically and Materially Non-linear Analysis which takes into account initial Imperfections (GMNIA)

Stress limitation approach is based on reduction of design resistance of membrane stress components in the tower shell. Meridional (longitudinal) σ_x , circumferential (tangential) σ_θ and in plane shear stresses $\tau_{x\theta}$, see Figure 3.3, have to be used in the design check.

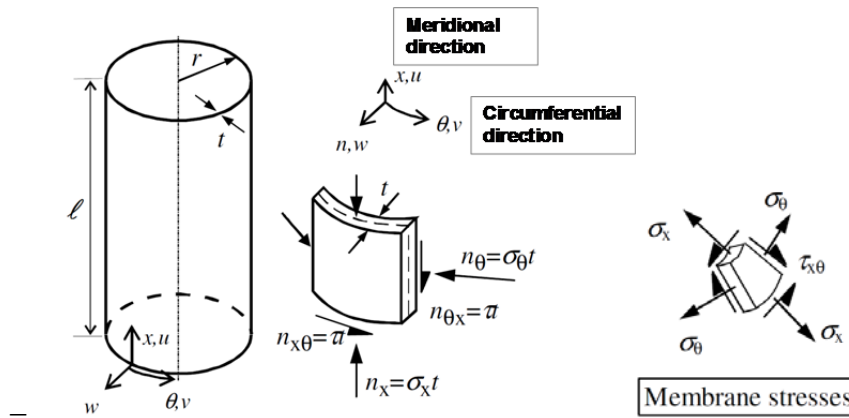


Figure 3.3: Stress directions in a cylindrical shell [42].

For the verification of the buckling strength of shells applying the stress design method the following equations have to be checked:

$$\begin{aligned}
 \sigma_{x,Ed} &\leq \sigma_{x,Rd} = \chi_x \cdot \frac{f_{yk}}{\gamma_M} \\
 \sigma_{\theta,Ed} &\leq \sigma_{\theta,Rd} = \chi_\theta \cdot \frac{f_{yk}}{\gamma_M} \\
 \tau_{x\theta,Ed} &\leq \tau_{x\theta,Rd} = \chi_t \cdot \frac{f_{yk}}{\sqrt{3} \times \gamma_M}
 \end{aligned} \tag{23}$$

The safety factor should be taken from relevant application standards or from EN 1993-1-1. However, the safety factor $\gamma_{M1} = 1.1$ is recommended for shell structures.

If more than one of the three above mentioned buckling-relevant membrane stresses are present, the following interaction check is recommended in EN 1993-1-6:

$$\left(\frac{\sigma_{x,Ed}}{\sigma_{x,Rd}}\right)^{k_x} + \left(\frac{\sigma_{\Theta,Ed}}{\sigma_{\Theta,Rd}}\right)^{k_{\Theta}} - k_i \left(\frac{\sigma_{x,Ed}}{\sigma_{x,Rd}}\right) \cdot \left(\frac{\sigma_{\Theta,Ed}}{\sigma_{\Theta,Rd}}\right) + \left(\frac{\tau_{x\Theta,Ed}}{\tau_{x\Theta,Rd}}\right)^{k_{\tau}} \leq 1 \quad (24)$$

The buckling interaction parameters k_x , k_1 , k_i and k_{Θ} are given in Annex D of EN 1993-1-6. However, in case of towers supporting wind energy converters contribution of the circumferential and shear stress component is often negligible.

The reduction factor χ is dependent on the shell slenderness $\bar{\lambda}$. According to EN 1993-1-6 they shall be determined as

$$\chi = 1 \quad \text{when} \quad \bar{\lambda} \leq \bar{\lambda}_0 \quad (25)$$

$$\chi = 1 - \beta \cdot \left(\frac{\bar{\lambda} - \bar{\lambda}_0}{\bar{\lambda}_p - \bar{\lambda}_0} \right)^{\eta} \quad \text{when} \quad \bar{\lambda}_0 < \bar{\lambda} < \bar{\lambda}_p \quad (26)$$

$$\chi = \left(\frac{\alpha}{\bar{\lambda}^2} \right) \quad \text{when} \quad \bar{\lambda}_p \leq \bar{\lambda} \quad (27)$$

Where:

α is elastic imperfection reduction factor,

β is plastic range factor,

η is interaction exponent,

$\bar{\lambda}_0$ is squash limit relative slenderness.

The above parameters may be obtained from Annex D of EN 1993-1-6 whereas the plastic limit relative slenderness should be calculated according to

$$\bar{\lambda}_p = \sqrt{\frac{\alpha}{1 - \beta}} \quad (28)$$

Influence of imperfections is introduced by meridional elastic imperfection reduction factor α_x which is dependent on fabrication tolerance quality class, see Equ. (29), Equ. (30) and Equ. (31).

$$\Delta w_k = \frac{1}{Q} \sqrt{\frac{r}{t}} \cdot t \quad (29)$$

$$\alpha_x = \frac{0,62}{1 + 1,91(\Delta w_k / t)^{1,44}} \quad (30)$$

$$\Delta w_k = \frac{1}{Q} \sqrt{\frac{r}{t}} \cdot t \quad (31)$$

Table 3.1: Fabrication tolerance quality class [42]

| Fabrication tolerance quality class | Description | Q |
|-------------------------------------|-------------|----|
| Class A | Excellent | 40 |
| Class B | High | 25 |
| Class C | Normal | 16 |

The relative slenderness for the different stress components to be considered should be obtained from Equ. (32).

$$\begin{aligned}\bar{\lambda}_x &= \sqrt{\frac{f_{yk}}{\sigma_{x,crit}}} \\ \bar{\lambda}_\theta &= \sqrt{\frac{f_{yk}}{\sigma_{\theta,crit}}} \\ \bar{\lambda}_r &= \sqrt{\frac{f_{yk}}{\sqrt{3}\tau_{x\theta,crit}}}\end{aligned}\quad (32)$$

In Annex D guidance is given for the calculation of the critical buckling stresses. The critical stress for meridional direction is determined according to Equ. (33).

$$\sigma_{x,Rcr} = 0,605EC_x \frac{t}{r} \quad (33)$$

The parameter C_x , see Equ. (34) depends on effect of boundary conditions and dimensionless length parameter ω , defined by Equ. (35)

$$C_x = 1,36 - \frac{1,83}{\omega} + \frac{2,07}{\omega^2} \quad \text{for short cylinders with: } \omega \leq 1,7$$

$$C_x = 1,0 \quad \text{for medium length cylinders with: } 1,7 \leq \omega \leq 0,5 \frac{r}{t} \quad (34)$$

$$C_x = C_{x,N} = 1 + \frac{0,2}{C_{xb}} \left[1 - 2\omega \frac{t}{r} \right] \geq 0,60 \quad \text{for long cylinders with: } \omega > 0,5 \frac{r}{t}$$

$$\omega = \frac{\ell}{r} \sqrt{\frac{r}{t}} = \frac{\ell}{\sqrt{rt}} \quad (35)$$

Boundary conditions and presence of stiffeners are important only in case of long cylinders, see Equ. (34). The case 3 from Figure 3.4, with flexible stiffeners, is recommended for long cylinders.

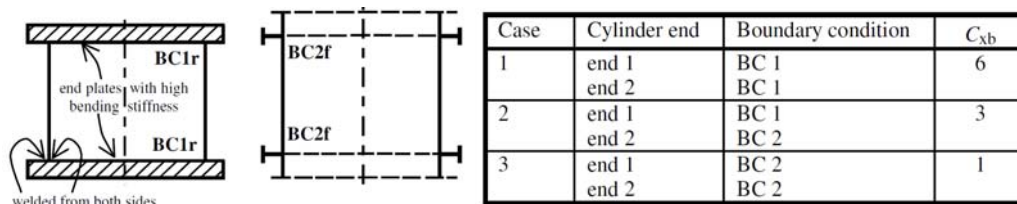


Figure 3.4: Influence of boundary condition on local shell buckling parameters [42]

Alternatively finite element methods may be used for the computation of the critical buckling stresses.

3.4 Flowchart

A design flowchart for calculation of reduced resistance to meridional stresses is shown in Figure 3.5. Firstly the relative slenderness λ is determined, influenced by the elastic critical stress which depends on boundary conditions and geometry. The reduction factor χ is then determined regarding by introducing equivalent geometrical imperfections.

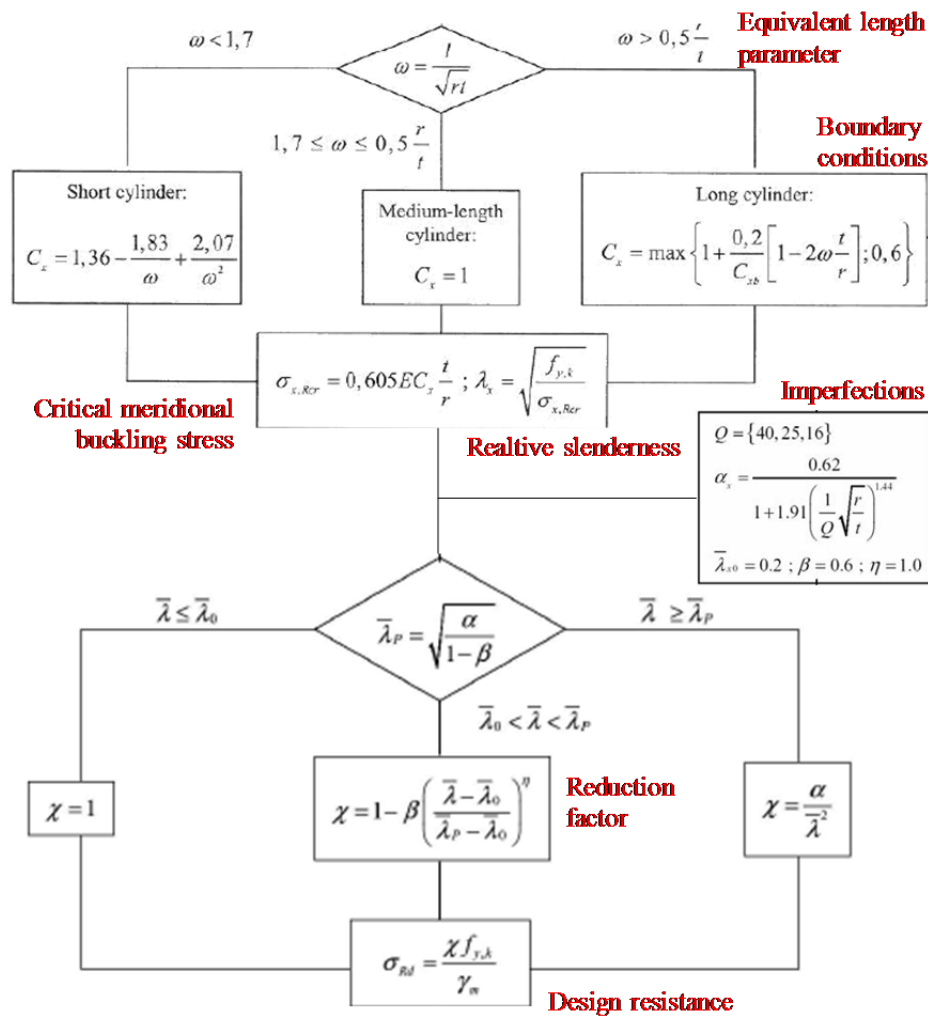


Figure 3.5: Flowchart for design check using buckling stress limitation

3.5 Numerical example

The example of shell buckling verification due to stresses in meridional direction is given for the middle conical segment of wind tower shown in Figure 1.1b. The segment consists of 11 sections with variable thicknesses and it is made of steel grade S355. Total length of the segment is $L = 26.62$ m. The design verification for the shell stability is given for the top section of the segment at 48.39 m height, with thickness $t = 16$ mm, lower shell diameter $D_1 = 3492$ mm, upper shell diameter $D_2 = 3448$ mm. Extreme values of design forces acting on the considered section of the tower are given in Table 2.8.

According to EN1993-1-6 §D2.2.2 [42], each cylindrical section j of equivalent length l_j , for buckling in the meridional direction should be treated as an equivalent cylinder of overall length $l = L$ with uniform L wall thickness $t = t_j$. Assuming that the boundary conditions at both ends of the cylinder are BC2, according to Figure 3.4, the dimensionless length ω and the parameter C_x parameter are therefore:

$$\omega = \frac{l}{\sqrt{rt}} = \frac{26620}{\sqrt{1746 \cdot 16}} = 159 > 0.5 \frac{r}{t} = 109 \rightarrow C_x = C_{x,N} \quad (36)$$

$$C_{x,b} = 1 \rightarrow C_{x,N} = \max\left(1 + \frac{0.2}{1} \left[1 - 2 \cdot 159 \frac{16}{1746}\right]; 0.6\right) = 0.617 \quad (37)$$

The characteristic imperfection amplitude Δw_k and the buckling parameter α_x , are calculated assuming the fabrication tolerance quality class B with $Q = 25$, see Table 3.1.

$$\Delta w_k = \frac{1}{Q} \sqrt{\frac{r}{t}} \cdot t = \frac{1}{25} \sqrt{\frac{1746}{16}} \cdot 16 = 6.68 \text{ mm} \quad (38)$$

$$\alpha_x = \frac{0.62}{1 + 1.91(\Delta w_k / t)^{1.44}} = \frac{0.62}{1 + 1.91(6.68/16)^{1.44}} = 0.40 \quad (39)$$

Other buckling parameters are adopted according to the design code recommendations:

$$\beta = 0.6$$

$$\eta = 1.0$$

$$\bar{\lambda}_{x0} = 0.2$$

The critical meridional buckling stress $\sigma_{x,Rcr}$ and the relative slenderness $\bar{\lambda}_x$ are therefore:

$$\sigma_{x,Rcr} = 0.605E \cdot C_x \frac{t}{r} = 0.605 \cdot 2.1 \cdot 10^5 \frac{16}{1746} = 1164 \text{ N/mm}^2 \quad (40)$$

$$\bar{\lambda}_x = \sqrt{\frac{f_y}{\sigma_{x,Rcr}}} = \sqrt{\frac{355}{1164}} = 0.55 \quad (41)$$

The plastic limit relative slenderness is obtained as:

$$\bar{\lambda}_p = \sqrt{\frac{\alpha_x}{1-\beta}} = \sqrt{\frac{0.40}{1-0.6}} = 1.0 \quad (42)$$

As the relative slenderness is within the limits $\bar{\lambda}_{x0} < \bar{\lambda}_x < \bar{\lambda}_p$, the reduction factor for buckling in meridional direction χ_x is obtained as:

$$\chi_x = 1 - \beta \cdot \left(\frac{\bar{\lambda}_x - \bar{\lambda}_{x0}}{\bar{\lambda}_p - \bar{\lambda}_{x0}} \right)^\eta = 1 - 0.6 \cdot \left(\frac{0.55 - 0.2}{1.0 - 0.2} \right)^{1.0} = 0.737 \quad (43)$$

The design value of meridional buckling resistances is obtained adopting the value of partial safety factor $\gamma_{M1} = 1.1$, according to EN1993-1-6 recommendation:

$$\sigma_{x,Rd} = \chi_x f_y / \gamma_{M1} = 0.737 \cdot 355 / 1.1 = 237 \text{ N/mm}^2 \quad (44)$$

The maximum design value of the resulting bending moment $M_{r,Ed} = 25,487 \text{ KNm}$ and the corresponding axial force $F_{z,Ed} = 1850 \text{ KN}$ are taken from the Table 2.8, and the design value of the meridional stress in the shell $\sigma_{x,Ed}$ is obtained using elastic cross section analysis.

$$W_{el} = \frac{(D^4 - (D - 2t)^4) \cdot \pi}{32 \cdot D} = 151.1 \cdot 10^6 \text{ mm}^3 \quad (45)$$

$$A = (D^2 - (D - 2t)^2) \cdot \pi / 4 = 174.7 \cdot 10^3 \text{ mm}^2$$

$$\sigma_{x,Ed} = \frac{M_{r,Ed}}{W_{el}} + \frac{F_{z,Ed}}{A} = \frac{25487 \cdot 10^6}{151.1 \cdot 10^6} + \frac{1850 \cdot 10^3}{174.7 \cdot 10^3} = 168.7 + 10.6 = 179 \text{ N/mm}^2 \quad (46)$$

Finally, the utilisation ratio below 1.0 is obtained, which means that the considered section is properly designed.

$$\frac{\sigma_{x,Ed}}{\sigma_{x,Rd}} = \frac{179}{237} = 0.75 < 1.0 \quad (47)$$

The calculation is not shown here, but the utilisation ratios of buckling due to circumferential and shear stresses are 0.001 and 0.08, respectively. Those values are practically negligible and therefore the interaction check is not needed.

4 FATIGUE

4.1 Introduction

The behaviour and structural design of support structures for multi-megawatt wind turbines, especially steel tubular towers and foundations is a main topic of the dissemination workshops developed within the project. This section is focused on fatigue analysis and design of tubular steel wind towers focusing on the connection between tower segments. It includes information concerning fatigue safety assessment in codes, especially in Eurocode 3 part 1-9 [17].

4.1.1 Stages of fatigue damage

Fatigue damage is associated to stresses or strains varying in time. The increase in the amplitude of variation of the stresses/strains will result in accelerated fatigue damage. When a structure is subjected to cyclic loading a fatigue crack nucleus can be initiated on a microscopically small scale followed by crack growing to a macroscopic size, and finally to failure in the last cycle of the fatigue life. In a structural element crack may initiate on the material surface (Figure 4.1) or in any spot where peak stresses appear, e.g. in the connection of the elements with other elements.

Different steel grades are expected to behave different when subjected to fatigue loading. Figure 4.2 shows the difference of grain in a micro scale observation and supports this conclusion. Nevertheless, Eurocode 3 [17] disregard differences in steel grades concerning fatigue resistance.

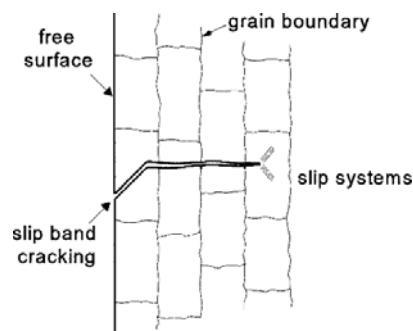


Figure 4.1: Crack initiation on material surface [20]

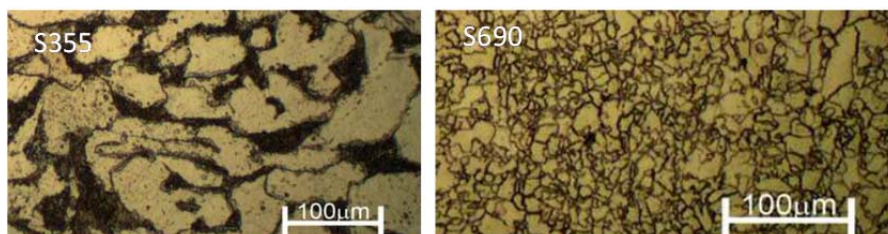


Figure 4.2: Microstructures of structural steels [21]

The fatigue life of structural components can be divided into two main phases, the crack initiation period and the crack growth period (Figure 4.3)

The life of un-notched components, for example, is dominated by crack initiation. In sharply notched parts or in parts containing crack-life defects, e. g. welded joints, the crack growth stage dominates and crack propagation data may be used in an assessment of fatigue life using fracture mechanics analysis. Therefore different test methods are necessary to assess the fatigue properties of these types of components.

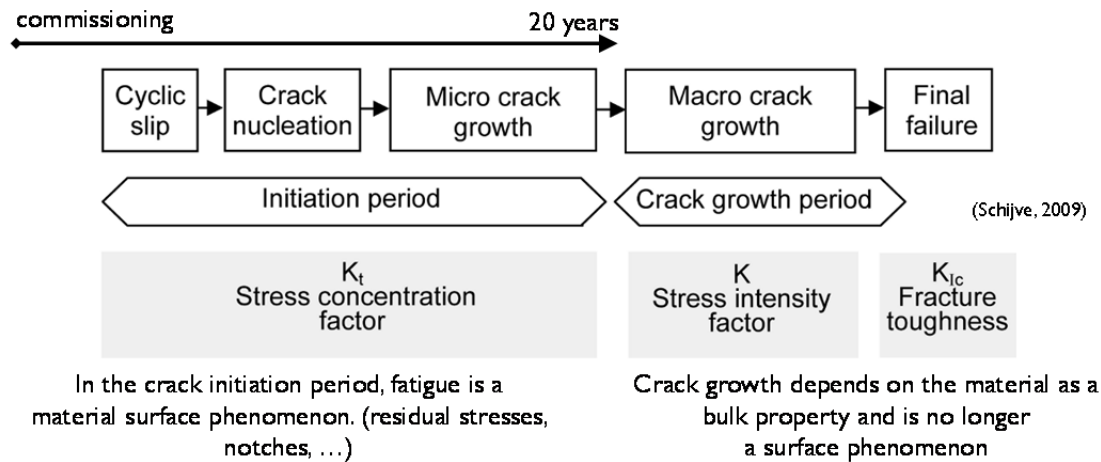


Figure 4.3: Different phases of fatigue life

4.1.2 Main factors influencing fatigue damage

The typical way to express fatigue damage for materials, mechanical components or structural details in high-cycle fatigue situations is to use $S-N$ curves, which relate the stress amplitude (or range) S with the number of cycles to failure N in a logarithmic scale.

The main parameters used to define $S-N$ curves are following:

- stress (strain) range $S = \sigma_{max} - \sigma_{min}$
- stress (strain) amplitude $A = \frac{\sigma_{max} - \sigma_{min}}{2}$
- stress (strain) ratio $R = \frac{\sigma_{min}}{\sigma_{max}}$
- stress (strain) mean value $\sigma_m = \frac{\sigma_{max} + \sigma_{min}}{2}$

These curves are proposed based on constant amplitude (or range) loading related to the fatigue life measured in number of cycles. Figure 4.4 shows typical $S-N$ curve (also called Wöhler curve or Fatigue Spectrum).

Some $S-N$ curves may exhibit a clear horizontal plateau for high fatigue lives (endurance limit), representing a fatigue limit. However, some $S-N$ curves may show a continuous reduction of fatigue strength for high fatigue lives, representing the case of a material/component not exhibiting a fatigue limit. The latter case corresponds to aluminium alloys and some high strength steels.

Fatigue life (i. e. number of load cycles up to fatigue failure) depends mainly on stress range (twice the stress amplitude) and stress concentration including residual stresses, which are of paramount importance for fatigue and are taken into account by defining representative 'details' that can be found in the structure. Also, some other important factors may influence the fatigue life, such as (Figure 4.5):

- type of material (ferrous and titanium alloys vs other materials)
- static strength of material
- stress mean value – in general, a tensile mean stress reduces fatigue life while a compressive mean stress increases life
- other effects such as size, surface finish, corrosion

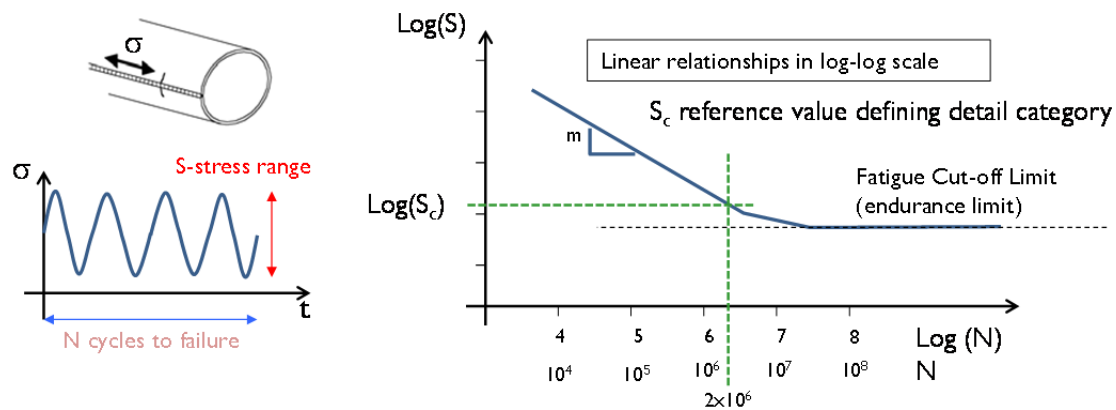


Figure 4.4: Relationship between constant stress amplitude and number of cycles to failure

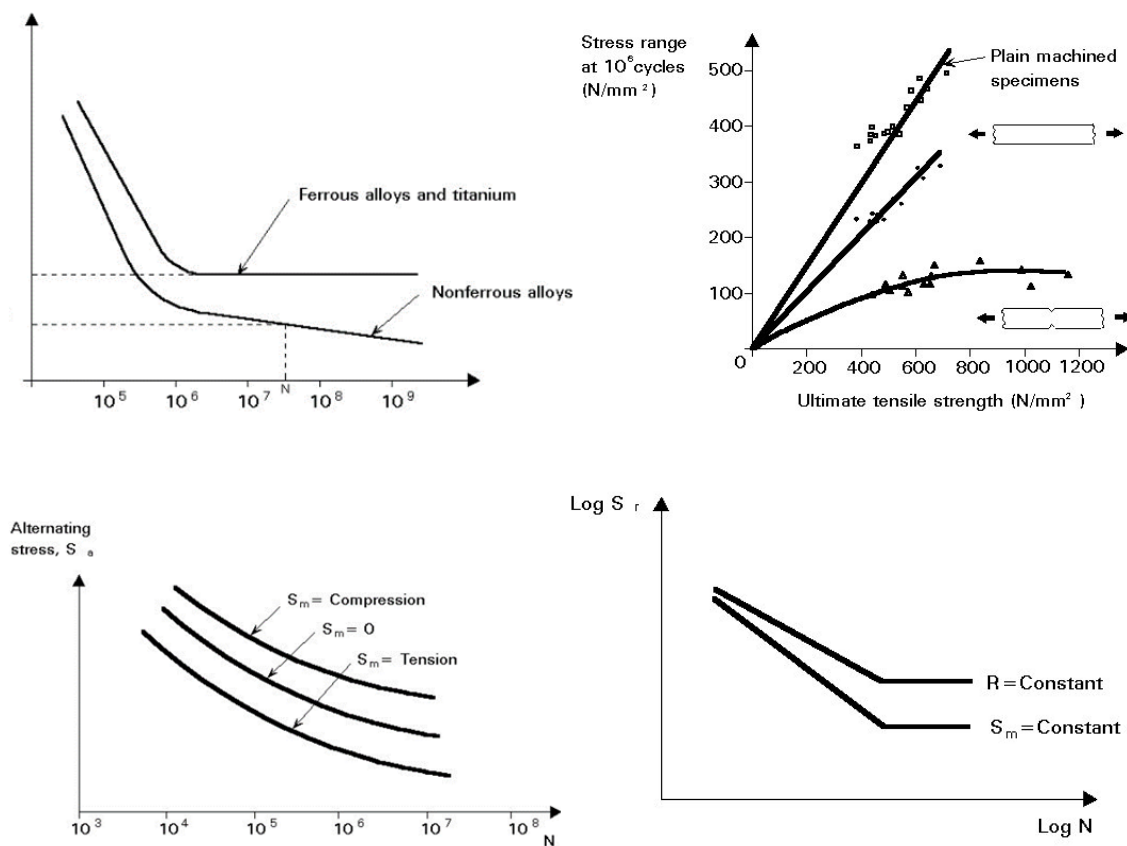


Figure 4.5: Effects modifying basic S-N data

4.2 Fatigue Safety Assessment in codes

4.2.1 Basis of structural design

The concepts of structural safety for Wind Turbines supporting structures are established in EN1990 [12] and in IEC 61400 [8]. The concept is based on the requirement of a certain level of reliability index, which in practice is obtained by imposing the use of two separate types of safety factors, the first multiplying the load effects and the second dividing the correspondent structural resistances. To achieve the targeted probability of failure or reliability level, the concept allows the use of the same safety factor for loads independent of the structural materials (strengths) used in the construction. The values to be used in the safety check depend on the target reliability defined mainly through the Limit State against which the structure has to be secured. Usually limit states are of 'Ultimate' type (e.g. cross-sectional resistance, member stability, fatigue, excessive deformation), of 'Serviceability' type (e.g. deformations, vibrations, cracks in concrete) or of 'Damage' type (e.g. damage in non-structural elements during earthquake).

The standard IEC61400-1 [8] also prescribes a Limit State approach for structural safety check in accordance with EN1990 [12]. Partial safety factors are defined and account for the uncertainties and variability in loads, the uncertainties in the analysis methods and the importance of structural components with respect to the consequences of failure. Nevertheless, different terminology is used in IEC61400-1 [8] to define limit states related to resistance and stability of members or cross-sections (U is used) and limit state related to fatigue (F is used).

To define the partial safety factor for loads in IEC61400-1 [8] a consequence of failure factor is defined according to the component classes. This consequence of failure factor, γ_n , is introduced to distinguish between:

- Component class 1: used for "fail-safe" structural components whose failure does not result in the failure of a major part of a wind turbine, for example replaceable bearings with monitoring.
- Component class 2: used for "non fail-safe" structural components whose failures may lead to the failure of a major part of a wind turbine.
- Component class 3: used for "non fail-safe" mechanical components that link actuators and brakes to main structural components for the purpose of implementing non-redundant wind turbine protection functions

For the ultimate limit state analysis (U), the following four types of analysis shall be performed where relevant:

1. ultimate strength;
2. stability analysis (buckling, etc.);
3. critical deflection analysis (mechanical interference between blade and tower).

Each type of analysis requires a different formulation of the limit state function and deals with different sources of uncertainties through the use of safety factors defined in section 2 of this document.

To assess fatigue damage appropriate fatigue calculation methodology is required. The standard allows the use of Miner's rule for the accumulation of damage. The limit state is reached when the accumulated damage index equals unity.

In general, fatigue damage calculations shall consider the formulation, including effects of both cyclic range and mean strain (or stress) levels. When details suffer major influence of residual stresses, such as in presence of welding in steel structure be performed on the basis of only the cyclic range, that is, on the basis of S-N curve defined for the fatigue detail under investigation.

The partial safety factors defined in standard IEC61400-1 [8] in case of fatigue verifications are the following:

- partial safety factor for loads, $\gamma_{Ff}=1.0$ for all design situations
- partial safety factor for resistances
 - damage tolerant method $\gamma_{mf}>0.90$
 - safe life method: $\gamma_{mf}=1.10$ (supporting structures for wind turbines are considered Component Class 2, i.e. failure leads to the failure of a major part of the wind turbine)

4.2.2 Eurocode 3 part 1-9

The relevant standard for steel structures design in Europe is the Eurocode 3, which includes the part 1-9 [17] dedicated to fatigue resistance calculations. In this standard two types of safety assessment are allowed, which are in agreement with the disposals found in IEC61400-1 [8]:

- damage tolerant method: should provide an acceptable reliability that a structure will perform satisfactorily for its design life, provided that a prescribed inspection and maintenance regime for detecting and correcting fatigue damage is implemented throughout the design life of the structure;
- safe life method: should provide an acceptable level of reliability that a structure will perform satisfactorily for its design life without the need for regular in-service inspection for fatigue damage. An acceptable reliability level may be achieved by adjustment of the partial factor for fatigue strength γ_{Mf} taking into account the consequences of failure and the design assessment used.

The required reliability can be achieved as follows:

- damage tolerant method (possible lower safety factors)
 - selecting details, materials and stress levels so that in the event of the formation of cracks a low rate of crack propagation and a long critical crack length would result,
 - provision of multiple load path
 - provision of crack-arresting details,
 - provision of readily inspectable details during regular inspections.
- safe-life method
 - selecting details and stress levels resulting in a fatigue life sufficient to achieve the β values equal to those for ultimate limit state verifications at the end of the design service life.

The design of wind turbine towers follows the 'safe life method' and, in the case of steel the fatigue strength is represented by "Wöhler" or "S-N" curves given in Eurocode 3 part 1-9 [17]. An overview of such curves is given in Figure 4.6.

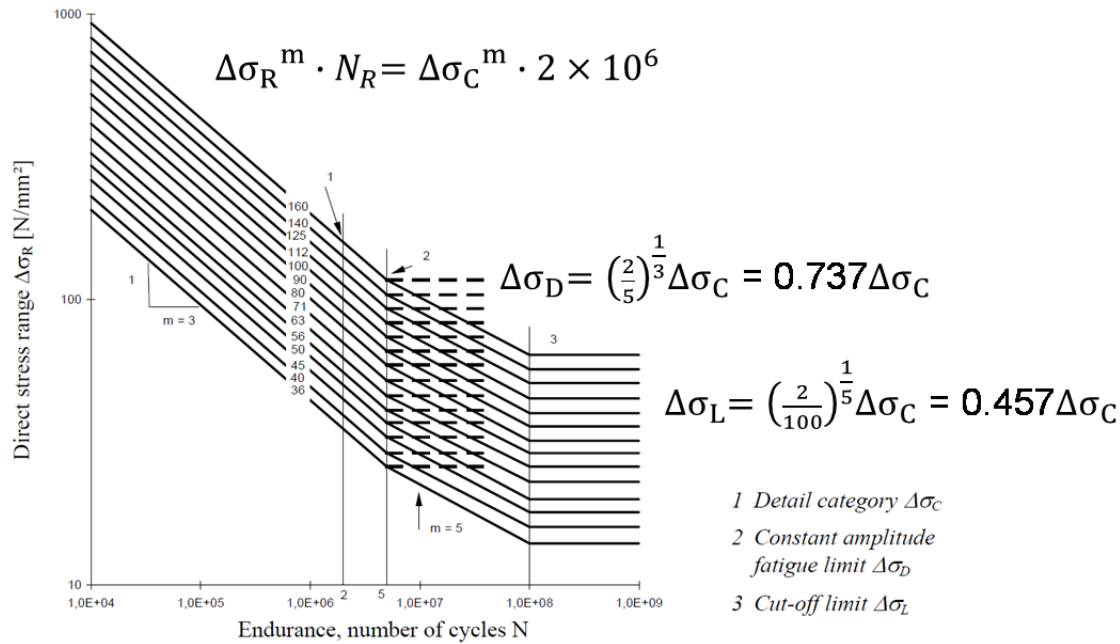


Figure 4.6: The fatigue strength for nominal stress ranges represented by a series of $\log\Delta\sigma_R$ vs $\log N$ curves given in EC3 part 1-9 [17]

| Detail category | Constructional detail | Description | Requirements |
|-----------------|---|--|--|
| 160 | <p>NOTE The fatigue strength curve associated with category 160 is the highest. No detail can reach a better fatigue strength at any number of cycles.</p> | <p><u>Rolled and extruded products:</u></p> <p>1) Plates and flats; 2) Rolled sections; 3) Seamless hollow sections, either rectangular or circular.</p> | <p><u>Details 1) to 3):</u></p> <p>Sharp edges, surface and rolling flaws to be improved by grinding until removed and smooth transition achieved.</p> |
| 71 | | <p><u>Transverse butt welds:</u></p> <p>3) Butt-welded end-to-end connections between circular structural hollow sections. 4) Butt-welded end-to-end connections between rectangular structural hollow sections.</p> | <p><u>Details 3) and 4):</u></p> <p>-Weld convexity $\leq 10\%$ of weld width, with smooth transitions. -Welded in flat position, inspected and found free from defects outside the tolerances EN 1090. -Classify 2 detail categories higher if $t > 8$ mm.</p> |
| 56 | | <p>11) Tube socket joint with 80% full penetration butt welds.</p> | <p>11) Weld toe ground. $\Delta\sigma$ computed in tube.</p> |
| 71 | | <p>12) Tube socket joint with fillet welds.</p> | <p>12) $\Delta\sigma$ computed in tube.</p> |
| 40 | | | |

Figure 4.7: Fatigue details given in EC3 part 1-9 [17] that can be found in tubular wind towers

If the stress amplitudes are below the *fatigue strength* of the material, then the number of load cycles no longer plays a role. If the stress amplitudes are higher, only a certain number of load fluctuations can be sustained. Different curves in Figure 4.6 correspond to different details depending on the structure and manufacturing process. Figure 4.7 shows some details that can be found in tubular wind towers with flange connections.

Figure 4.8 shows S-N curves obtained from measurements performed in a wind tower, from design curve given by the manufacturer and from the fatigue detail 71 defined in EC3 [17]. The measured stress corresponds to vertical stress component in the shell obtained from strain measurements near the bottom cross section of the tower.

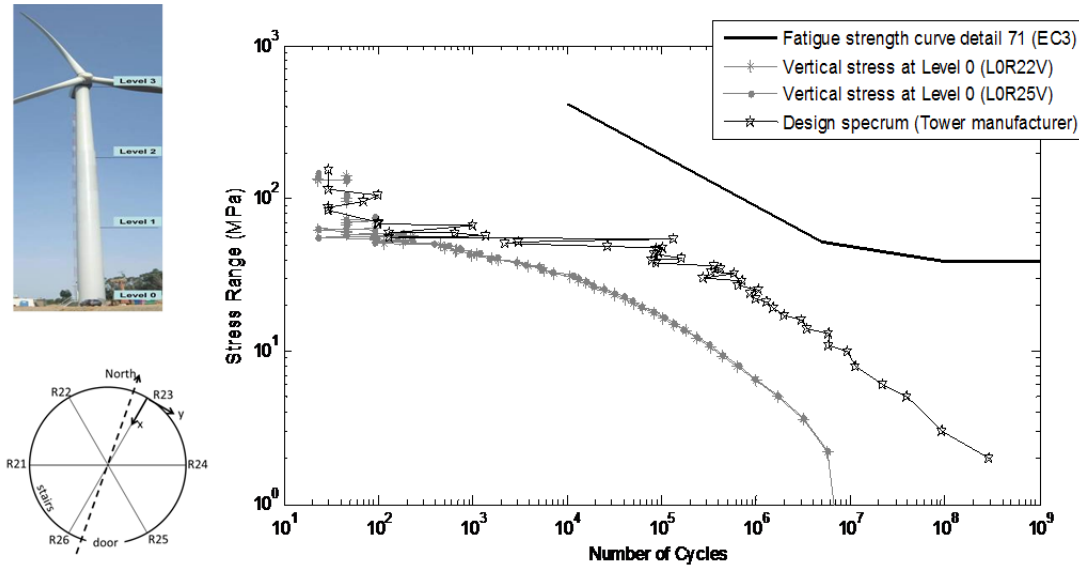


Figure 4.8: Comparison of S-N curves obtained from measurements in a wind tower, from design curve given by the manufacturer and from the fatigue detail 71 defined in EC3 [17]

4.2.3 Fatigue verification formats

The fatigue assessment should be based on damage accumulation based on linear cumulative damage calculation, using e.g. the Palmgren-Miner rule, or on equivalent stress range. The first approach needs the full fatigue spectra of the load (effect) and of the resistance. The second approach is simpler and only needs the comparison of the load (effect) range with the respective resistance range for a reference number of cycles.

The fatigue assessment based on the Palmgren-Miner rule is performed using a linear cumulative damage calculation that generates the damage index D_d as follows:

$$D_d = \sum_i \frac{n_i}{N_i} \leq 1.0 \quad (48)$$

This Miner's summation uses the number of cycles n_i from the load (effect) fatigue spectrum and the number of cycles N_i from the design fatigue resistance spectrum (see Figure 4.9). The applied load (effect) ranges $\Delta\sigma_i$ should be multiplied by the safety factor for loads γ_{FF} and the fatigue strength values $\Delta\sigma_c$ should be divided by the safety factor for materials γ_{mf} in order to obtain the corresponding number of cycles n_i or N_i for each band in the spectrum.

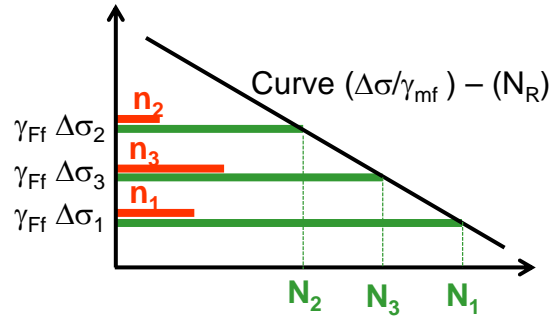


Figure 4.9: Scheme of the parameters n_i and N_i in the damage index formula $D_i = n_i / N_i$

The second approach for fatigue safety check is based on the concept of equivalent constant amplitude load (effect) range (Damage Equivalent Load, DEL), which is the constant-amplitude range that would result in the same fatigue life as for the design spectrum, when the comparison is based on a Miner's summation. To define DEL a reference number of cycles N_{ref} must be defined. According to Eurocode 3 part 1-9 [17] the design value of DEL to be used for the fatigue assessment should be the stress ranges $\gamma_{Ff} \Delta\sigma_{E,2}$ corresponding to $N_C = 2 \times 10^6$ cycles.

In non-welded details or stress-relieved welded details, the mean stress influence on the fatigue strength may be taken into account by determining a reduced effective stress range $\Delta\sigma_{E,2}$ in the fatigue assessment when part or all of the stress cycle is compressive as schematically presented in Figure 4.10.

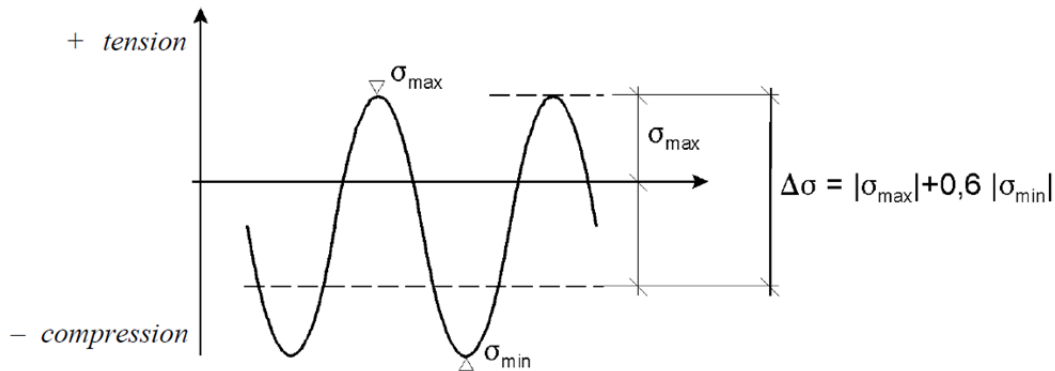


Figure 4.10: Mean stress influence on the fatigue strength in non-welded details or stress-relieved welded details

The fatigue safety check is based on the constant amplitude DEL range ($\Delta\sigma_{E,ref}$) associated with a reference number of cycles (N_{ref}) as follows:

$$\Delta\sigma_{E,ref} \leq \Delta\sigma_c \quad (49)$$

When the fatigue load (effect) spectrum ($\Delta\sigma_i - n_i$) is available, the constant amplitude DEL range ($\Delta\sigma_{E,ref}$) associated with a reference number of cycles (N_{ref}) and a certain slope m of the resistance curve S-N can be obtained using following calculations:

$$\left(\frac{\Delta\sigma_i}{\Delta\sigma_{E,ref}} \right)^m = \frac{N_{ref}}{N_i} \quad (50)$$

$$D_d = \sum_i \frac{n_i}{N_i} = \sum_i \frac{n_i \Delta\sigma_i^m}{N_{ref} \Delta\sigma_{E,ref}^m} \quad (51)$$

when considering $D_d=1.0$ the constant amplitude DEL range is obtained as follows (see Figure 4.11):

$$\Delta\sigma_{E,ref} = \left(\sum_i \frac{n_i \Delta\sigma_i^m}{N_{ref}} \right)^{\frac{1}{m}} \quad (52)$$

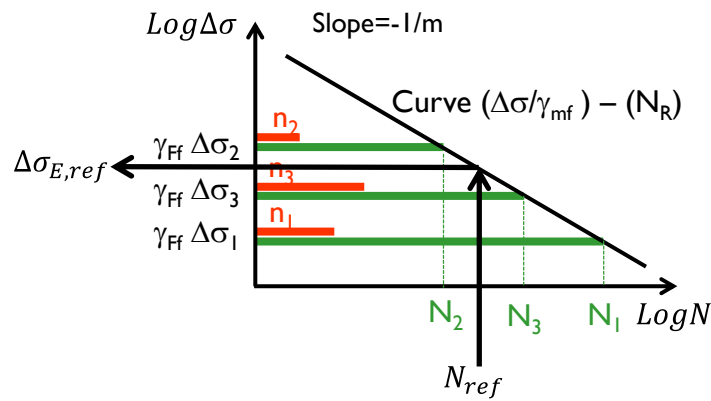


Figure 4.11: Scheme for the calculation of DEL associated to a certain N_{ref} and slope m

Eurocode 3 part 1-9 [17] defines the reference number of cycles $N_{ref} = 2 \times 10^6$ corresponding to the Damage Equivalent Load (DEL) $\Delta\sigma_{E,2}$. If a different N_{ref} is defined for the DEL $\Delta\sigma_{E,ref}$ following conversion can be performed:

$$\Delta\sigma_{E,2} = \left(\frac{N_{ref}}{2 \times 10^6} \right)^{\frac{1}{m}} \Delta\sigma_{E,ref} \quad (53)$$

4.2.4 Example: Tubular steel tower

The fatigue spectrum represented in Figure 4.12 describes the relation between ΔM_y and the number of cycles in a circular hollow cross section of a wind tower with geometrical characteristics given in Table 4.1.

Table 4.1: Geometry and properties of the section

| Diameter (m) | Thickness (m) | Area (m ²) | Moment of Inertia (m ⁴) |
|--------------|---------------|------------------------|-------------------------------------|
| 4.30 | 0.030 | 0.4053 | 0.937 |

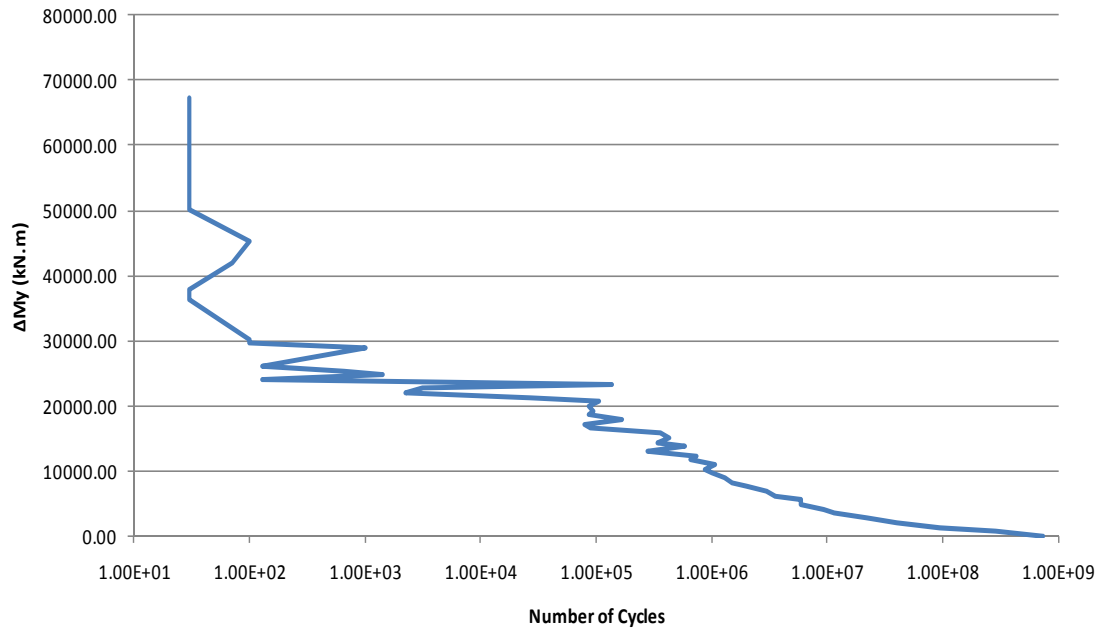


Figure 4.12: Fatigue spectrum corresponding to the bending moment M_y in a circular hollow cross section

According to the presented spectrum, stress variations can be obtained as follows:

$$\Delta\sigma = \frac{M_y d}{2I} \quad (54)$$

The fatigue assessment based on the Palmgren-Miner rule is performed using a linear cumulative damage calculation that generates the damage index D_d as follows:

$$D_d = \sum_i \frac{n_i}{N_i} \leq 1.0 \quad (55)$$

The values n_i are provided according to the given spectrum for each value of $\gamma_{Ff} \Delta\sigma_i$ and the value N_i , which represents the ‘resistant’ number of cycles is obtained with the EC3-1-9 (chapter 7) approach from the factored $\Delta\sigma/\gamma_{Mf} - N_R$ curve of stress range of $\gamma_{Ff} \Delta\sigma_i$. According to IEC 61400 guideline [8], $\gamma_{Ff} = 1.00$ and $\gamma_{Mf} = 1.10$. The number of cycles $N_{ref} = 2 \times 10^6$ is obtained from EC3-1-9 [17], which is also used to choose the curve representing the fatigue detail. Since the tubular tower is manufactured from rolled steel plates using full penetration but welding the representative fatigue detail will be the Detail 71 (Figure 4.13) and therefore

the curve $\Delta\sigma_c=71\text{MPa}$ shall be chosen in Figure 4.14 to compute the damage index. Figure 4.15 represents graphically the procedure to compute the damage index.









| Detail category | Constructional detail | Description | Requirements |
|-----------------|---|---|---|
| 160 |    | <u>Rolled and extruded products:</u> 1) Plates and flats; 2) Rolled sections; 3) Seamless hollow sections, either rectangular or circular. | <u>Details 1) to 3):</u> Sharp edges, surface and rolling flaws to be improved by grinding until removed and smooth transition achieved. |
| 140 |  | 11) Automatic longitudinal seam weld without stop/start positions in hollow sections | 11) Free from defects outside the tolerances of EN 1090. Wall thickness $t \leq 12,5 \text{ mm}$. |
| 125 |  | 11) Automatic longitudinal seam weld without stop/start positions in hollow sections | 11) Wall thickness $t > 12,5 \text{ mm}$. |
| 90 |  | 11) with stop/start positions | |
| 70 |  | <u>Transverse butt welds:</u> 3) Butt-welded end-to-end connections between circular structural hollow sections. | <u>Details 3) and 4):</u> -Weld convexity $\leq 10\%$ of weld width, with smooth transitions. -Welded in flat position, inspected and found free from defects outside the tolerances EN 1090. -Classify 2 detail categories higher if $t > 8 \text{ mm}$. |
| 56 |  | 4) Butt-welded end-to-end connections between rectangular structural hollow sections. | |

Figure 4.13: Representative fatigue details obtained from EC3 part 1-9 [17]

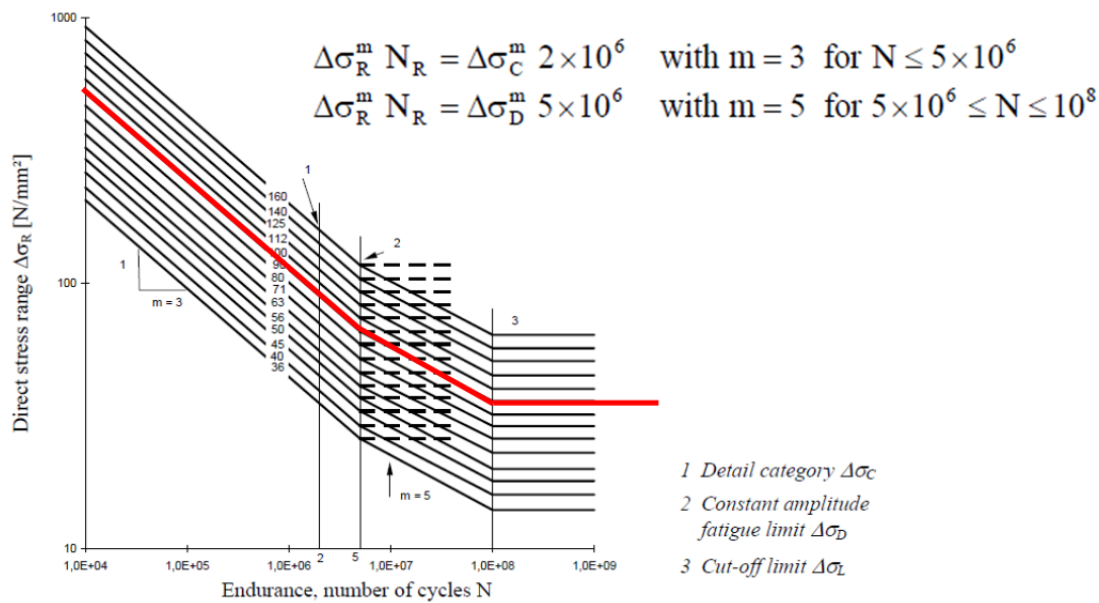


Figure 4.14: S-N curves for different details in steel structures defined in EC3 part 1-9 [17]

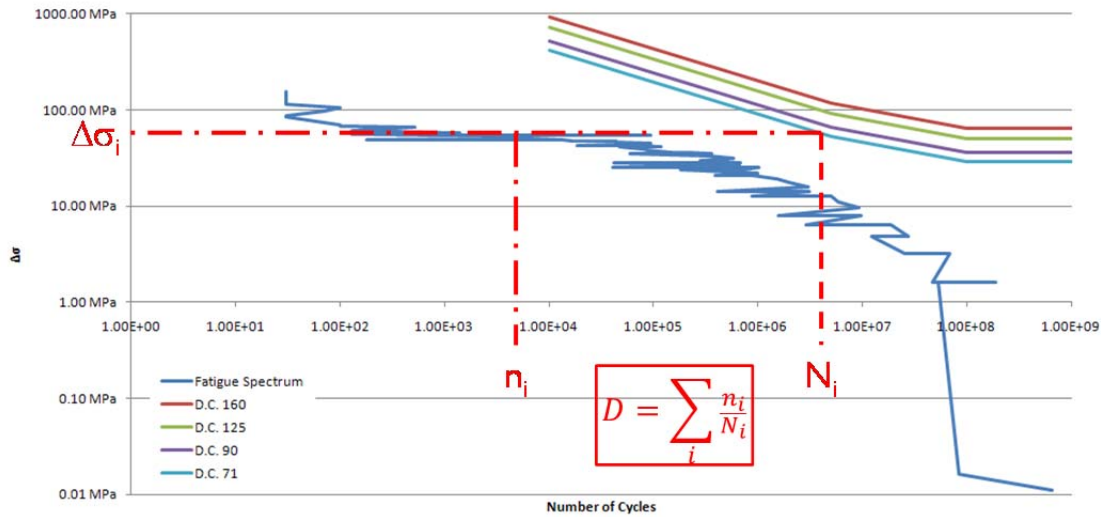


Figure 4.15: Scheme to compute the damage index

The damage equivalent load procedure can be used in alternative to previous procedure. In that case the damage equivalent stress can be computed from the fatigue spectrum given in Figure 4.12 and considering the different values of m defined in Figure 4.14. To compute the DEL $\Delta\sigma_{E,2}$ for $N_{ref}=2 \times 10^6$ following equation is used:

$$DEL = \Delta\sigma_{E,2} = \left(\sum_i \frac{n_i \Delta\sigma_i^m}{2 \times 10^6} \right)^{\frac{1}{m}} \quad (56)$$

Fatigue check corresponds to the evaluation of following expression:

$$\gamma_{Ff} \Delta\sigma_{E,2} \leq \sqrt[m]{D_d} \frac{\Delta\sigma_c}{\gamma_{Mf}} \quad (57)$$

where $D_d = 1.0$ is the admissible damage of the structure and $\Delta\sigma_c = 71 \text{ MPa}$ is the considered detail category. Since m varies between 3 and 5 for different number of cycles the value $m=4$ can be used in this equation. Furthermore $\gamma_{Ff} = 1.00$ and $\gamma_{Mf} = 1.10$.

Connection 2: $\sigma_{ult,Ed} = 171 \text{ N/mm}^2$

4.2.5 Fatigue design loads for connections

Similar to the static loads, the fatigue loads are provided in the form of load tables with Damage Equivalent Loads (DEL) for different tower sections. The DELs are given for each load component, whereas a common practice is the use of a single Wöhler slope of $m = 4$. The DEL for the two flange sections can thus be simplified as given in Table 4.2.

Table 4.2: Damage Equivalent Loads at the flange sections ($m = 4$ and $N_{ref} = 2 \cdot 10^8$).

| | Height | ΔF_x | ΔF_y | ΔF_z | ΔM_x | ΔM_y | ΔM_z |
|----------------|--------|--------------|--------------|--------------|--------------|--------------|--------------|
| | mm | kN | kN | kN | kN.m | kN.m | kN.m |
| Flange1 | 21770 | 96 | 67 | 29 | 3342 | 4243 | 1229 |

| | | | | | | | |
|----------------|-------|----|----|----|------|------|------|
| Flange2 | 48390 | 81 | 61 | 29 | 1707 | 2359 | 1229 |
|----------------|-------|----|----|----|------|------|------|

In general, consideration of the rotor thrust (Fx), tilting moment (My) and torsional moment (Mz) is sufficient. Tilting and torsional moment can be considered as orthogonal, so that the damages from tensile stresses (from My and Fx) can be derived separately from those from shear stresses (from Mz). As they usually are much smaller, the damages from shear stresses will be neglected. This leads to

$$\text{Connection 1: } \sigma_{z,DEL} = 22.4 \text{ N/mm}^2$$

$$\text{Connection 2: } \sigma_{z,DEL} = 21.4 \text{ N/mm}^2$$

This DEL method is only applicable as long as a linear relation between load-actions and member stresses exists. For fatigue design of bolts in flange connections an extremely non-linear relation has to be taken into account, which means that the complete Rainflow matrix has to be considered for the fatigue design. As no complete Rainflow matrices are available for the given design example, Rainflow matrices for damages caused by one cycle per load variation range ΔZ are determined in the following.

4.2.5.1 Fatigue design for flange connection

For ring-flange connections, with common wind-tower dimensions, the required stiffnesses C_S and C_D can be approximated by (see also Seidel):

- Bolt stiffness C_S :

$$C_S = \frac{1}{\int_0^{\ell_s} \frac{1}{E_S A_S(x)} dx} \approx \frac{E_{bolt} \cdot A_{nom}}{2 \cdot t_{fl}}$$

$$\text{Flange 1: } C_{S,1} \approx \frac{210000 \cdot 1385}{2 \cdot 90} = 1615833 \text{ N/mm}$$

$$\text{Flange 2: } C_{S,2} \approx \frac{210000 \cdot 1018}{2 \cdot 75} = 1425200 \text{ N/mm}$$

- Clamp solid stiffness C_D :

$$C_D = \frac{1}{2 \cdot \int_0^{t_F} \frac{1}{E_D A_D(x)} dx} \approx \frac{E_{fl} \cdot \pi}{4 \cdot 2 \cdot t_{fl}} \cdot \left[\left(d_{washer} + \frac{2 \cdot t_{fl}}{10} \right)^2 - d_0^2 \right]$$

$$\text{Flange 1: } C_{D,1} \approx \frac{210000 \cdot \pi}{4 \cdot 2 \cdot 90} \cdot \left[\left(78 + \frac{2 \cdot 90}{10} \right)^2 - 45^2 \right] = 6589098 \text{ N/mm}$$

$$\text{Flange 2: } C_{D,2} \approx \frac{210000 \cdot \pi}{4 \cdot 2 \cdot 75} \cdot \left[\left(66 + \frac{2 \cdot 75}{10} \right)^2 - 39^2 \right] = 5541769 \text{ N/mm}$$

For the given calculation example the method acc. to Schmidt/Neuper has been chosen, as it is the one most commonly used. All required curve parameters of this tri-linear model are summarized in Table 4.3.

Table 4.3: Curve parameters of tri-linear Schmidt/Neuper bolt-load function model

| Curve parameter | Flange 1 | Flange 2 |
|--|----------|----------|
| $p = \frac{C_S}{C_S + C_D}$ | 0.197 | 0.205 |
| $q = \frac{C_D}{C_S + C_D}$ | 0.803 | 0.795 |
| $\lambda^* = \frac{0.7 \cdot a + b}{0.7 \cdot a}$ | 2.176 | 2.331 |
| $Z_I = \frac{a - 0.5 \cdot b}{a + b} \cdot F_{p,C}$ | 229.1 kN | 141.0 kN |
| $Z_{II} = \frac{1}{\lambda^* \cdot q} \cdot F_{p,C}$ | 406.3 kN | 275.1 kN |

The final bolt-load is than given by

$$Z \leq Z_I \quad \rightarrow \quad F_{t,I} = F_{p,C} + p \cdot Z$$

$$Z_I < Z \leq Z_{II} \quad \rightarrow \quad F_{t,II} = F_{p,C} + p \cdot Z_I + \left[\lambda^* \cdot Z_{II} - (F_{p,C} + p \cdot Z_I) \right] \cdot \frac{Z - Z_I}{Z_{II} - Z_I}$$

$$Z > Z_{II} \quad \rightarrow \quad F_{t,III} = \lambda^* \cdot Z$$

A re-adjustment of the pre-load $F_{p,C}$ of all bolts within 6-month is assumed, thus 90% of the nominal pre-load can be taken into account acc. to DIBt-Guideline. Figure 4.16 shows the resulting bolt-load functions for flange connection 1 and 2.

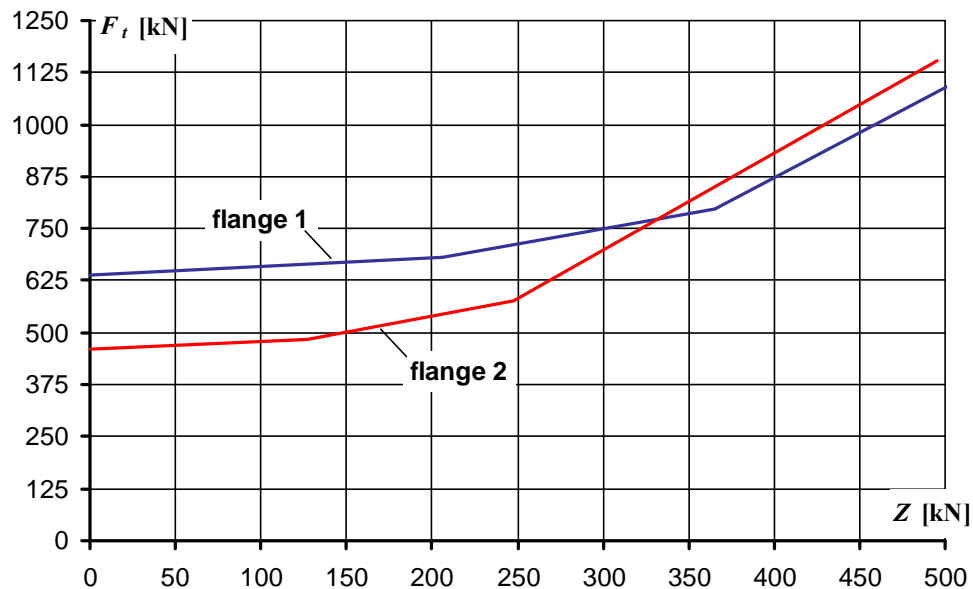


Figure 4.16: Bolt load functions of connection 1 & 2 acc. to Schmidt/Neuper

For the exemplary determination of Rainflow matrices only loads will be considered, which produce stresses up to ~80% of the bolts yield strength, i.e. $Z_{max} = 350$ kN for flange 1 and $Z_{max} = 250$ kN for flange 2. It is assumed that the probability of occurrence of higher loads is too small to be considered in fatigue calculations. The results are presented in Table 4.4.

Table 4.4: Relationship between load Z_{Ed} in the shell segment and resulting bolts force $F_{t,Ed}$ in load steps of 50 kN

| | Flange 1 | Flange 2 |
|----------|------------|------------|
| Z [kN] | $F_{t,Ed}$ | $F_{t,Ed}$ |
| 0 | 639.0 | 459.0 |
| 50 | 648.8 | 469.2 |
| 100 | 658.7 | 479.5 |
| 150 | 668.5 | 502.6 |
| 200 | 678.4 | 540.7 |
| 250 | 711.5 | 582.7 |
| 300 | 747.9 | 699.3 |
| 350 | 784.3 | 815.8 |

With the tensile stress area A_s of the used bolts, matrices can be determined, which summarize the bolt stress variation ranges $\Delta\sigma_N$ in function of the shell stress variation $\Delta Z = Z_{max} - Z_{min}$. Table 4.5 and Table 4.6 show the resulting matrices for flange 1 and 2.

Table 4.5: Resulting axial stress variation ranges $\Delta\sigma_N$ in bolts in function of load ranges $Z_{max} - Z_{min}$ in Flange 1

| $\Delta\sigma_N$ [N/mm ²] | from Z_{min} [kN] | | | | | | | |
|---------------------------------------|---------------------|-------|-------|-------|------|------|------|-----|
| to Z_{max} [kN] | 0 | 50 | 100 | 150 | 200 | 250 | 300 | 350 |
| 0 | | | | | | | | |
| 50 | 8.8 | | | | | | | |
| 100 | 17.6 | 8.8 | | | | | | |
| 150 | 26.4 | 17.6 | 8.8 | | | | | |
| 200 | 35.1 | 26.4 | 17.6 | 8.8 | | | | |
| 250 | 64.7 | 55.9 | 47.1 | 38.3 | 29.5 | | | |
| 300 | 97.1 | 88.4 | 79.6 | 70.8 | 62.0 | 32.5 | | |
| 350 | 129.6 | 120.8 | 112.0 | 103.3 | 94.5 | 64.9 | 32.5 | |

Table 4.6: Resulting axial stress variation ranges $\Delta\sigma_N$ in bolts in function of load ranges $Z_{max} - Z_{min}$ in Flange 2

| $\Delta\sigma_N$ [N/mm ²] | from Z_{min} [kN] | | | | | |
|---------------------------------------|---------------------|-------|-------|------|------|-----|
| to Z_{max} [kN] | 0 | 50 | 100 | 150 | 200 | 250 |
| 0 | | | | | | |
| 50 | 12.5 | | | | | |
| 100 | 25.0 | 12.5 | | | | |
| 150 | 53.3 | 40.8 | 28.3 | | | |
| 200 | 100.0 | 87.5 | 75.0 | 46.7 | | |
| 250 | 151.4 | 138.9 | 126.4 | 98.1 | 51.4 | |

As the method used to determine the bolt force functions does not consider bending stresses, the Wöhler curve for bolts in tension given in EN1993-1-9 has to be reduced to detail category 36* (cp. []). In addition the reduction factor

$$k_s = (30/d)^{0.25}$$

is used as all bolts have nominal diameters d larger than 30 mm. Following the recommendations from DIBt- and GL-Guideline, no endurance limit is considered. The resulting properties of the Wöhler curves for the bolts are shown in Table 4.7.

Table 4.7: Properties of the considered Wöhler curves 36*, cp.

| | Bolt | k_s | $\Delta\sigma_C$ with $N_C = 2 \cdot 10^6$ | $\Delta\sigma_D$ with $N_D = 10^7$ |
|----------|------|-------|--|------------------------------------|
| Flange 1 | M42 | 0.919 | 36.8 | 21.1 |
| Flange 2 | M36 | 0.955 | 38.2 | 22.0 |

Finally the single damages can be derived by

$$D_i = \frac{n_{E,i}}{N_{R,i}}$$

with

$$N_{R,i} = \left\{ \begin{array}{ll} N_C \cdot \left(\frac{\Delta\sigma_C / \gamma_{Mf}}{\gamma_{Ff} \cdot \Delta\sigma_N} \right)^3 & \text{if } \gamma_{Ff} \cdot \Delta\sigma_N \geq \Delta\sigma_D / \gamma_{Mf} \\ N_D \cdot \left(\frac{\Delta\sigma_D / \gamma_{Mf}}{\gamma_{Ff} \cdot \Delta\sigma_N} \right)^5 & \text{if } \Delta\sigma_N < \Delta\sigma_D / \gamma_{Mf} \end{array} \right\} \text{ with } \gamma_{Mf} = 1.15 \text{ and } \gamma_{Ff} = 1.0.$$

As no occurrences $n_{E,i}$ of the single load variation ranges $\Delta\sigma_N$ are given within this specific calculation example, Rainflow matrices for the damages produced by unique load cycles are calculated. The results are presented in Table 4.8 and

Table 4.9.

Table 4.8: Rainflow matrix for damages caused by one cycle per load variation range ΔZ in flange 1

| D_i [cycle ⁻¹] | from Z_{min} [kN] | | | | | | | |
|------------------------------|---------------------|-----------|-----------|-----------|-----------|-----------|-----------|-----|
| to Z_{max} [kN] | 0 | 50 | 100 | 150 | 200 | 250 | 300 | 350 |
| 0 | | | | | | | | |
| 50 | 2.51 E-09 | | | | | | | |
| 100 | 8.05 E-08 | 2.51 E-09 | | | | | | |
| 150 | 2.79 E-07 | 8.05 E-08 | 2.51 E-09 | | | | | |
| 200 | 6.62 E-07 | 2.79 E-07 | 8.05 E-08 | 2.51 E-09 | | | | |
| 250 | 4.13 E-06 | 2.66 E-06 | 1.59 E-06 | 8.58 E-07 | 3.93 E-07 | | | |
| 300 | 1.40 E-05 | 1.05 E-05 | 7.69 E-06 | 5.41 E-06 | 3.64 E-06 | 5.23 E-07 | | |
| 350 | 3.32 E-05 | 2.69 E-05 | 2.15 E-05 | 1.68 E-05 | 1.29 E-05 | 4.18 E-06 | 5.23 E-07 | |

Table 4.9: Rainflow matrix for damages caused by one cycle per load variation range ΔZ in flange 2

| D_i [cycle ⁻¹] | from Z_{min} [kN] | | | | | |
|------------------------------|---------------------|-----------|-----------|-----------|-----------|-----|
| to Z_{max} [kN] | 0 | 50 | 100 | 150 | 200 | 250 |
| 0 | | | | | | |
| 50 | 1.20 E-08 | | | | | |
| 100 | 2.14 E-07 | 1.20 E-08 | | | | |
| 150 | 2.07 E-06 | 9.27 E-07 | 3.09 E-07 | | | |
| 200 | 1.37 E-05 | 9.15 E-06 | 5.76 E-06 | 1.39 E-06 | | |
| 250 | 4.74 E-05 | 3.66 E-05 | 2.75 E-05 | 1.29 E-05 | 1.85 E-06 | |

4.2.5.1 Fatigue design

For the fatigue design verification of the bolts the load variation ranges due to lateral contraction of the shell has to be checked. In accordance with chapter the pre-load variation $\Delta F_{p,C}$ of the bolts is given by

$$\Delta F_{p,C} = \beta \cdot \frac{\nu \cdot \sum (\Delta \sigma_{z,i} \cdot s_i)}{\delta_{joint} \cdot E_{shell}}$$

- with β : empirical determined correction factor taken as $\beta = 1.25$
 ν : Poisson ration taken as $\nu = 0.3$
 $\Delta \sigma_z$: maximum stress variation range in the net cross section of the tower cross section i , taken as $\Delta \sigma_z = c_{net} / c \cdot \sigma_{ult,Rd}$
 s_i : shell thickness of the tower cross section i
 δ_{joint} : elastic resilience of bolted connection
 E_{shell} : Young-modulus of tower shell material

Note: Comparison of the calculated values with test results show that in 5 % of the cases the given approach leads to slightly unsafe results due to local effects in the friction connection. Therefore a correction factor $\beta = 1.25$ has been included to obtain always safe results.

As the shell stresses are transferred from one tower segment to the other stepwise within the friction connection, cp. Figure 4.17, the sum $\Sigma(\Delta\sigma_{z,i} \cdot s_i)$ can be simplified by

$$\Sigma(\Delta\sigma_{z,i} \cdot s_i) \cong \Delta\sigma_{z,mean} \cdot s_{mean}$$

with $\Delta\sigma_{z,mean}$: mean stress variation range of the net cross section of both tower cross sections

s_{mean} : mean shell thickness of both tower cross sections

As the stress variation ranges in the bolts are linear correlated to the load actions, the DEL method can be applied.

All intermediate results for the determination of the resulting DEL pre-load variation range acc. to chapter is given in Table 4.10.

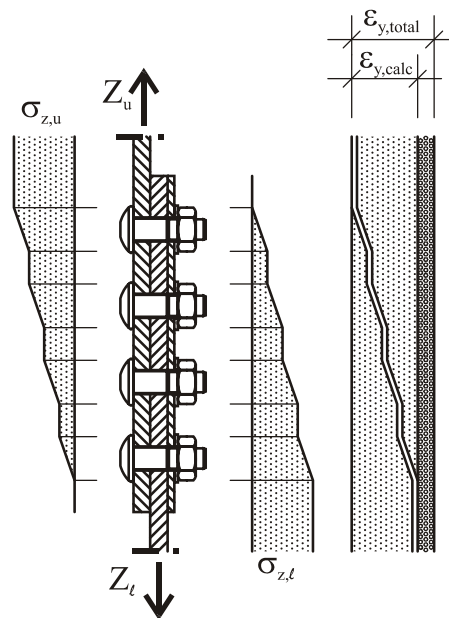


Figure 4.17: Sketch of idealised stress distribution in tower shells within the friction connection zone and considered lateral contraction $\varepsilon_{y,total} (=1.25 \cdot \varepsilon_{y,calc})$ of the shell

Table 4.10: Resulting pre-load variation range in bolts; all input parameters are summarized in Table 5.5

| Description | Equation / Parameter | Connection 1 | Connection 2 |
|---|--|-------------------------|-------------------------|
| Mean shell thickness | s_{mean} | 20.5 mm | 15.5 mm |
| Maximum stress in "mean shell" | $\max \Delta\sigma_{z,mean} = \frac{c_{mean} - d_0}{c_{mean}} \cdot \sigma_{ult,Ed}$ | 314.2 N/mm ² | 230.1 N/mm ² |
| elastic resilience of bolt head | $\delta_{head} = \frac{\ell_{head}}{E_{bolt} \cdot A_{nom}}$ | 5.053 E-08 | 5.053 E-08 |
| elastic resilience of shank | $\delta_{shank} = \frac{\ell_i}{E_{bolt} \cdot A_i}$ | 2.546 E-07 | 2.223 E-07 |
| elastic resilience of unengaged loaded part of thread | $\delta_{freethread} = \frac{\ell_{thread}}{E_{bolt} \cdot A_{d_3}}$ | 1.486 E-07 | 1.009 E-07 |

| | | | |
|---|--|-----------------|-----------------|
| elastic resilience of engaged bolt thread | $\delta_{eng,thread} = \frac{\ell_{eng,thread}}{E_{bolt} \cdot A_{d_3}}$ | 8.084 E-08 | 8.084 E-08 |
| elastic resilience of nut | $\delta_{nut} = \frac{\ell_{nut}}{E_{nut} \cdot A_{nom}}$ | 1.376 E-07 | 1.376 E-07 |
| elastic resilience of the preloaded bolt | $\delta_{bolt} = \delta_{head} + \delta_{shank} + \delta_{free\ thread} + \delta_{eng\ thread} + \delta_{nut}$ | 6.722 E-07 | 5.922 E-07 |
| elastic resilience of clamping package | $\delta_{cp} = \frac{2 \cdot \ln \left[\frac{(d_w + d_0) \cdot (d_w + \ell_{cp} \cdot \tan \varphi - d_0)}{(d_w - d_0) \cdot (d_w + \ell_{cp} \cdot \tan \varphi + d_0)} \right]}{E_{cp} \cdot \pi \cdot d_0 \cdot \tan \varphi}$ | 1.150 E-07 | 1.070 E-07 |
| total resilience of the joint | $\delta_{joint} = \delta_{bolt} + \delta_{cp}$ | 7.872 E-07 | 6.992 E-07 |
| Maximum resulting pre-load variation range in bolts | $\max \Delta F_{p,C} = \beta \cdot \frac{\nu \cdot \max \Delta \sigma_{z,mean} \cdot s_{mean}}{\delta_{joint} \cdot E_{shell}}$ | -23.54 kN | -12.24 kN |
| Pre-load variation range in bolts for the DEL in net shell cross section | $\Delta F_{p,C,DEL} = \beta \cdot \frac{\nu \cdot \Delta \sigma_{z,DEL,net} \cdot s_{mean}}{\delta_{joint} \cdot E_{shell}}$ | -2.70 kN | -1.53 kN |

The fatigue stress of the pre-loaded bolts at $N_{ref} = 2 \cdot 10^8$ cycles can be calculated with a Wöhler curve with constant slope $m = 4$, which is common practice in wind-tower design, see also. For the pre-loaded bolts detail category 50 is used acc. to EN 1993-1-9. This leads to

$$\text{Characteristic fatigue resistance } (N_{ref} = 2 \cdot 10^8): \quad \Delta \sigma_{bolt,R} = 50 \cdot \left(\frac{2 \cdot 10^6}{2 \cdot 10^8} \right)^{\frac{1}{4}} = 15.81 \text{ N / mm}^2$$

$$\text{DEL in bolts of connection 1:} \quad \Delta \sigma_{bolt,1,DEL} = \frac{F_{p,C,DEL}}{A_s} = \frac{2700}{560.6} = 4.82 \text{ N / mm}^2$$

$$\text{DEL in bolts of connection 2:} \quad \Delta \sigma_{bolt,2,DEL} = \frac{F_{p,C,DEL}}{A_s} = \frac{1530}{560.6} = 2.73 \text{ N / mm}^2$$

The final fatigue design verification than reads

$$\frac{\gamma_{Ff} \cdot \Delta \sigma_{DEL}}{\Delta \sigma_R / \gamma_{Mf}} \leq 1 \quad \text{with } \gamma_{Mf} = 1.15 \text{ and } \gamma_{Ff} = 1.0.$$

$$\rightarrow \text{Connection 1:} \quad 0.35 < 1$$

$$\rightarrow \text{Connection 2:} \quad 0.20 < 1$$

The fatigue design of the shell is done in the same way using detail category 90

$$\text{Characteristic fatigue resistance:} \quad \Delta \sigma_{shell,R} = 90 \cdot \left(\frac{2 \cdot 10^6}{2 \cdot 10^8} \right)^{\frac{1}{4}} = 28.46 \text{ N / mm}^2$$

With the damage equivalent stresses of the gross cross section given in chapter 4.2.5 the final fatigue design verification leads to

$$\rightarrow \text{Connection 1:} \quad 0.91 < 1$$

→ Connection 2: $0.86 < 1$

The general fatigue safety of the “finger cut” of the friction connection can be improved by a smother cutting line, which leads to a smaller geometrical notch at finger base. Figure 4.18 gives an example for such an improvement by using a clothoidal cut instead of a circular cut.

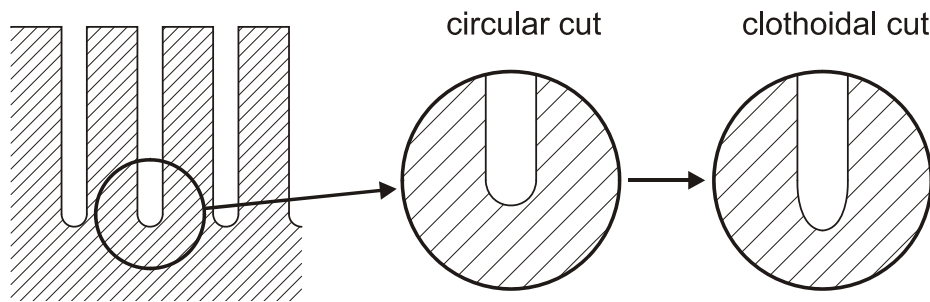


Figure 4.18: Scheme of circular and clothoidal finger cutting lines, respectively

This type of cutting would also improve the quality of the cutting edge itself, as the change-over from linear to curved cutting is easier to handle for the cutting-machine and thus will improve the fatigue safety even more as the metallurgical and physical notch will become smaller.

5 CONNECTIONS

5.1 General

The connection between two segments of a steel tubular tower is most commonly realized as a flange connection. However, recent research results offer a competitive alternative: friction connections with long open slotted holes. By their use, the fatigue resistance of the flanges may be overcome as the limiting design criterion. Additionally, the assembly process on site will be accelerated. For design purpose, it is assumed that the resistance of the three dimensional connection detail, which is loaded mostly in bending, can be described by the resistance of a segment with a single bolt and bolt row, respectively. The segment width c is equivalent to the arc length between two bolt holes or bolt rows in the tension zone of the shell.

In general, the following design checks for tower connections (bolts and tower shell) are required:

- Resistance at the Ultimate Limit State (ULS)
- Fatigue design (FLS)
- Resistance at the Serviceability Limit State (SLS):
 - Flange opening at the bolt axis (flange connections only!)
 - Flange / shell yielding
 - Bolt yielding (flange connections only!)

The following calculation example will concentrate on the ULS of the bolts for both connection details.

5.2 Flange connection

The following chapters describe the theoretical background, give a numerical example and propose a flowchart to design for flange connections used in towers of wind turbines.

Ring flange connections with preloaded high strength bolts are used for in-situ execution. Most commonly "L" model [33] is used although in exceptional cases of large towers and "T" model is used. The flange connection should be designed so no opening under service loads appears. After the flanges separate two failure modes are possible: rupture in the bolts or the plastic joint in the tower shell.

To simplify the design, only one segment of the tower flange is considered, see Figure 5.1, where the tension stresses acting in the tower shell are integrated into a concentrated load Z .

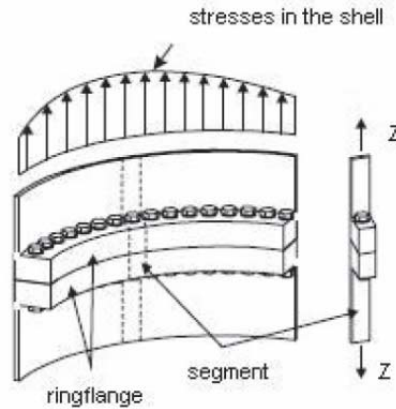


Figure 5.1: Segment approach for flange connections [1]

5.2.1 Theoretical background

5.2.1.1 Bolt forces

The analytical determination of the real structural behaviour of a preloaded ring-flange connection of tubular tower segments under bending is rather complicated. For the time being the best way to consider all redistribution and load shifting effects within the 3D-structure is by numerical simulations. Thereby the entire joint is to be discretised by means of volumetric brick-elements. However, due to the high degree of contact-surfaces needed, such FE-simulations are too labour-intensive for the usual tower design. Therefore, common practise is to use segment models, allowing for a simple and realistic determination of the relevant internal forces, such as bolt loads, see Figure 5.2 a). As a result of these segment models the tension force Z in the shell can be obtained by the integral of the axial stress σ_x over the cross-sectional area of the shell strip width c .

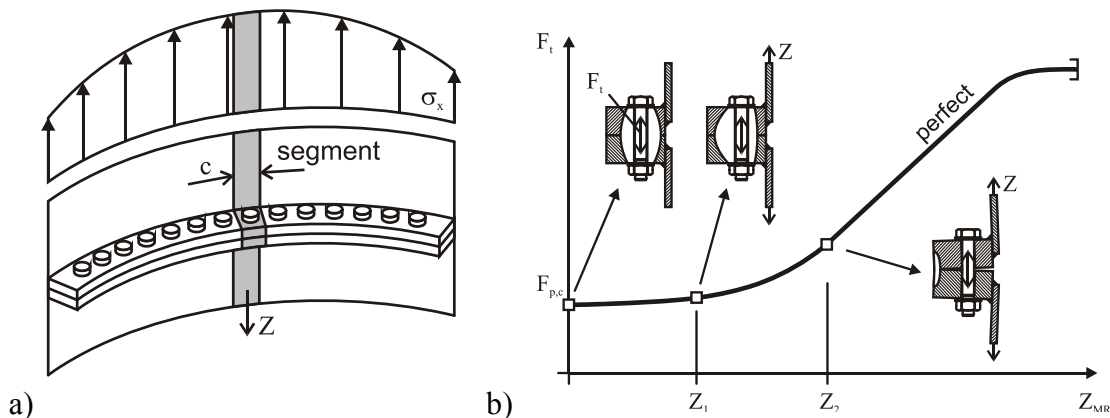


Figure 5.2: Segment model of L-shaped ring-flange connection

By means of this simplified 2-D model the design for ultimate and fatigue limit state can be realised in a more reasonable way. Thereby the smaller the radius R of the tube is the more the ring effects have to be taken into account. The general procedure for both design verifications is described more in detail later on in the present chapter.

For the fatigue limit state the determination of the exact bolt-loads in function of the shell force Z plays an essential role. Load carrying behaviour of the segment follows the nonlinear graph shown in Figure 5.2 b). For small tension forces Z in the tower shell, as shown at the beginning, the inclination in bolt force F_s is low, keeping the force within the band of pretension force $F_{p,c}$. An increase in load Z relieves the pressure acting in the contact zone between the flanges. Thus, as soon as the flange starts to unclench, the bolt force rises (between Z_1 and Z_2). The relation between the two forces after Z_2 keeps about linear until yielding of the bolt starts and final rupture occurs.

The general behaviour of a preloaded bolt in L-shaped ring-flange connections can be also described detailed as follows:

1. For segment forces $Z \leq 0$ the flange zone under compression (clamp solid) has the shape of a paraboloid of revolution [28], cp. Figure 5.3 a), and the bolt loads F_t keep almost constant at the level of $F_{p,C}$, thus $F_t \approx F_{p,C} \approx \text{const.}$
2. With increasing segment force $Z \leq Z_1$ the clamp solid begins to move in direction of the flange edge and the bolt load F_t slightly increases.
3. From a certain segment force Z_1 on the shifting of the clamp solid develops faster and the flange connection begins to open, which leads to an expeditious increase of bolt load F_t .
4. When reaching segment force Z_2 the interface of the flanges stays only in contact at the flange edges and the structural behaviour of the connection corresponds to the pure edge bearing model. The bolt load F_t increases linearly in function of the tension force Z in the shell.
5. When reaching the elastic limit of the bolt (Z_3) the slope of the bolt-load-function $F_t(Z)$ decreases and the connection reaches its limit due to plastification of the bolt.

5.2.1.2 Influence of flange imperfections on bolt forces

Imperfections due to uncertainties out of manufacturing such as inclinations or gaps between the flanges cannot be avoided. These imperfections can significantly influence the actual loads in the bolts in the region affected and thus the performance of the entire connection. Figure 5.3 shows the qualitative shape of the clamp solid after preloading of the bolt for different types of imperfection.

Jakubowski [29] indicates the following three types of imperfection, which can occur in any combination:

1. rotation symmetric or local taper with flange sided gap, case b) in Figure 5.3
2. rotation symmetric or local taper with tube sided gap, case c) in Figure 5.3
3. local parallel gap, case d) in Figure 5.3

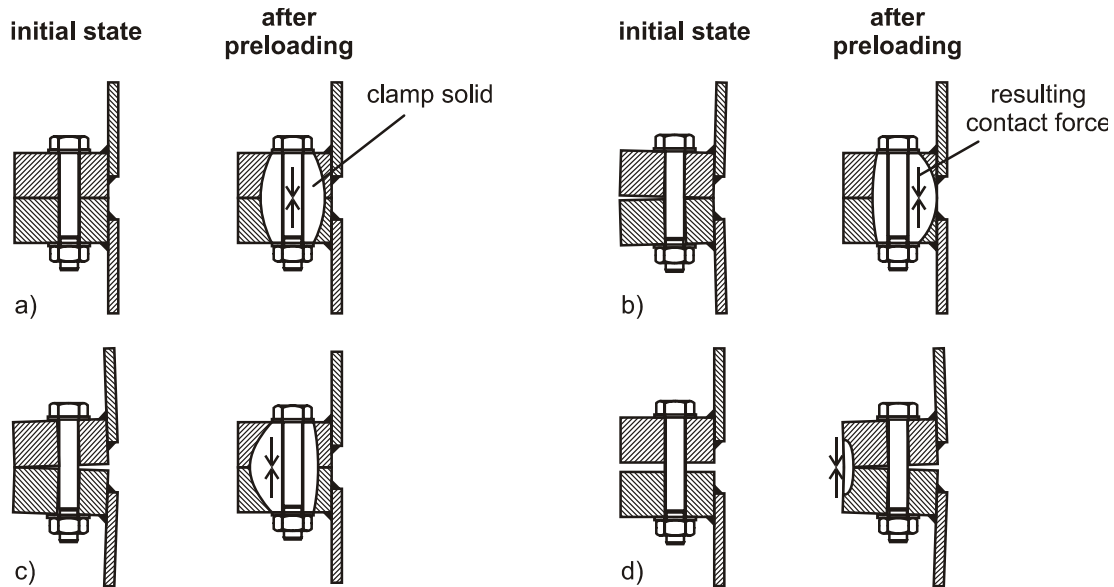


Figure 5.3: Position of clamp solid in L-flange in a perfect (a) and different imperfect connections (b)(c)(d); qualitative shape acc. to [29]

Local taper and parallel gap imperfections have the most detrimental impact on ultimate as well as fatigue resistance of the flange connection. Figure 5.4 shows the influence of these imperfections on the bolt load. The shift of bolt-load function $F_t(Z)$ increases considerably the load variation ranges in the bolt δF_t and thus the fatigue load. This fact should be considered to gain a save sided fatigue design.

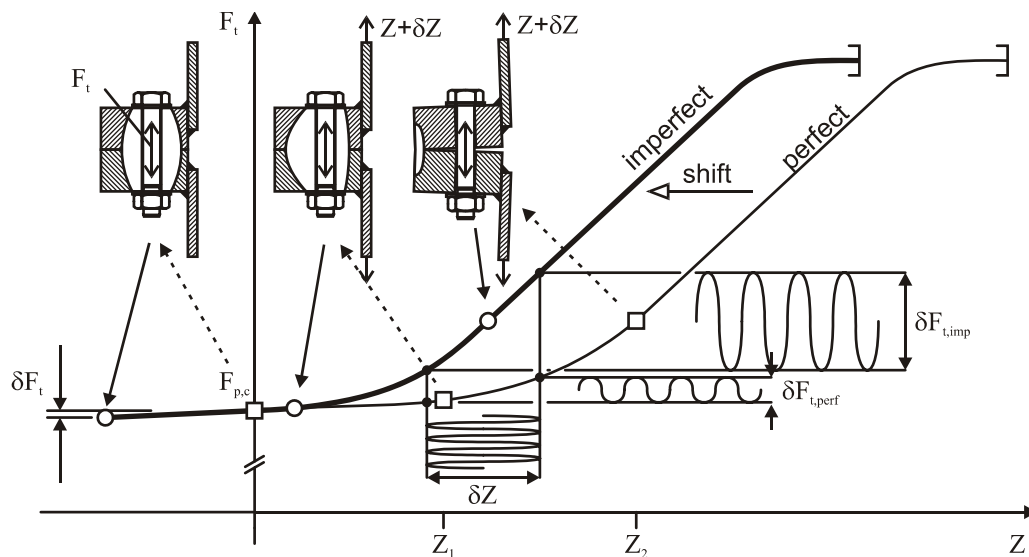


Figure 5.4: Influences of flange imperfections on the bolt force function

5.2.1.3 Ultimate limit state

The verification in the ultimate limit state (ULS) is usually done according to the plastic hinge theory. Even though bolts in ring-flange connections have to be preloaded, the pre-tensioning load in bolts has not to be considered for the ULS verification. According to [33] three different failure mechanisms must be checked in L-shaped ring-

flange connections, whereas the lowest resistance $Z_{ult,i}$ is governing the design, cp. Figure 5.5:

1. Yielding (failure) of the bolt; this governs failure mechanism if flanges and shells are rather stiff compared to the bolt. The ultimate resistance of the segment then equals to the tensional resistance of the bolt:

$$Z_{ult,1} = F_{t,Rd} \quad (58)$$

2. Yielding (failure) of the bolt and at the same time plastic hinge in shell; the ultimate resistance of this failure mode is given by:

$$Z_{ult,2} = \frac{F_{t,Rd} \cdot a + M_{N,pl,Rd,sh}}{a + b} \quad (59)$$

3. Plastic hinge in shell and flange (failure of connection); the bolt load stays below its tensile resistance ($F_{t,Ed} < F_{t,Rd}$). The ultimate resistance of this failure mode thereby reads:

$$Z_{ult,3} = \frac{M_{N,pl,Rd,sh} + M_{pl,Rd,fl,net}}{b} \quad (60)$$

- with
- Z_{ult} = Ultimate tensile resistance force of the segment
 - $F_{t,Ed}$ = Design tensile force in bolt
 - $F_{t,Rd}$ = Design tensile resistance of the bolt
 - $M_{N,pl,Rd,sh}$ = Design plastic bending resistance of the shell considering M - N -interaction
 - $M_{pl,Rd,fl,net}$ = Design plastic bending resistance of the flange with deduction of bolt hole
 - a = Distance between flange edge and axis of bolt
 - b = Distance between axis of bolt and shell

$$M_{N,pl,Rd,sh} = \left[1 - \left(\frac{Z_{ult}}{N_{pl,Rd,sh}} \right)^2 \right] \cdot M_{pl,Rd,sh} \quad (61)$$

$$F_{t,Rd} = \frac{0.9 \cdot f_{ub} \cdot A_s}{\gamma_{M2}} \quad (62)$$

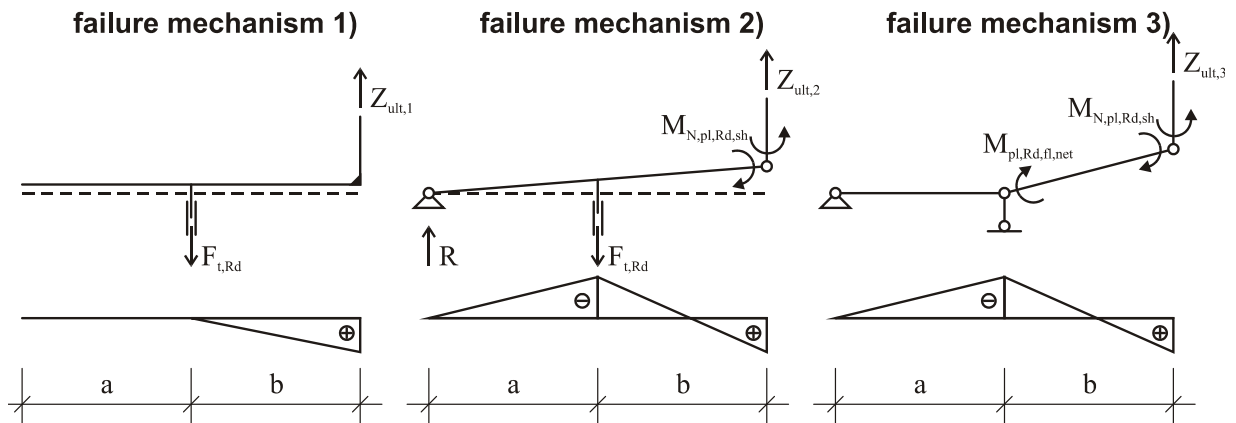


Figure 5.5: Plastic hinge models for the determination of the ultimate resistance of L-shaped ring-flange connections acc. to Petersen [33]

5.3 Friction connection

The following chapters describe the theoretical background, gives a numerical example and propose a flowchart to design for the innovative in HISTWIN developed so-called "HISTWIN-connection" used in towers of wind turbines.

Friction connections with normal clearance holes have been used in structural engineering for decades. Their behaviour has been extensively examined by various researchers and is comprehensively described by Kulak et al. [44]. Slip resistant joints rely on load transfer between the joined elements due to friction, which is ensured by a clamping force provided by preloaded high strength bolts, see Figure 5.6a.

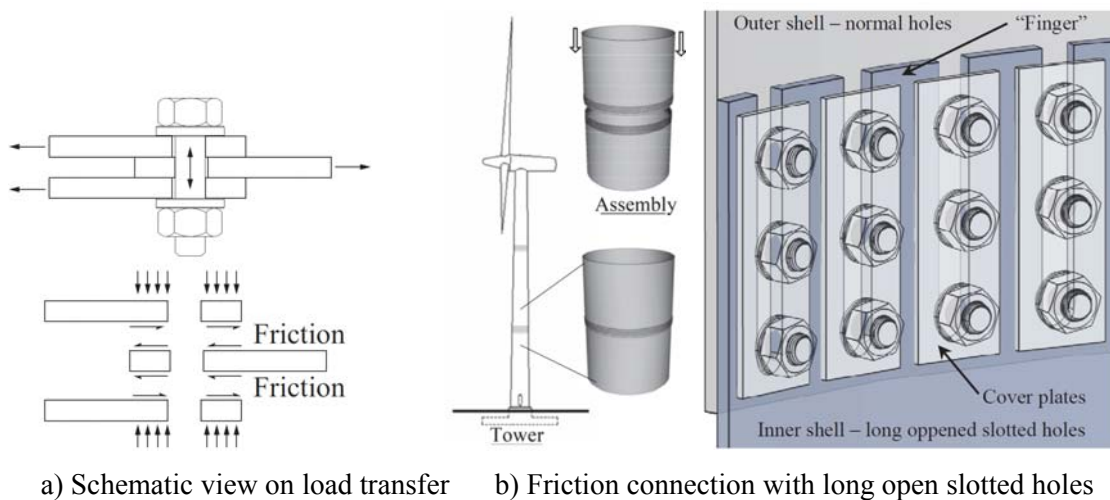


Figure 5.6: Friction connection

Friction connections are very efficient for cyclic wind loading which varying between tension and compression. Due to preloaded bolts and force transfer by friction, stress concentration does not appear. This structural detail belongs to fatigue **class 100** [33], which is much above fatigue detail of the L-flange which is between class 36 and 71. In many cases this fatigue criterion of the connection governs the design of the tower.

Veljkovic et al. [45] suggest substituting normal clearance holes on the lower tower section with long open slotted holes with the covered plates, which are depicted in Figure 5.6b. The remaining steel parts between the long open slotted holes are with respect to their visual appearance designated as "fingers". The on top opened bolt hole shall ease the assembly process. On the inside of the tower, cover plates shall be mounted to ensure an equal distribution of pressure and to facilitate the assembly process.

5.3.1 Theoretical background

The structural design of friction connections in general is regulated in various standards and guidelines [44], [34], [35]. As an example, the design procedure according to EN 1993-1-8 [35] is shown here. The ultimate resistance of the friction connection corresponds to its ultimate slip resistance. The friction connection with long open slotted holes is a single lap joint, thus providing one friction surface $n = 1$. Recent findings in the HISTWIN2 [46] project have shown that the second friction surface is activated after the ultimate limit state is reached. It can be easily determined according to the following hand-calculation procedure:

- Determination of the ultimate slip design resistance $Z_{s,Rd}$ of one bolt row of the friction joint (segment model):

$$Z_{s,Rd} = \frac{n_r \cdot \mu \cdot k_s \cdot F_{p,C}}{\gamma_{M3}} \quad (63)$$

- with
- n_r : number of bolts per slotted hole
 - μ : slip factor
 - k_s : reduction factor for long slotted holes
 - $F_{p,C}$: characteristic preload force in bolt
 - γ_{M3} : partial safety factor taken as $\gamma_{M3} = 1.25$

- Equilibrium in friction joint:

$$Z_{s,Rd} \stackrel{!}{=} Z_{Ed} \quad (64)$$

- Determination of the corresponding maximum tension stress in shell $\sigma_{x,t}$ due to tension force Z_{Ed} in segment model, cp. Figure 5.7:

$$Z_{Ed} = A_{shell} \cdot \sigma_{mean} = c \cdot s_{mean} \cdot \sigma_{mean} \cong c \cdot s_{mean} \cdot \sigma_{x,t} \quad (65)$$

- with
- A_{shell} : area of cross section of segment model
 - σ_{mean} : mean of tension/compression stress in segment model
 - $\sigma_{x,t}$: maximum tension/compression stress in shells
 - c : segment width = distance between two bolt rows
 - s_{mean} : mean shell thickness of the two connected tower segments

- Determination of the corresponding load P_{Ed} for the 4-point-bending test.

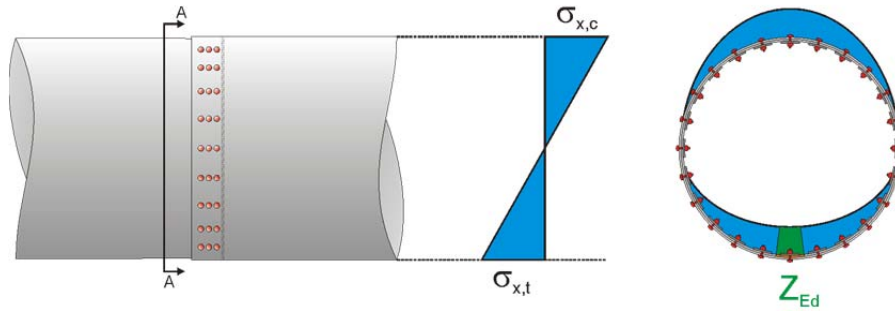


Figure 5.7: Stress distribution in shell and tension force Z_{Ed} of segment model

Due to lateral contraction of the tower shell under bending the forces in the preloaded bolts vary. This load-variation depends on the shell stresses as well as the bolt and connection geometry and its range has to be checked with regard to the fatigue safety of the connection. In accordance [27] the load variation range $\Delta F_{p,C}$ in the preloaded bolts of a friction connection can be determined by the equation

$$\Delta F_{p,C} = \beta \cdot \frac{\nu \cdot \sum (\Delta \sigma_{x,i} \cdot s_i)}{\delta_{joint} \cdot E_{shell}} \quad (66)$$

- with β : empirical determined correction factor taken as $\beta = 1.25$
 ν : Poisson ration taken as $\nu = 0.3$
 $\Delta \sigma_x$: maximum stress variation range in the net cross section of the tower cross section i
 s_i : shell thickness of the tower cross section i
 δ_{joint} : elastic resilience of bolted connection
 E_{shell} : Young-modulus of tower shell material.

The required elastic resilience of the bolted connection can be calculated acc. to [28] by

$$\delta_{joint} = \delta_{bolt} + \delta_{cp} \quad (67)$$

- with δ_{bolt} : elastic resilience of the preloaded bolt
 δ_{cp} : elastic resilience of clamping package (steel shells + cover-plate + washers).

According to [28] the resilience of the bolt takes into account not only its elastic deformation within the clamp length but also any elastic deformations, which occur outside this region and also have an effect on the deformation behaviour of the bolt in the joint. Thus the geometry of the whole bolt has to be considered. A bolt as given in Figure 5.8 consists of a number of individual elements, which can readily be substituted by cylindrical bodies of various length i and cross sections A_i . These cylindrical elements are arranged in a row, so that the total resilience of the bolt is given by

$$\delta_{bolt} = \delta_{head} + \delta_{shank} + \delta_{free\ thread} + \delta_{eng.\ thread} + \delta_{nut} \quad (68)$$

with δ_{head} : elastic resilience of bolt head

$$\delta_{head} = \frac{\ell_{head}}{E_{bolt} \cdot A_{nom}}$$

with $\ell_{head} = \alpha \cdot d$: substitutional extension length of bolt head

with $\alpha = 0.5$ for hexagon head bolts

$\alpha = 0.25$ for rivet head bolts

$$A_{nom} = \frac{\pi}{4} \cdot d^2 : \text{nominal cross section of bolt}$$

E_{bolt} : Young's-modulus of bolt material
 d : nominal diameter of bolt shank

δ_{shank} : elastic resilience of shank

$$\delta_{shank} = \sum \frac{\ell_i}{E_{bolt} \cdot A_i}$$

with ℓ_i : length of shank body i

$$A_i = \frac{\pi}{4} \cdot d_i^2 : \text{nominal cross section of bolt shank body } i$$

$\delta_{free\ thread}$: elastic resilience of unengaged loaded part of thread

$$\delta_{free\ thread} = \frac{\ell_{thread}}{E_{bolt} \cdot A_{d_3}}$$

with ℓ_{thread} : free length of unengaged loaded thread

$$A_{d_3} = \frac{\pi}{4} \cdot d_3^2 : \text{nominal cross section of bolt thread}$$

d_3 : minor diameter of bolt thread

$\delta_{eng.\ thread}$: elastic resilience of engaged bolt thread

$$\delta_{eng.\ thread} = \frac{\ell_{eng.\ thread}}{E_{bolt} \cdot A_{d_3}}$$

with $\ell_{eng.\ thread} = 0.5 \cdot d$: length of engaged loaded thread

δ_{nut} : elastic resilience of nut

$$\delta_{nut} = \frac{\ell_{nut}}{E_{nut} \cdot A_{nom}}$$

with $\ell_{nut} = 0.4 \cdot d$: substitutional extension length of nut

E_{nut} : Young's-modulus of nut material

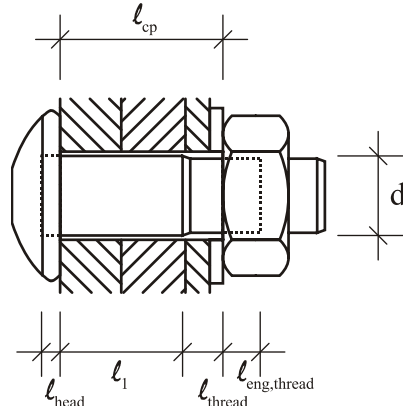


Figure 5.8: Division of a bolt into individual cylindrical solids and deformation regions outside the bolt [28]

Considering that the bolted joint is concentrically clamped and the deformation cone can spread without hindrance up to the interface ($D_A \geq D_K$), cp. Figure 5.9, the elastic resilience of clamping package can be determined acc. to the following equation:

$$\delta_{cp} = \frac{2 \cdot \ln \left[\frac{(d_w + d_0) \cdot (d_w + \ell_{cp} \cdot \tan \varphi - d_0)}{(d_w - d_0) \cdot (d_w + \ell_{cp} \cdot \tan \varphi + d_0)} \right]}{E_{cp} \cdot \pi \cdot d_0 \cdot \tan \varphi} \quad (69)$$

with d_w : outside diameter of the plane head bearing surface of the bolt, cp.

Figure 5.9

d_0 : diameter of bolt hole

ℓ_{cp} : length of clamping package, cp. Figure 5.8

φ : angle of deformation cone taken as $\varphi = 35^\circ$

E_{cp} : Young's-Modulus of clamping package material (shell, cover-plate, washer)

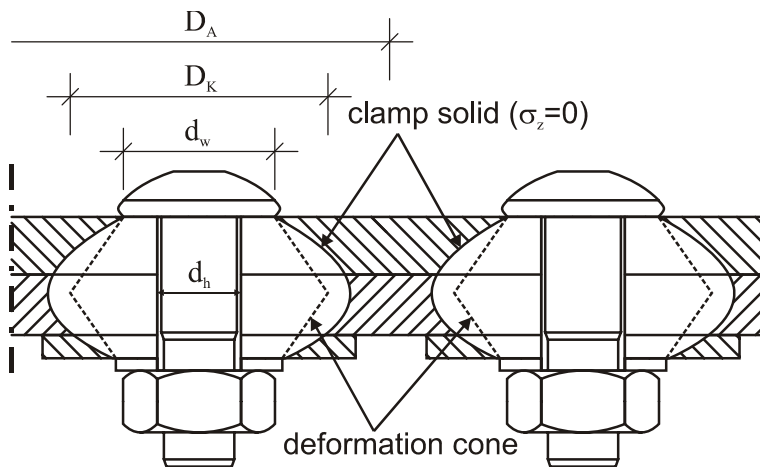


Figure 5.9: Clamp solid and calculation model at a bolted joint [28]

5.3.2 Flowchart (Excel-Tool)

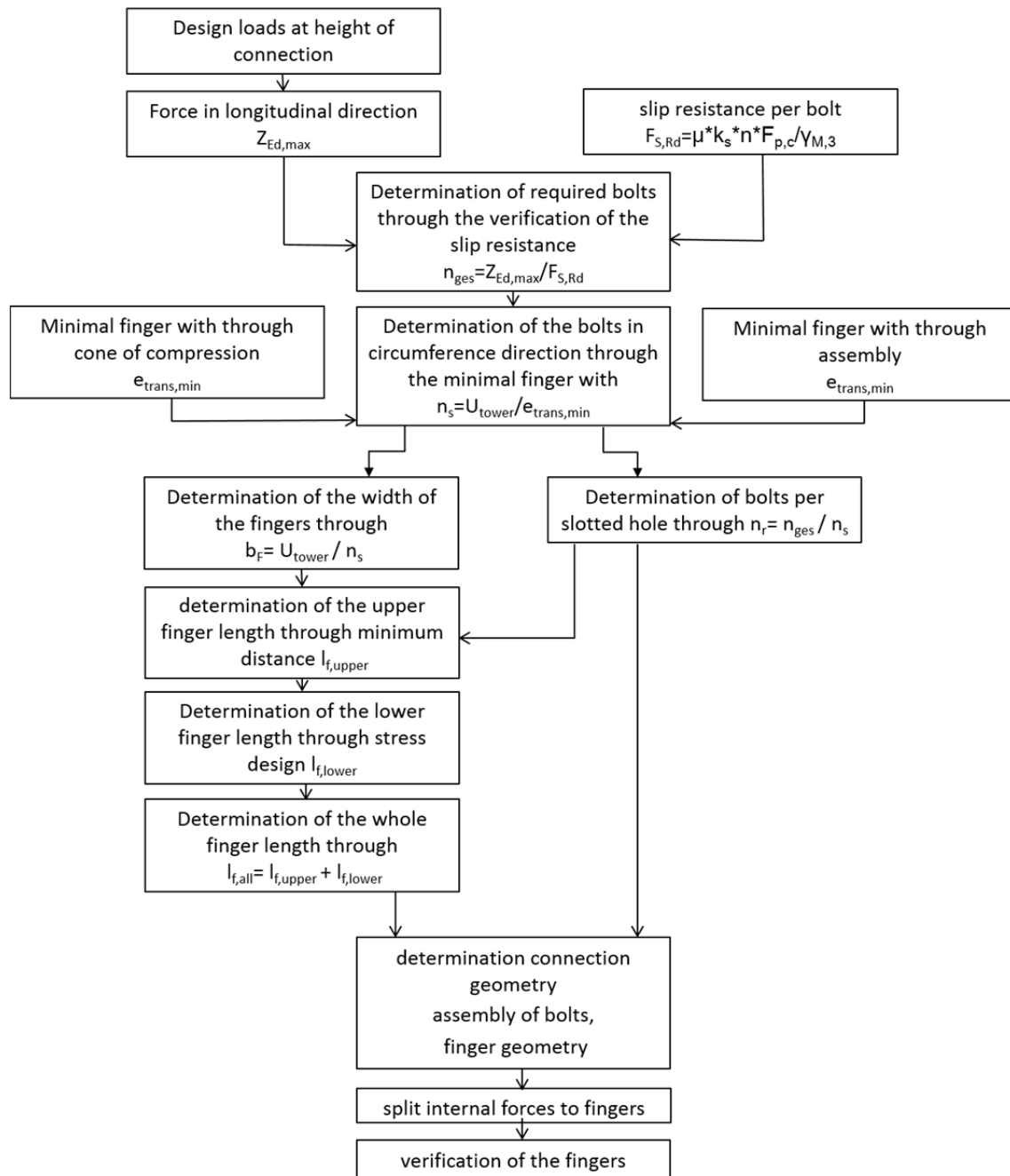


Figure 5.10: Flowchart for designing connection

5.4 Numerical examples

5.4.1 Flange connection

For a specific load case the design loads can be linearly interpolated between two given sections.

The design loads for the two flange sections can thus be simplified as in Table 5.4. The safety factor is taken as 1.35.

Table 5.1: Extreme design loads at the flange sections

| | Height | F _x | F _y | F _z | F _r | M _x | M _y | M _z | M _r |
|-----------------|--------|----------------|----------------|----------------|----------------|----------------|----------------|----------------|----------------|
| | mm | kN | kN | kN | kN | kNm | kNm | kNm | kNm |
| Flange 2 | 48390 | -864 | 7 | -1846 | 864 | 1635 | -25168 | -1363 | 25221 |
| Flange 1 | 21770 | -886 | 27 | -2443 | 886 | 1129 | -48617 | -1368 | 48631 |

The effects of shear stresses on the resistance of the flanges are neglected and only the load components inducing longitudinal stresses in the shell are considered. The maximum design stress in the tower shell thus becomes:

$$\sigma_{ult,Ed} = \frac{M_r}{W_i} - \frac{F_z}{A_i}$$

with

M_r, F_z Extreme design loads at height of flange section i acc. to Table 5.4
 W_i, A_i Cross section resistances of tower tube at height of flange section i

This leads to the following maximum tensile stresses in the tower shell

Connection 1: $\sigma_{ult,Ed} = 195 \text{ N/mm}^2$

Connection 2: $\sigma_{z,DEL} = 21.4 \text{ N/mm}^2$

This DEL method is only applicable as long as a linear relation between load-actions and member stresses exists. For fatigue design of bolts in flange connections an extremely non-linear relation has to be taken into account, which means that the complete Rainflow matrix has to be considered for the fatigue design. As no complete Rainflow matrices are available for the given design example, Rainflow matrices for damages caused by one cycle per load variation range ΔZ are determined in the following.

5.4.1.1 Flange geometry

The dimensions and material properties of the relevant flange of tower joint 1 and 2 are given in Figure 5.11 and Figure 5.12.

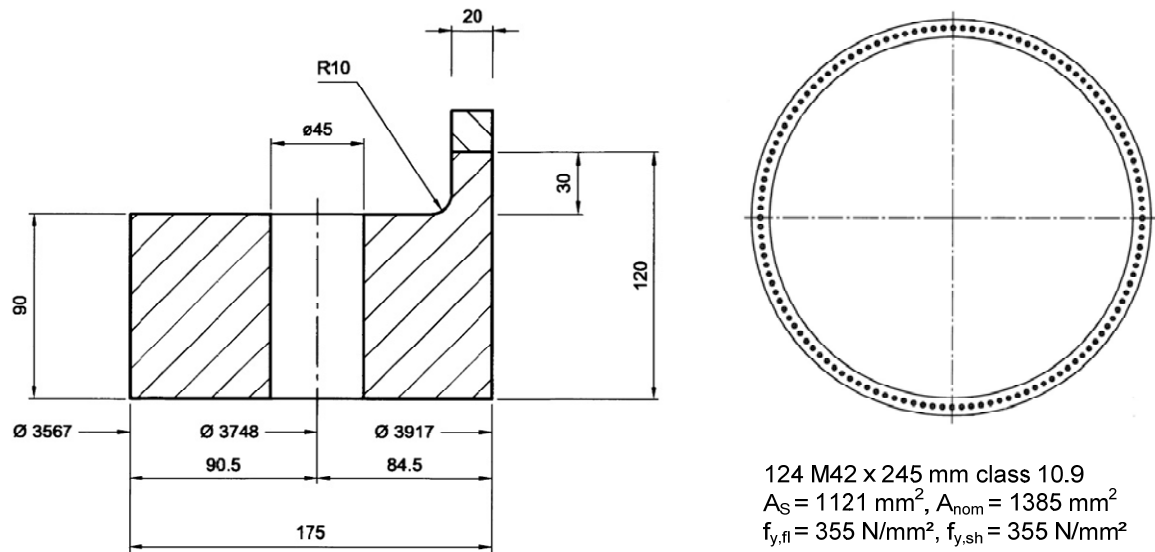


Figure 5.11: Flange 1 - Dimensions and material properties of upper flange in tower joint 1

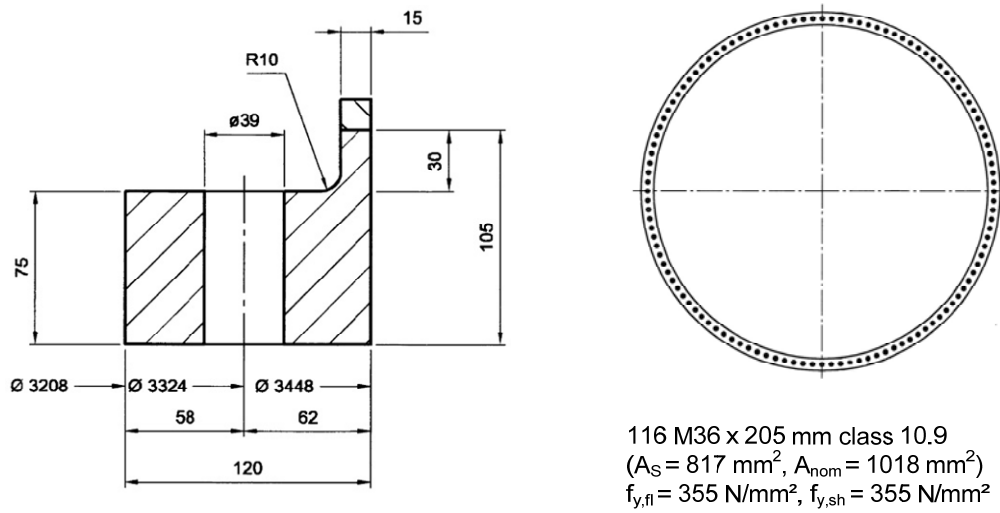


Figure 5.12: Flange 2 - Dimensions and material properties of upper flange in tower joint 2

5.4.1.2 Ultimate Limit State

The ultimate resistance of the flange can be calculated acc. to chapter 5.2 of this documentation. With the given dimensions for:

Flange 1:

$$a = 90.5 \text{ mm}$$

$$b = 84.5 - \frac{20}{2} = 74.5 \text{ mm}$$

$$c = 95 \text{ mm}$$

$$t_{fl} = 90 \text{ mm}$$

$$s = 20 \text{ mm}$$

Flange 2:

$$a = 58.5 \text{ mm}$$

$$b = 62 - \frac{15}{2} = 54.5 \text{ mm}$$

$$c = 90 \text{ mm}$$

$$t_{fl} = 75 \text{ mm}$$

$$s = 15 \text{ mm}$$

and the design resistances of the single components

- Design tensile resistance of bolts:

$$F_{t,Rd} = \frac{0.9 \cdot f_{ub} \cdot A_s}{\gamma_{M2}}$$

$$\text{Flange 1: } F_{t,Rd,1} = \frac{0.9 \cdot 100 \cdot 11.21}{1.25} = 807.1 \text{ kN}$$

$$\text{Flange 2: } F_{t,Rd,2} = \frac{0.9 \cdot 100 \cdot 8.17}{1.25} = 588.2 \text{ kN}$$

- Design plastic bending resistance of shell

$$M_{pl,Rd,sh} = \frac{W_{pl,sh} \cdot f_{y,sh}}{\gamma_{M0}} = \frac{c \cdot s^2 \cdot f_{y,sh}}{4 \cdot \gamma_{M0}}$$

$$\text{Flange 1: } M_{pl,Rd,sh,1} = \frac{9.5 \cdot 2.0^2 \cdot 35.5}{4 \cdot 1.1} = 306.6 \text{ kNcm}$$

$$\text{Flange 2: } M_{pl,Rd,sh,2} = \frac{9.0 \cdot 1.5^2 \cdot 35.5}{4 \cdot 1.1} = 163.4 \text{ kNcm}$$

- Design plastic resistance of shell

$$N_{pl,Rd,sh} = \frac{A_{sh} \cdot f_{y,sh}}{\gamma_{M0}} = \frac{c \cdot s \cdot f_{y,sh}}{\gamma_{M0}}$$

$$\text{Flange 1: } N_{pl,Rd,sh,1} = \frac{9.5 \cdot 2.0 \cdot 35.5}{1.1} = 613.2 \text{ kNcm}$$

$$\text{Flange 2: } N_{pl,Rd,sh,2} = \frac{9.0 \cdot 1.5 \cdot 35.5}{1.1} = 435.7 \text{ kNcm}$$

- Design plastic bending resistance of shell considering M - N -interaction

$$M_{N,pl,Rd,sh} = \left[1 - \left(\frac{Z_{ult}}{N_{pl,Rd,sh}} \right)^2 \right] \cdot M_{pl,Rd,sh}$$

- Design plastic bending resistance of net cross-section of flange

$$M_{pl,Rd,fl,net} = \frac{W_{pl,net,fl} \cdot f_{y,fl}}{\gamma_{M0}} = \frac{(c - d_0) \cdot t_{fl}^2 \cdot f_{y,fl}}{4 \cdot \gamma_{M0}}$$

$$\text{Flange 1: } M_{pl,Rd,fl,net,1} = \frac{(9.5 - 4.5) \cdot 9.0^2 \cdot 35.5}{4 \cdot 1.1} = 3267.6 \text{ kNcm}$$

$$\text{Flange 2: } M_{pl,Rd,fl,net,2} = \frac{(9.0 - 3.9) \cdot 7.6^2 \cdot 35.5}{4 \cdot 1.1} = 2314.6 \text{ kNcm}$$

the ultimate resistance of the flange connection can be determined acc. to the plastic hinge theory described on page 75 of this report. It is given by the minimum value of

$$\text{Min} \{Z_{ult,1}; Z_{ult,2}; Z_{ult,3}\}$$

with

$$Z_{ult,1} = F_{t,Rd}$$

$$\text{Flange 1: } Z_{ult,1} = 807.1 \text{ kN}$$

$$\text{Flange 2: } Z_{ult,1} = 588.2 \text{ kN}$$

$$Z_{ult,2} = \frac{F_{t,Rd} \cdot a + M_{N,pl,Rd,sh}(Z_{ult,2})}{a + b}$$

$$= -\frac{N_{pl,Rd,sh}^2 \cdot (a + b)}{2 \cdot M_{pl,Rd,sh}} + N_{pl,Rd,sh} \cdot \sqrt{1 + \frac{N_{pl,Rd,sh}^2 \cdot (a + b)^2 + 4 \cdot F_{t,Rd} \cdot a \cdot M_{pl,Rd,sh}}{4 \cdot M_{pl,Rd,sh}^2}}$$

$$\text{Flange 1: } Z_{ult,2} = 451.2 \text{ kN}$$

$$\text{Flange 2: } Z_{ult,2} = 311.6 \text{ kN}$$

$$Z_{ult,3} = \frac{M_{N,pl,Rd,sh}(Z_{ult,3}) + M_{pl,Rd,fl,net}}{b}$$

$$= -\frac{N_{pl,Rd,sh}^2 \cdot b}{2 \cdot M_{pl,Rd,sh}} + \sqrt{\frac{N_{pl,Rd,sh}^4 \cdot b^2}{4 \cdot M_{pl,Rd,sh}^2} + \frac{M_{pl,Rd,fl,net} + M_{pl,Rd,sh}}{M_{pl,Rd,sh}} \cdot N_{pl,Rd,sh}^2}$$

$$\text{Flange 1: } Z_{ult,3} = 456.9 \text{ kN}$$

$$\text{Flange 2: } Z_{ult,3} = 426.0 \text{ kN}$$

This leads to the ultimate resistance of the connections as summarized in Table 5.2. The design verification is given in Table 5.3.

Table 5.2: Ultimate resistance of flange connection 1 and 2

| | Failure mode acc. to plastic hinge theory from Petersen [33] | Ultimate tensile force in segment shell $Z_{ult,Rd}$ [kN] | Ultimate tensile stress in tower shell $\sigma_{ult,Rd}$ [N/mm ²] |
|-----------------|--|---|---|
| Flange 1 | "2" = Yielding of bolt in combination with a plastic hinge in shell | 451.2 | 237.5 |
| Flange 2 | "2" = Yielding of bolt in combination with a plastic hinge in shell | 311.6 | 230.8 |

Table 5.3: Design verification of connection flange 1 & 2

| | Resulting maximum tensile stresses in tower shell $\sigma_{ult,Ed}$ [N/mm ²] | Design verification $\sigma_{ult,Ed} / \sigma_{ult,Rd}$ [-] |
|-----------------|---|---|
| Flange 1 | 195 | 0.82 |
| Flange 2 | 171 | 0.74 |

5.4.2 Friction connection

The characteristic loads for the top of tower can thus be simplified as in Table 5.4, which are used as input for the Excel-Tool. The values become designed automatically by the Excel-Tool.

Table 5.4: Extreme characteristic loads at the top of tower

| | Height | F _x | F _y | F _z | F _r | M _x | M _y | M _z | M _r |
|-----------------|--------|----------------|----------------|----------------|----------------|----------------|----------------|----------------|----------------|
| | mm | kN | kN | kN | kN | kNm | kNm | kNm | kNm |
| Flange 1 | 21170 | -598,7 | -6,8 | -1079,5 | -1079,5 | 1480,7 | -1665,4 | -1021,4 | 1994 |

In a first step the global stresses at the tower tube are calculated. So, the maximum design stress in the tower shell becomes:

$$\sigma_{ult,Ed} = \frac{N_{Ed}}{A_i} + \frac{M_r}{W_i} + \frac{V_{y,Ed} \cdot s_x}{I_{xx} \cdot t} + \frac{M_T}{W_T}$$

with

M_r, F_Z Extreme design loads at height of connection i
 W_i, A_i Cross section resistances of tower tube at height of connection i

This leads to the following maximum tensile stresses in the tower shell

$$\text{Connection 1: } \sigma_{ult,Ed} = 111 \text{ N/mm}^2$$

5.4.2.1 Geometry of friction connection

A sketch of the clamping package geometry is given in Figure 5.13.

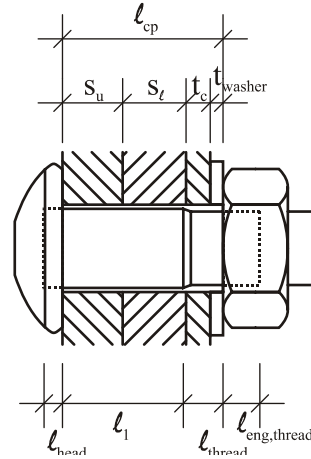


Figure 5.13: Dimensions of friction connection

The tower is made of steel S460. For the tower joint pre-loaded high-strength friction grip bolts of type M42 12.9 are used. The dimensions of the clamping packages are summarized in Table 5.5. The number of required bolts and bolt-rows is determined within the next chapter.

Table 5.5: Dimensions of friction connection

| Detail | Connection 1 [mm] |
|--|----------------------|
| Shell thickness upper tower shell s_u | 40 |
| Shell thickness lower tower shell s_l | 40 |
| Thickness of cover plate t_c | 8 |
| Diameter of bolt whole d_0 | 45 |
| Nominal diameter of bolt shank d | 42 |
| Outside diameter of the plane head bearing surface of the bolt d_w | 71 |
| Thickness of washer t_{washer} | 4 |

5.4.2.2 Ultimate limit state

The static resistance at the Ultimate Limit State can be defined as the slip resistance of friction connection on the one hand (which is critical both in pressure and tension) and the yield resistance of the finger (net shell cross section) on the other hand.

As dead weight components add to the bending effect, the highest design loads are found in the compressed zone. In tension the unfavourable effects of negative transversal strains were found to have only little effect on the resistance. By symmetry it can be assumed that the positive transversal strains will not have a significant influence either. Thus it is a slightly conservative but reasonable design assumption to consider loads from the compressed zone of the connection and resistance from the tensile zone.

Assuming that the longitudinal stresses are uniformly distribution over the shell segment width c , the design resistance of the friction joint is given by the minimum

value of maximum slip resistance of the friction connection and the cross sectional resistance of the segment finger (net cross section of shell).

From this follows a maximum allowable stress $\sigma_{ult,Rd}$ in the gross cross section of the tower shell of

$$\sigma_{ult,Rd} = \min \left\{ \frac{n_s \cdot \mu \cdot k_s \cdot F_{p,C}}{c \cdot s \cdot \gamma_{M3}}; \frac{c - d_0}{c} \cdot \frac{f_{y,shell}}{\gamma_{M0}} \right\}$$

with n_r : number of bolts per slotted hole

μ : slip factor

k_s : reduction factor for long slotted holes taken as $k_s = 0.63$
from preliminary small scale tests

$F_{p,C}$: characteristic preload force in bolt taken as $F_{p,C} = \frac{0.7 \cdot f_{ub} \cdot A_s}{\gamma_{M7}}$

c : width of shell segment (belonging to one bolt row)

s : shell thickness

d_0 : diameter of bolt hole and width of finger cut, resp.

$f_{y,shell}$: characteristic yield strength of tower shell material

γ_{M0} : partial factor taken as $\gamma_{M0} = 1.0$

γ_{M3} : partial factor taken as $\gamma_{M3} = 1.25$

γ_{M7} : partial factor taken as $\gamma_{M7} = 1.1$

Table 5.6 and

Table 5.7 summarize the results for different slip factors for the contact surface in the friction joint. The connections are optimized for the extreme loads given in Table 5.4.

Table 5.6: Ultimate resistance of friction connection 1; Contact surface painted with zinc primer

| <u>Zinc coating</u> → $\mu = 0.45$ | Connection 1 |
|--|---------------------|
| Number of slotted holes n_s | 56 |
| Number of bolts per slotted hole n_r | 5 |
| Number of bolts in connection | 280 |
| Diameter of tower D [mm] | 3915 |
| Width of shell segment c [mm] | 211.24 |
| Net width of shell segment $c_{net} = c - d_0$ [mm] | 166.24 |
| Cross section reduction due holes and cuts c_{net} / c | 0.79 |
| Max slip resistance at ULS [N/mm ²] | 115 |
| Max allowable stress in gross cross section [N/mm ²] | 279 |
| Ultimate resistance of connection $\sigma_{ult,Rd}$ [N/mm²] | 115 |

Table 5.7: Ultimate resistance of friction connection 1; Tower shell made of weathering steel

| <u>Weathering steel</u> $\rightarrow \mu = 0.79$ | Connection 1 |
|--|---------------------|
| Number of slotted holes n_s | 56 |
| Number of bolts per slotted hole n_r | 3 |
| Number of bolts in connection | 168 |
| Diameter of tower D [mm] | 3915 |
| Width of shell segment c [mm] | 211,24 |
| Net width of shell segment $c_{net} = c - d_0$ [mm] | 166,24 |
| Cross section reduction due holes and cuts c_{net} / c | 0.79 |
| Max slip resistance at ULS [N/mm ²] | 121 |
| Max allowable stress in gross cross section [N/mm ²] | 279 |
| Ultimate resistance of connection $\sigma_{ult,Rd}$ [N/mm²] | 121 |

6 DOOR OPENING

Openings in the tower shell are made for two reasons: for the door at the lower segment of the tower which is used for maintenance, and for ventilation usually at the lower and top segment of the tower. A possible layout for a bottom door opening is shown in Figure 6.1. Two possibilities exist for stiffening of the door opening, by adding a stiffener or by increasing the plate thickness in the area around the door opening.

Several failure modes in the ultimate limit state can develop in the area of the opening: buckling of the shell adjacent to the opening due to increased stresses and disturbed boundary conditions, compressive plastic yielding in the areas of stress concentration and tensile rupture due to occurrence of maximum principal stresses mostly above the opening. Resistance of the tower segment is reduced due to presence of the opening, see Figure 6.2. The level of reduction depends on successfulness of the stiffening.

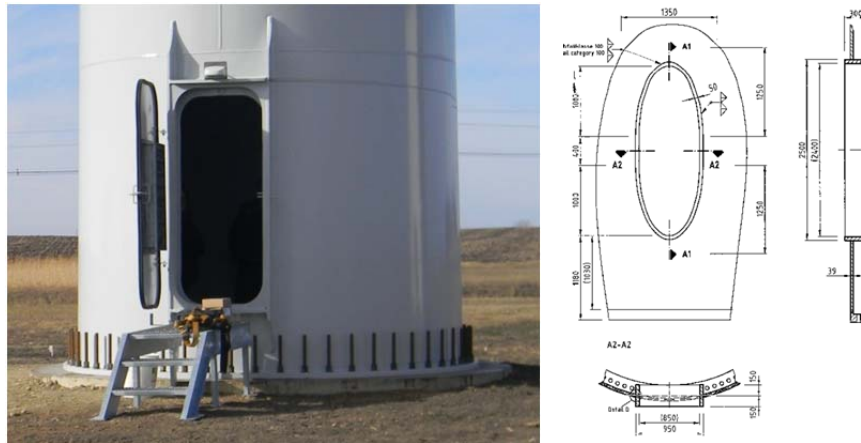


Figure 6.1: Typical layout of the door opening in the lower segment of the tower shell.

Fatigue limit state is especially important because presence of the opening and stiffening around it imposes stress concentrations. It is supposed that stress concentrations are located around the narrow perimeter of the opening, see Figure 6.2.

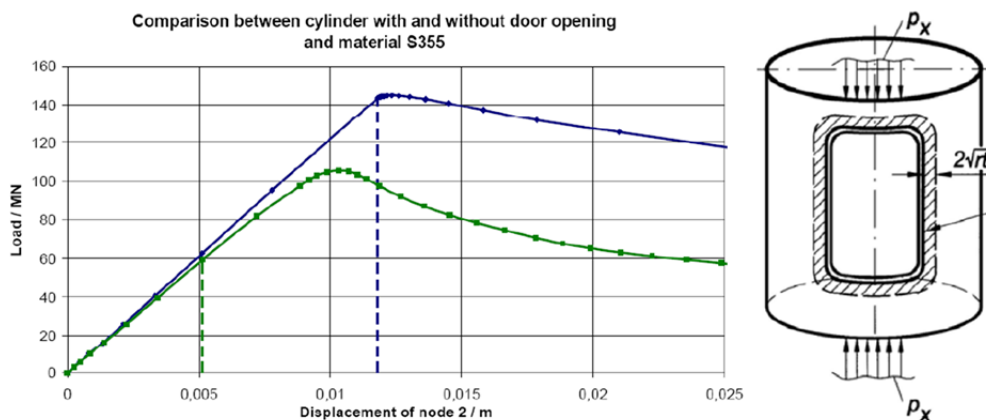


Figure 6.2: Influence of the door opening on the bending moment resistance of the connection [39].

6.1 Stability

Stress limit approach for the buckling design of the door opening region is approximate and recommendations are limited only for few simple geometry cases. Tower manufacturers usually use complicated geometry of the opening and various stiffening approaches in order to optimise the buckling and fatigue performance. Therefore, design approaches relaying on Finite Element Analysis (FEA) are used for design check of the door opening region. Two approaches, MNA/LBA and GMNIA, see section 3.2, are often used and therefore described in more details here.

6.1.1 MNA/LBA approach

MNA/LBA method is analogical to the basic general method in the Eurocode 3. Load amplification factors obtained from linear bifurcation analysis (LBA) r_{Rcr} and materially nonlinear analysis (MNA) r_{Rpl} are used to obtain the relative slenderness $\bar{\lambda}_{ov}$ of the structure zone around the opening, see Equ. (70):

$$\bar{\lambda}_{ov} = \sqrt{r_{Rpl} / r_{Rcr}} \quad (70)$$

Using MNA and LBA the boundary conditions, material properties and geometry of the structure are taken into account. The imperfections are adopted in the same manner as in the case of the stress limit approach and overall reduction factor χ_{ov} is determined following the appropriate part of the procedure shown in section 3.3. Final verification for the MNA/LBA method is made by providing the buckling resistance ratio $r_{Rd} \geq 1.0$:

$$\begin{aligned} r_{Rk} &= \chi_{ov} r_{Rpl} \\ r_{Rd} &= r_{Rk} / \gamma_{M1} \end{aligned} \quad (71)$$

6.1.2 GMNIA approach

GMNIA approach comprises all issues in one analysis: boundary conditions, material properties, geometry and imperfections.

Imperfections should be introduced in form of equivalent geometric imperfections covering: geometric imperfections in form of deviations from perfect middle surface (out of roundness, eccentricities, dimples), see Figure 6.3, irregularities near welds, material imperfections (residual stresses, inhomogeneities, etc.). The pattern of the equivalent geometric imperfections should be chosen in such a form that it has the most unfavourable effect. Often, it is hard to find the most unfavourable pattern. Therefore, the eigen-mode affine pattern from LBA can be used as initial imperfections.

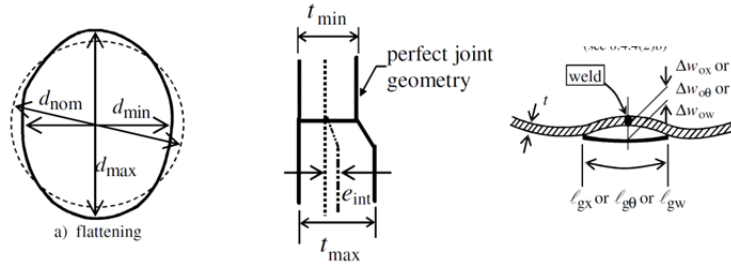


Figure 6.3: Imperfections of the tower shell.

An example of LBA of the tower shell in the door opening region is shown in Figure 6.4. For such analysis the geometry and boundary conditions needs to be properly defined. Fixed boundary conditions can be used at the bottom of the tower, while the upper cross-section of the modelled segment can be kinematically constrained to the central point which is used to apply the loads. The design loads at the top of the segment, with dominant bending action, or similar arbitrary loads, should be applied to the model in order to obtain the load amplification factors. If the design loads are applied to the model, the load amplification factors can be used for MNA/LBA approach and the eigen-mode shapes can be used as imperfections for GMNIA approach.

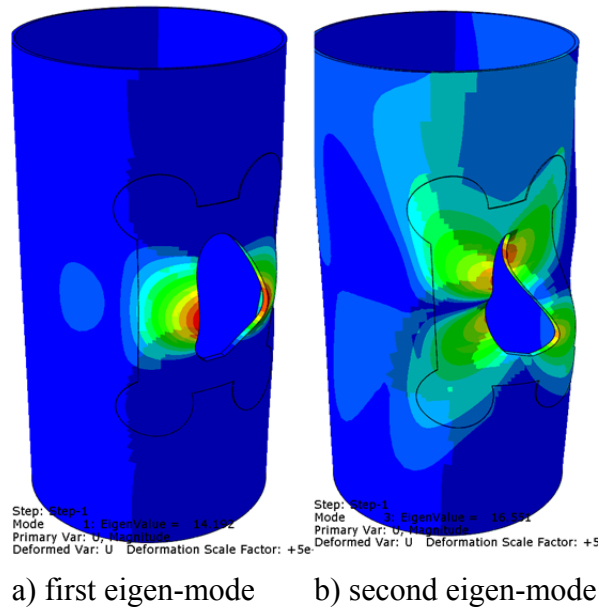


Figure 6.4: Example of LBA of the door opening region.

The amplitude of adopted equivalent geometrical imperfection is dependent on the fabrication tolerance quality class. The maximum deviation from the perfect geometry should be taken as the larger of:

$$\begin{aligned} \Delta w_{0,eq,1} &= \ell_g U_{n1} \\ \Delta w_{0,eq,2} &= n_i t U_{n2} \end{aligned} \quad (72)$$

Where:

- l_g is the relevant gauge length according to EN1993-1-6 §8.4.4(2)
- t is the local shell wall thickness,
- n_i is the multiplier to achieve an appropriate tolerance level ($n_i = 25$ is recommended by EN1993-1-6),
- U_{n1}, U_{n2} are the dimple imperfection amplitude parameters for the relevant fabrication tolerance quality class, see Table 6.1.

Table 6.1: Fabrication tolerance quality class for GMNIA

| Fabrication tolerance quality class | Description | Recommended value of U_{n1} | Recommended value of U_{n2} |
|-------------------------------------|-------------|-------------------------------|-------------------------------|
| Class A | Excellent | 0,010 | 0,010 |
| Class B | High | 0,016 | 0,016 |
| Class C | Normal | 0,025 | 0,025 |

In shell buckling analysis it is substantial to check which sign of the imperfection will produce the most unfavourable effects. According to EN1993-1-6, the sign of the equivalent geometrical imperfection form should be chosen in such manner that it will produce deformations towards the centre of the shell curvature. However, it is recommended to perform GMNIA with both negative and positive sign of the imperfection shape.

The geometrically and materially nonlinear analysis should be performed with imperfections introduced to the model in a stress-free state and the design loads should be applied. The same segment model which is used for LBA and MNA can be used but with differed analysis parameters. The material model for the shell and the stiffeners, if any, should be adopted following EC3 design rules, i.e. simple elastic-plastic material model without hardening, limited to the yield strength f_y .

For such a sophisticated analysis standard solvers based on Newton-Raphson methods experience convergence issues and usually stops before reaching the ultimate limit load. Generally, for post critical FEA, the static RIKS solvers based on arc-length method, see Figure 6.5 are mostly able to find solution during the unloading process. In more demanding cases, when the static RIKS solver also experiences convergence issues, more robust quasi-static analysis using explicit dynamic solvers can be used. Those analyses are more complicated for implementation due to influence of inertia and special care must be taken in validation of the results.

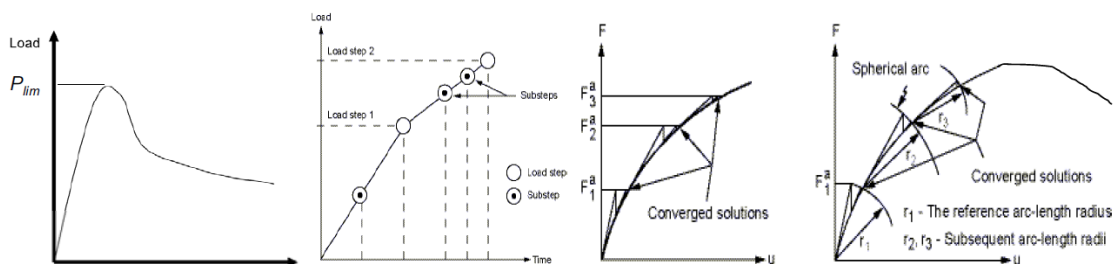


Figure 6.5: Principles of the arc-length method suitable for post critical FEA.

Once the ultimate load and the unloading path in GMNIA are obtained, the buckling verification must be performed considering several criteria. According to EN1993-1-6

following failure criteria should be traced to determine the lowest design load amplification factor $r_{R,GMNIA}$, see Figure 6.6.

- C1: The maximum load factor (limit load).
- C2: The bifurcation load factor, where this occurs during the loading path before reaching the limit load.
- C3: Load factor at the largest tolerable deformation.

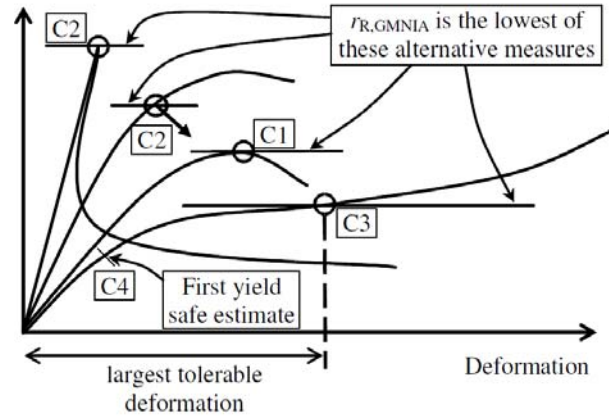


Figure 6.6: Load amplification factor criteria for GMNIA approach.

According to EN1993-1-6 the largest tolerable deformation may be considered as the greatest local rotation of the shell surface $\beta < 0.1$ in radians, in absence of more specific requirement.

Throughout the design process, the GMNIA results must be compared to the results of the analysis without imperfections GMNA and the analysis without material nonlinearity GNA in order to assure that the adopted material model and the imperfections are appropriate and give unfavourable results.

Finally, the buckling strength verification in GMNIA is obtained by providing the design buckling resistance ratio $r_{Rd} \geq 1$:

$$\begin{aligned} r_{Rk} &= k_{GMNIA} r_{R,GMNIA} \\ r_{Rd} &= r_{Rk} / \gamma_{M1} \end{aligned} \tag{73}$$

The ability of the used software and modelling technique to reliably asses true behaviour of certain structure type under specific nature of loading should be put to test. The calibration factor k_{GMNIA} is needed to take into account the reliability of the numerical model used for GMNIA. For example, by means of modelling technique the following aspects may have great influence on the results:

- Numerical method (finite element, finite strip, ...)
- Geometrical model complexity (e.g. simplified or detailed)
- Finite element type (shell, solid, linear, quadratic, ...),
- Mesh density,
- Solver type (Static, RIKS, Explicit, ...)
- Load application (imposing deformations, stresses, forces, ...),
- Boundary conditions,

- Material models (elastic, plastic, damage, ...)
- Application of imperfections,
- Assessment of results.

The calibration factor is obtained by comparison of FEA results to simple case with well-known results either from theory or tests. The simple model should be built and analysed using the same software, modelling technique, solver, etc. The calibration factor k_{GMNIA} is obtained as follows:

$$k_{GMNIA} = \frac{r_{Rk,known,check}}{r_{R,GMNIA,check}} \quad \text{or} \quad k_{GMNIA} = \frac{r_{R,test,known,check}}{r_{R,GMNIA,check}} \quad (74)$$

Where:

| | |
|--------------------------|--|
| $r_{Rk,known,check}$ | is the known characteristic value from theory, |
| $r_{R,test,known,check}$ | is the known test result, |
| $r_{R,GMNIA,check}$ | is the calculation outcome of the FEA conforming to theory case or the test. |

If the test results are used to determine k_{GMNIA} , and it exceeds 1.0 then it should be adopted as $k_{GMNIA} = 1.0$. If the established theory results are used to determine k_{GMNIA} , then the obtained value must lie inside the range: $0.8 < k_{GMNIA} < 1.2$. Otherwise, the used GMNIA procedure is considered inappropriate and other software must be used or the modelling technique needs to be improved. Once established, for the certain structure type, nature of loading, software and modelling technique, the same k_{GMNIA} can be used for further design checks using GMNIA procedure.

7 FOUNDATIONS

There are many options available for the wind tower foundations and the optimal foundation configuration is dependent on the size of the wind-turbine and site-specific geotechnical and loading conditions. The wind tower foundation structures are subjected to strong overturning moments and therefore have to exhibit sufficient resistance against compressive and uplift forces. In most cases, the wide variations between compressive and uplift (tensile) forces are dependent on the wind forces and occasionally on the horizontal seismic actions. A series of structural and geotechnical design checks are needed in order to ensure that the foundation type, size, and placement are capable of resisting the most unfavourable load combination. Within the framework of HISTWIN project, emphasis was given on the shallow foundations, which is the most commonly used foundation type for land-based wind turbines. Slab foundations consist of circular or rectangular or polygonal footings, which add vertical weight to the tower thus decreasing the eccentricity of the vertical load. The mass and dimensions of the slab are determined so that the weight of the turbine, the tower and the foundation itself are capable of resisting the overturning moment from the horizontal load on the turbine structure. Circular slab foundations are considered the most efficient structural solution for the shallow foundations, as the maximum overturning moments are likely to happen in any direction. For construction easiness, in particular to the formwork, a polygonal shape is often preferred for the slab foundation. It is worth noting that an octagonal base, with the same area of the circular foundation, is the most adequate solution.



Figure 7.1: A circular (left) and polygonal (right) slab foundation

To optimize the solution, the slab is in general tapered with a pedestal at the centre where the tower base is clamped. Anchoring of the wind turbine steel tower to the reinforced concrete pedestal by means of preloaded anchors is one of the two most commonly configurations used, the other being the embedment of the lowest course of the shell to the foundation. The two solutions are illustrated in Figure 7.2.



Figure 7.2: A foundation with the steel ring embedded in the concrete (left) and with partially prestressed anchors (right)

Figure 7.3 depicts detailing and in site arrangement of the anchors of a wind tower foundation. In this type of solution, although no special benefit is gained concerning the plastic limit state, preloading to the anchors is mandatory for the fatigue limit state, the safety requirements of which otherwise are not met by conventional anchoring. Anchors are partially prestressed, at a level of about 50%, which is a good compromise, satisfying the verifications of the anchors against fatigue in one hand and keeping the R.C. foundation local strain within the acceptable margins, on the other.

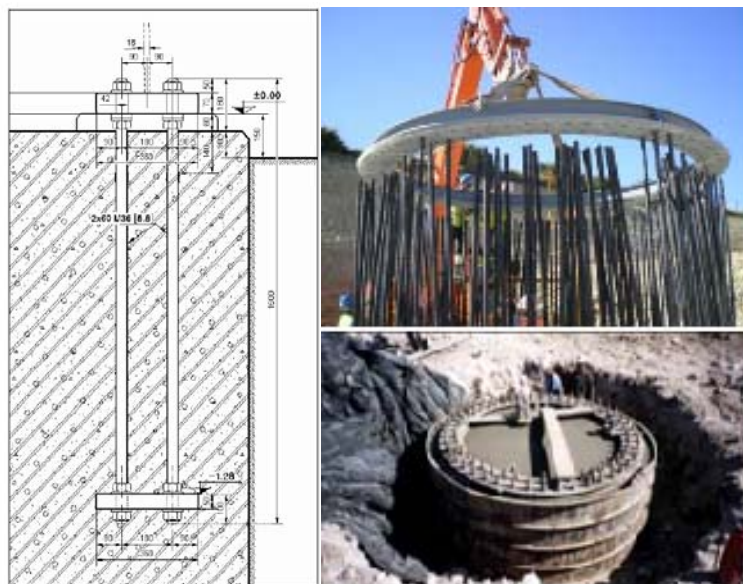


Figure 7.3: Detail to anchors (left) and in-site arrangement of anchors (right)

The anchoring system consists of a set of partially prestressed anchors at a circumferential arrangement, connecting the base plate of the tower to the circular washer plate embedded in the R.C. pedestal. The uplift forces are counterbalanced by the resistance of the embedded plate, while the shear force is delivered by the friction between the base plate and the (preferably non-shrink) grout, at the top of the pedestal. The PE covering of the anchor body establishes the absence of any cohesion between the anchors and the concrete, allowing thus the preloading, as soon as the R.C. elements develop their full capacity.

Inevitably, the complicity of the configuration results in an equally complicated stress state and therefore a finite element model is required for the competent discretization of the foundation and the anchoring system. Furthermore, it is highly recommended that this model should be built together with the one of the tower, in order that the 2nd order effects of the later and the contribution of the soil structure interaction are properly taken into account.

7.1 Finite element structural foundation models

Within HISTWIN Project, FE models for both foundation types have been developed. The structural design is based on nonlinear analysis [GMNA], due to the presence of non-linear elements (unilateral contact and cable type elements).

7.1.1 Modelling of the foundation in case of partially prestressed anchors

In the FE structural model of the foundation with partially prestressed anchors, the foundation, including the non-shrink mortar to the top of pedestal, are modeled by means of brick elements, as depicted in Figure 7.4. The footing is supported to the ground via unilateral contact elastic springs, having a constant per area unit equal to the soil subgrade reaction modulus. Corresponding horizontal springs are necessary for the global equilibrium of the structure.

The base plate is rigidly attached to the shell of the tower and it is connected to the non-shrink mortar elements through unilateral contacts with friction links. The embedded in the interior of the pedestal washer plate is modeled using plate elements. The washer plate is connected to the superjacent concrete elements through unilateral contact conditions. The partially prestressed anchors are linear elements of cable type, active in tension only. Each anchor is represented by a single element, attached solely to the two steel flanges, excluding any connection to the concrete and the non-shrink mortar. The partially prestressed anchors are linear elements of cable type, active in tension only. Each anchor is represented by a single element, attached solely to the two steel flanges, excluding any connection to the concrete and the non-shrink mortar.

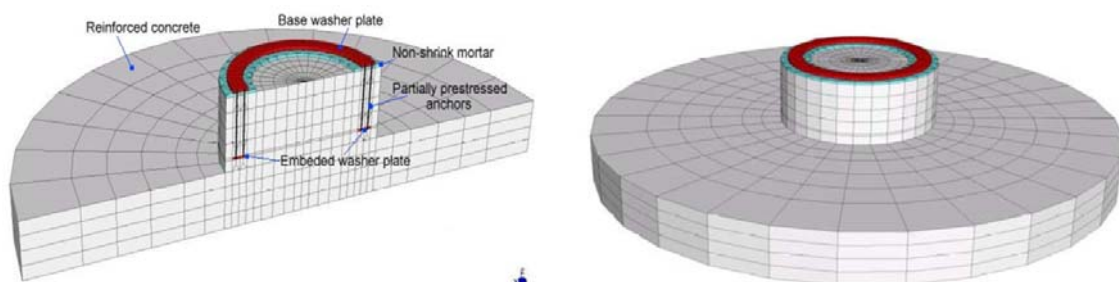


Figure 7.4: Cross section of the foundation FE model (left) and the foundation FE model (right)

Regarding the direct estimation of the anchor forces by hand calculation, such a task is practically not feasible, since the position of the neutral line of the anchoring system can be determined only with the introduction of the elasticity conditions, which requires an iterative calculation procedure. A less accurate assessment of the anchor forces can be

achieved with the aid of a simpler Finite Element model, including only the bottom flanges (with unilateral elastic support) and the anchors (see Figure 7.5).

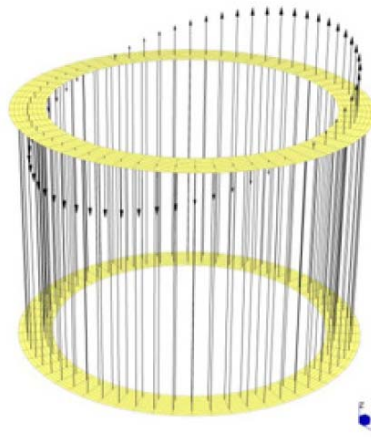


Figure 7.5: Alternative FE model for the estimation of anchor forces

For the design of the foundation – anchoring system, the verification should cover all of the following structural components, also depicted in Figure 7.6:

- Washer and base plates (Von Misses stresses)
- Prestressed anchors (tensile forces)
- Non-shrink mortar (compressive and shear stresses)
- Concrete (compressive, shear and punching shear stresses)
- Reinforcement bars
- Rigid body equilibrium for the structure.

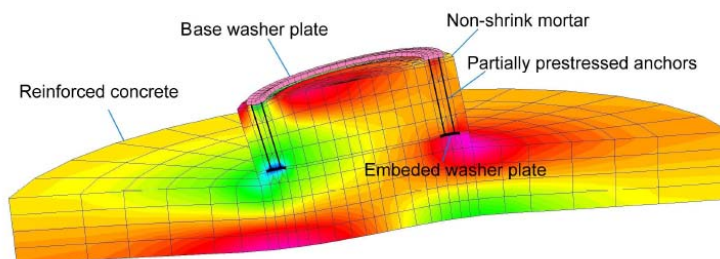


Figure 7.6: Structural components of FE foundation model

7.1.2 Modelling of the foundation in case of embedding the tower to the concrete

In the FE structural model of the foundation in case of embedding the tower to the concrete, the foundation is modeled again using brick elements, as shown in Figure 7.7. In the position where the shell elements of the tower are inserted to the concrete, there is a small gap left between the embedded shell elements and the brick elements of the foundation. The connection is performed through unilateral contact with friction elements. The overall system is assumed to be elastically supported to the foundation base, taking account of the soil-structure interaction. The foundation has been introduced by means of brick elements, elastically supported to the ground, through unilateral contact and friction conditions.

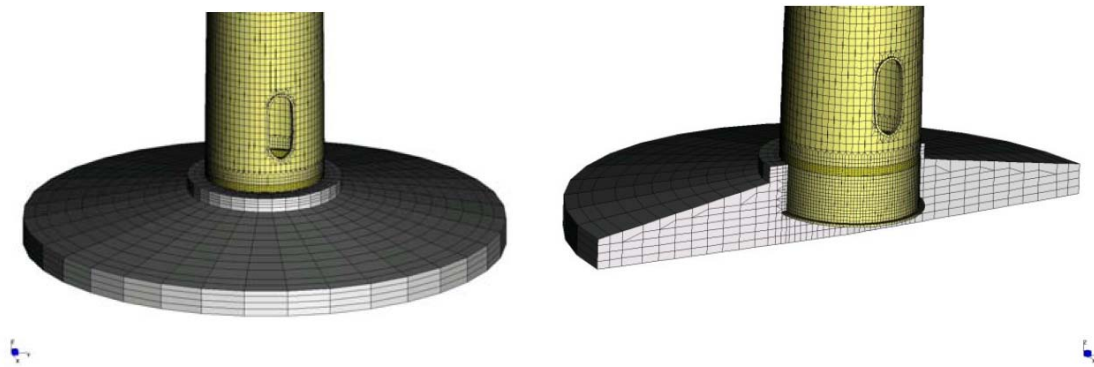


Figure 7.7: Model of the embedded tower to the foundation

7.2 Design of shallow foundations

For the design of shallow circular foundations the following checks in order to access about the foundation stability and resistance should be considered:

- Pressure on the foundation for non-factored loads – in this verification it is estimated the maximum applied stress in the base of the foundation (circular foundation).
- Verification of the compressed area - for characteristics loads, at least 50% of the base area must be compressed which can be fulfilled when $e < 0.59R$. This verification is only applied to the wind action.
- Limit state of equilibrium according to EC7-1 - in this verification it is checked if the resistant bending moment due to the vertical forces is enough to ensure about the equilibrium of the foundation when subjected to the overturning moment [47].
- Soil bearing capacity according to EC7-1 - in this case it is guaranteed that the maximum applied pressure in the base of the foundation is lower than the bearing capacity of the soil. This verification is considered for three types of combinations according to the EC7-1 (ULS-GEO, ULS-STR and accidental combination for seismic loads) [47].
- Soil bearing capacity according to EC8-5 - this part of Eurocode (Annex F) presents a formulation for foundation stability taking into account the soil inertia (kinematic effect) [48]. In reference Seismic Assessment and Improvement of building foundations is presented that the drained response is much more sensitive to inertia loading than undrained one.
- Soil bearing capacity according to DNV for extremely eccentric loading – This verification reflects the failure of the soil under the unloaded part of foundation area (Rupture 2) [49].
- Base sliding – it is checked that the friction resistant forces between the base of the foundation and the soil beneath (related to the vertical forces) are higher than the acting horizontal forces on the tower and turbine structures. In this verification, the torsional contribution of M_z is also considered.

Safety factors are defined in EC7-1 [47]. The vertical dead loads (mass and self-weights) and the load cases are usually defined directly from the load cases presented by

the technical specifications of the turbine manufacturer. For the safety verifications of the foundation, the loads are reduced to the base of the foundation.

The flowchart of the foundation design (geotechnical & structural & connection) is presented in Figure 7.8.

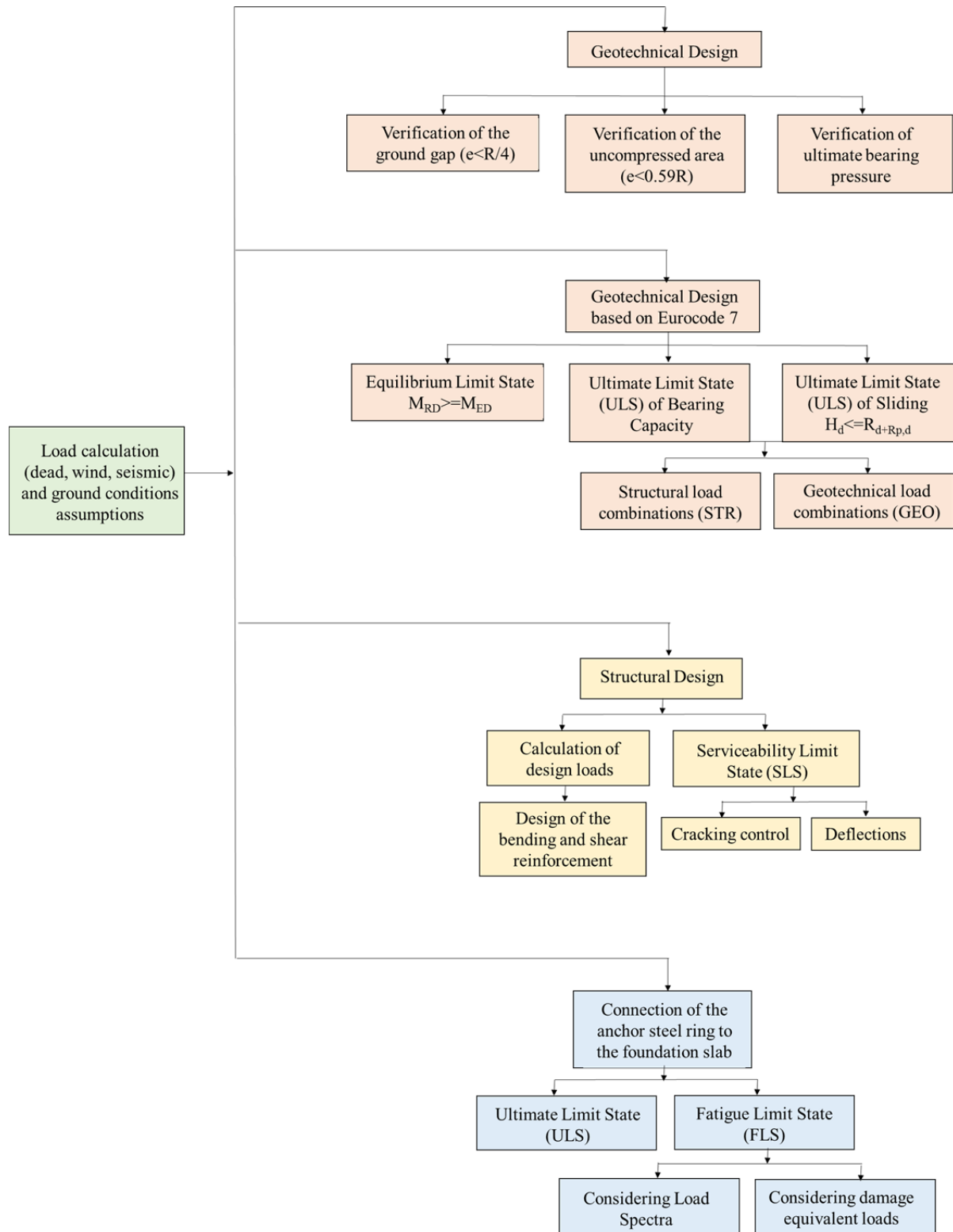


Figure 7.8: Flowchart of foundation design

7.3 Numerical example of the foundation for the MM92 evolution – 80 m wind turbine

7.3.1 Introduction

This part presents the analysis and design of the foundation for the MM92 evolution wind turbine, for a 80 m hub height. It is based on the following documents:

- T-2.9-TT.00.26-A-E – REpower MM92 – Specifications for foundation design. Tower with 80.00 m Hub Height. Rotor Blades LM45.3p RE45.2. Wind Zone III DIBt (2004) and class 2a, IEC, 07.09.2007 [50]
- V-1.1-FG.00.00-A-(F) – “General Specifications for the Design of Onshore-Foundations”, REpower Systems AG, 14.10.2008 [50]

An optimized solution is sought, given the design specifications provided by REpower. Geotechnical design is also checked using the specifications from Eurocode 7 [47], for a given type of ground conditions. Once a geometric solution was achieved, the structural design was performed, based on Eurocode 2 and RSAEEP codes. The corresponding results are presented in this part.

Given the type of loading, the most efficient structural solution is a circular shallow foundation. Regarding construction easiness, in particular formwork, a polygonal shape is often preferred. An octagonal base, with the same area of the circular foundation is the most adequate solution. Figure 7.9 presents the geometry of such a foundation.

Due to past difficulties in similar works, and also considering Repower’s specifications concerning minimum concrete type to use in the zone around the anchor flange, the concreting of the foundation may be performed in three phases. After placing the steel can and all the reinforcement bars, the first concreting shall be made up to the level H1 (Figure 7.9) and shall be done with concrete C30/37. The second concreting phase, being placed immediately after the conclusion of phase 1 without any interruption of the concreting process, shall be performed up to level H2, with concrete C35/45, as defined on document [50]. The third concreting phase can be done two or three days after the second phase and corresponds to the height between the referred level (H2) and the top of the foundation. Before performing this concreting, the best procedures shall be done to ensure the best connection between old and new concrete. As a minimum, the surface of the old concrete must be rough and cleaned with compressed air jet.

7.3.2 Codes and regulations

The following codes and regulations were considered for the foundation design:

- IEC 61400-1:1999(E) – Wind turbine generator systems – Part 1: Safety requirements.
- EN 1990 – Basis of design for structural eurocodes
- EN 1992-1-1:2004 – Eurocode 2: Design of concrete structures – Part 1: General rules and rules for buildings.
- EN 1997-1:2004 – Eurocode 7: Geotechnical design – Part 1: General rules

- REBAP – Regulamento de Estruras de Betão Armado e Pré-esforçado
- RSAEEP – Regulamento de Segurança e Acções para Estruturas de Edifícios e Pontes

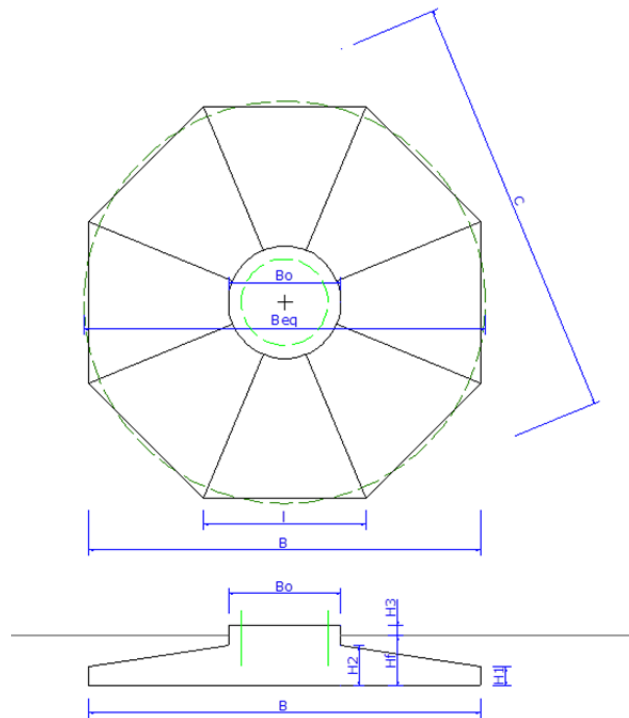


Figure 7.9: Foundation steel ring embedded in the foundation concrete slab

7.3.3 Loads

7.3.3.1 Coordinate system

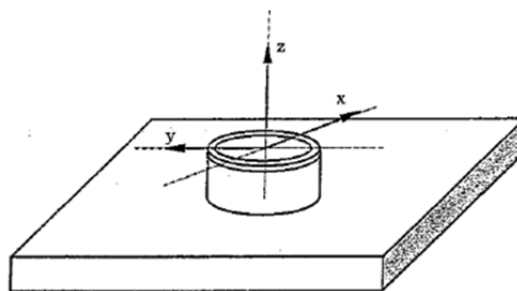


Figure 7.10: Coordinate reference system

All the loads correspond to a height indication of 2,00 m above ground level. In the subsequent safety verifications, the loads are reduced to the base of the foundation using the following expressions:

$$F_{z(b)} = |F_z| + G_{2m_tower} + G_{foundation} + G_{balast} \quad (75)$$

$$F_{res(b)} = F_{res} \quad (76)$$

$$M_{res(b)} = M_{res} + F_{res} * (2,0 + H_f) \quad (77)$$

7.3.3.2 Dead loads

According the technical specifications for the MM92 – 80 system, the mass and self-weight of the tower and equipment are presented in Table 7.1.

Table 7.1: Self-weight

| Item | Mass (ton) | Weight (kN) |
|---------------------------------|--------------|----------------|
| Tower | 146,5 | 1 437,2 |
| Rotor w/ blades | 41,3 | 405,2 |
| Nacelle without rotor (Winergy) | 67,5 | 662,2 |
| Total | 255,3 | 2 504,5 |

On the following calculations, the vertical load to be considered will be obtained directly from the load cases provided by REpower [50].

7.3.3.3 Wind loads

The load cases defined by REpower [50], including dead loads, for structural and geotechnical design of the foundation are presented in

Table 7.2, Table 7.3 : Load cases, at a 2,00 m above ground surface, for geotechnical design of the foundation and

Table 7.4.

Table 7.2 : Load cases, at a 2,00 m above ground surface, for structural design of the foundation

| Case | Reference | M _{res} (kNm) | M _z (kNm) | F _{res} (kN) | F _z (kN) | γ _F | obs. |
|------|---------------|---------------------------|---------------------------|--------------------------|--------------------------|----------------|---|
| S1 | dlc1511_0_gt2 | 69 107 | 1 363 | 874 | 3 175 | Incl. | maximum reference moment (w/ γ _F =1,35) (*) |
| | dlc1511_0_gt2 | 51 530 | 1 010 | 647 | 2 352 | Excl. | associated characteristic moment (*) |
| S2 | dlc6145120E | 61 458 | 1 218 | 871 | 2 366 | Excl. | maximum characteristic moment (*) |
| | dlc6145120E | 67 473 | 1 339 | 958 | 2 603 | Incl. | associated reference moment (w/ γ _F =1,10) (*) |
| S3 | dlc6145300E | 66 970 | 1 043 | 975 | 2 495 | Incl. | maximum reference force (w/ γ _F =1,10) (*) |
| | dlc6145300E | 61 001 | 948 | 886 | 2 268 | Excl. | associated characteristic force (*) |
| S3 | dlc6145300E | 61 001 | 948 | 886 | 2 268 | Excl. | maximum characteristic force (*) |
| | dlc6145300E | 66 970 | 1 043 | 975 | 2 495 | Incl. | associated reference force (w/ γ _F =1,10) (*) |
| S4 | dlc1624352_e | 27 366 | 6 476 | 276 | 3 010 | Incl. | maximum reference torsion (w/ γ _F =1,35) (*) |
| | dlc1624352_e | 20 610 | 4 797 | 204 | 2 230 | Excl. | associated characteristic torsion (*) |
| S5 | dlc1624352_e | 10 084 | 5 482 | 130 | 2 376 | Excl. | maximum characteristic torsion (**) |
| | dlc1624352_e | 10 962 | 6 030 | 143 | 2 614 | Incl. | associated reference torsion (w/ γ _F =1,10) (**) |

(*) Rotor blade: LM45.3p (**) Rotor blade: RE45.2

Table 7.3 : Load cases, at a 2,00 m above ground surface, for geotechnical design of the foundation

| Case | Standard | Combination | Reference | $M_{res,k}$ (kNm) | $F_{res,k}$ (kN) | $ F_{z,k} $ (kN) | Safety factors to be applied γ_F |
|------|----------|-------------|-------------|----------------------|---------------------|---------------------|--|
| G1 | DIBt | DIBt caso 1 | dlc6145352C | 55 159 | 768 | 2 145 | 1,35 |
| G2 | | DIBt caso 3 | dlc6145120E | 61 458 | 871 | 2 366 | 1,10 |

Table 7.4 : Load case, at 2,00 m above ground surface, for "ground gap" verification

| Case | Reference | $M_{res,k}$ (kNm) | $F_{res,k}$ (kN) | $ F_{z,k} $ (kN) | Safety factors to be applied γ_F |
|------|--------------|----------------------|---------------------|---------------------|--|
| G5 | "Ground gap" | 26 826 | 302 | 2 401 | 1,00 |

7.3.3.4 Seismic loads

The seismic loads were computed based on the Portuguese code (RSAEEP) considering the following conditions:

- Zone: A ($\alpha = 1,0$)
- Ground condition: Type II (from very stiff to medium stiff cohesive soils, dense non-cohesive soils)
- Damping coefficient: 0,02 (steel)
- Behaviour factor: 1,00
- Seismic action: Type 1 and Type 2

A modal response spectrum analysis was performed and the first 12 modes were determined as shown in Table 7.5.

Table 7.5 : Natural modes

| Mode | Period (Sec) | Frequency (Cyc/sec) |
|------|-----------------|------------------------|
| 1 | 2,69 | 0,37 |
| 2 | 2,69 | 0,37 |
| 3 | 0,34 | 2,96 |
| 4 | 0,34 | 2,96 |
| 5 | 0,12 | 8,43 |
| 6 | 0,12 | 8,43 |
| 7 | 0,10 | 9,87 |
| 8 | 0,06 | 16,34 |
| 9 | 0,06 | 16,34 |
| 10 | 0,04 | 26,25 |
| 11 | 0,04 | 26,25 |
| 12 | 0,03 | 34,34 |

Using the response spectra defined by RSAEP, the reactions obtained are presented in Table 7.6.

Table 7.6 : Reactions for seismic actions

| Seismic action | F _x (kN) | F _y (kN) | F _z (kN) | M _x (kN*m) | M _y (kN*m) | M _z (kN*m) | M _{res,k} (kN*m) | F _{res,k} (kN) |
|----------------|------------------------|------------------------|------------------------|--------------------------|--------------------------|--------------------------|------------------------------|----------------------------|
| Type 1 | 235 | 78 | 0 | 3 365 | 10 197 | 0 | 10 738 | 248 |
| Type 2 | 286 | 95 | 0 | 6 024 | 18 255 | 0 | 19 223 | 302 |

The load combinations with the seismic action as the leading variable action are obtained with the expression of Equ. (78):

$$S_d = G_k + 1,5 \cdot E_k + \psi_2 \cdot W_k \quad (78)$$

The loads to be superimposed to the seismic loads are defined in [50] and are listed on Table 7.7.

Table 7.7 : Design loads, to be superimposed to the seismic loads, applied 2 m above the ground surface

| Case | Reference | M _{res,k} (kNm) | F _{res,k} (kN) | F _{z,k} (kN) | Safety factors to be applied, γ_F |
|------|--------------------|-----------------------------|----------------------------|----------------------------|--|
| | Dlc_1_2s_14352.int | 30 900 | 367 | 2 497 | 1,00 |

The resulting structural design load combination is:

Table 7.8 : Design loads, for structural design, applied 2 m above the ground surface

| Case | M _{res,d} (kNm) | M _{z,d} (kNm) | F _{res,d} (kN) | F _{z,d} (kN) |
|------|-----------------------------|---------------------------|----------------------------|--------------------------|
| S6 | 59 734,34 | 0 | 819,38 | -2 497,00 |

It will be seen later that this case is not critical in the structural design.

7.3.4 Ground conditions

The ground conditions are not known at the present time, therefore the following characteristics were assumed throughout the analysis:

- Allowable pressure under the foundation: $\sigma_{adm} = 250$ kPa
- Shear strength angle: $\varphi' = 30^\circ$
- Unit weight: $\gamma = 18$ kN/m³
- Ground water table deeper than 2B
- Modulus: $40 \text{ MPa} < E_{s,dyn} < 200 \text{ MPa}$

A detailed subsurface investigation should be performed, adapted to the site conditions, in order to determine the actual ground conditions. The execution of bore-holes, with SPT tests, will provide critical data to establish a correct geological-geotechnical model. Regarding the determination of the dynamic moduli ($E_{s,dyn}$ and $G_{s,dyn}$), geophysical methods such as cross-hole wave propagation and seismic refraction techniques can be used. The later should be interpreted together with the information obtained in the bore-holes.

7.3.5 Geometry

Several different foundation configurations were studied. Table 7.9 presents some of them. The adopted solution corresponds to Model 3. The safety verifications were performed with a circular equivalent foundation, with diameter B_{eq} (see Table 7.10). The concrete unit weight is 25 kN/m^3 , whilst the ballast's placed on top the foundation weight is 18 kN/m^3 . No water pressure was considered.

Table 7.9 : Geometry of the models considered

| Model | H_f (m) | H_1 (m) | H_2 (m) | H_3 (m) | B_0 (m) | B (m) | C (m) | l (m) | B_{eq} (m) | $V_{concrete}$ (m^3) | $V_{ballast}$ (m^3) |
|-------|--------------|--------------|--------------|--------------|--------------|------------|------------|------------|-----------------|------------------------------------|-----------------------------------|
| 1 | 2,50 | 0,95 | 2,00 | 0,00 | 5,60 | 16,80 | 18,18 | 6,96 | 17,25 | 348 | 120 |
| 2 | 2,00 | 0,95 | 1,50 | 0,00 | 5,60 | 18,00 | 19,59 | 7,73 | 18,59 | 337 | 70 |
| 3 | 2,00 | 0,95 | 2,00 | 0,50 | 5,60 | 17,00 | 18,40 | 7,04 | 17,50 | 357 | 134 |
| 4 | 1,50 | 0,95 | 1,50 | 0,50 | 5,60 | 18,10 | 19,59 | 7,49 | 18,59 | 338 | 81 |
| 5 | 2,00 | 2,00 | 2,00 | 0,50 | 5,60 | 16,60 | 17,97 | 6,88 | 17,05 | 469 | 0 |
| 6 | 1,00 | 1,00 | 1,00 | 0,50 | 5,60 | 20,00 | 21,65 | 8,28 | 20,54 | 344 | 0 |

Table 7.10 : Geometry of the adopted foundation (model 3)

| | |
|---------------------------------------|---------------|
| $n =$ | 8 |
| $\theta (^{\circ}) =$ | 22,5 |
| $B \text{ (m)} =$ | 17,00 |
| $C \text{ (m)} =$ | 18,40 |
| $B_{eq} \text{ (m)} =$ | 17,46 |
| $H_f \text{ (m)} =$ | 2,00 |
| $H_1 \text{ (m)} =$ | 0,95 |
| $H_2 \text{ (m)} =$ | 2,00 |
| $H_3 \text{ (m)} =$ | 0,50 |
| $B_0 \text{ (m)} =$ | 5,60 |
| $l \text{ (m)} =$ | 7,04 |
| $A \text{ (m}^2\text{)} =$ | 239,42 |
| $A' \text{ (m}^2\text{)} =$ | 22,17 |
| $V_{concrete} \text{ (m}^3\text{)} =$ | 356,82 |
| $W_f \text{ (kN)} =$ | 8 920 |
| $V_{ballast} \text{ (m}^3\text{)} =$ | 134,33 |
| $W_{ballast} \text{ (kN)} =$ | 2 418 |
| $W_f + W_b \text{ (kN)} =$ | 11 338 |

For this geometry, the loads at the base of the foundation, for the different load combinations to be used on the geotechnical foundation design are presented in Table 7 11.

Table 7.11 : Characteristic values of the loads at the foundation base (model 3)

| Case | Reference | $M_{res(b)}$ (kNm) | $F_{res(b)}$ (kN) | $ F_{z(b)} $ (kN) | Safety factors to be applied γ_F |
|------|-------------|-----------------------|----------------------|----------------------|--|
| G1 | dlc6145352C | 58 230,89 | 767,99 | 13 482,88 | 1,35 |
| G2 | dlc6145120E | 64 941,79 | 870,93 | 13 704,33 | 1,10 |
| G5 | Ground gap | 28 034,85 | 302,16 | 13 739,56 | 1,35 |

7.3.6 Safety verification – Geotechnical design

7.3.6.1 Verification of the ground gap

No inactive area at the base of a gravity foundation is admissible for the tower moment specified by REPower. No safety factors have to be applied. It has to be proven that the eccentricity of the total vertical load (turbine, foundation slab, pedestal, ballast, etc) due to the tower moment for a circular foundation is

$$e < R/4 \quad (79)$$

7.3.6.2 Verification of the uncompressed area

For the unscaled ultimate loads ($\gamma_F=1,0$) not more than 50% of the base may be without compression. No safety factors have to be applied. It has to be proven that the resultant of all forces (tower moment, turbine, foundation slab, pedestal, ballast) is within a circle such that for circular bases

$$e < 0,59 * R \quad (80)$$

7.3.6.3 Soil bearing pressures for circular bases

- Ultimate bearing pressure at the edge of the foundation for the unfactored loads:

$$\sigma_{\max} = K * |F_{z(b)}| / (\pi * R^2) \quad (81)$$

where K is a coefficient obtained from Figure 7.11.

- Ultimate average bearing pressure for the unfactored loads:

$$\sigma_{\text{med}} = |F_{z(b)}| / A_{\text{eff}} \quad (82)$$

where

$$\alpha = 2 * \arccos(e / R) \quad (83)$$

$$A_{\text{eff}} = R^2 * (\alpha - \sin \alpha) \quad (84)$$

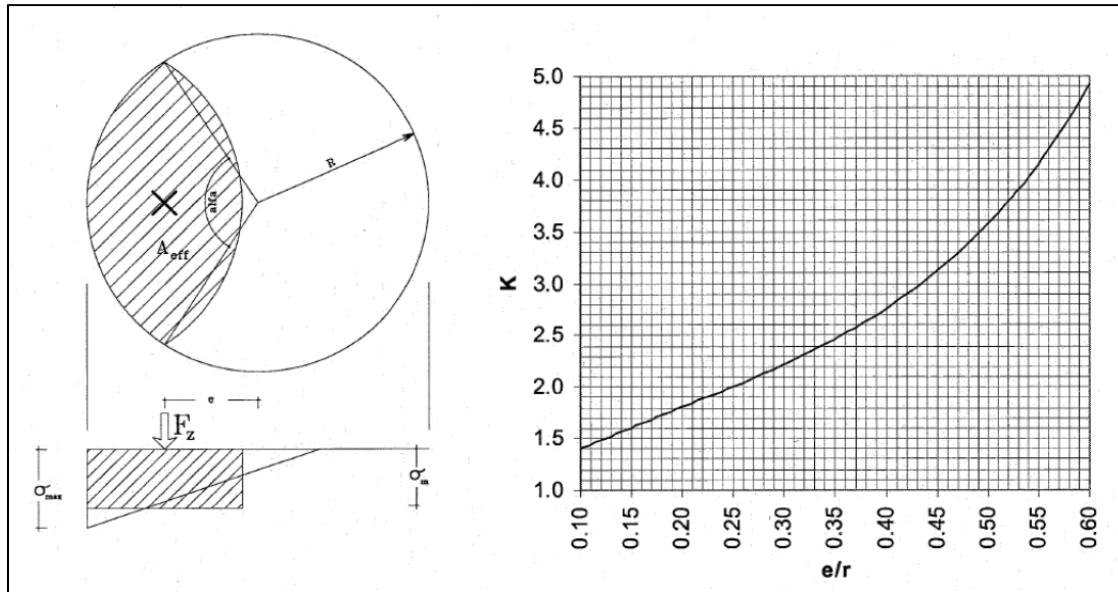


Figure 7.11: Soil bearing pressure distributions [50]

7.3.6.4 Results

The results from the safety verifications presented in the previous points are presented on Table 7.12.

Table 7.12 : Results from the safety verification (model 3)

| Case | Reference | e (m) | e/R | e/R <0.25 ? | e/R <0.59 ? | K | σ_{\max} (kPa) | α (°) | A_{eff} (m ²) | σ_{med} (kPa) |
|------|-------------|----------|------|-------------------|-------------------|-----|--------------------------|-----------------|---------------------------------------|--------------------------------|
| G1 | dlc6145352C | 4,32 | 0,49 | | OK | 3,5 | 197 | 120,7 | 95,01 | 142 |
| G2 | dlc6145120E | 4,74 | 0,54 | | OK | 4,0 | 229 | 114,2 | 82,47 | 166 |
| G5 | Ground gap | 2,04 | 0,23 | OK | | 1,9 | 109 | 153,0 | 168,82 | 81 |

7.3.6.5 Parametric study of the geometry

A parametric study of the geometry, guaranteeing the safety of the previous points, was undertaken and the results are presented in Table 7.13. The maximum and average soil bearing pressures was computed for the most unfavourable load case, and the results are unfactored.

Table 7.13 : Results from the parametric study

| Model | H _f (m) | H ₁ (m) | H ₂ (m) | H ₃ (m) | B ₀ (m) | B (m) | C (m) | V _{concrete} (m ³) | V _{balast} (m ³) | σ_{\max} (kPa) | σ_{med} (kPa) |
|-------|-----------------------|-----------------------|-----------------------|-----------------------|-----------------------|----------|----------|--|--|--------------------------|--------------------------------|
| 1 | 2,50 | 0,95 | 2,00 | 0,00 | 5,60 | 16,80 | 18,18 | 348 | 120 | 249 | 181 |
| 2 | 2,00 | 0,95 | 1,50 | 0,00 | 5,60 | 18,00 | 19,59 | 337 | 70 | 204 | 145 |
| 3 | 2,00 | 0,95 | 2,00 | 0,50 | 5,60 | 17,00 | 18,40 | 357 | 134 | 229 | 166 |
| 4 | 1,50 | 0,95 | 1,50 | 0,50 | 5,60 | 18,10 | 19,59 | 338 | 81 | 199 | 141 |
| 5 | 2,00 | 2,00 | 2,00 | 0,50 | 5,60 | 16,60 | 17,97 | 469 | 0 | 247 | 178 |
| 6 | 1,00 | 1,00 | 1,00 | 0,50 | 5,60 | 20,00 | 21,65 | 344 | 0 | 146 | 104 |

7.3.6.6 Geotechnical design according to Eurocode 7

In this section, the design according to EC7 is presented, for the ground conditions specified earlier. The characteristic values of the loads were already set in For this geometry, the loads at the base of the foundation, for the different load combinations to be used on the geotechnical foundation design are presented in Table 7.11.

Table 7.11.

7.3.6.6.1 Load combinations

The partial safety coefficients adopted by EC7 are the following:

Table 7.14 : Partial factors adopted by EC7

| | Verification | Actions (γ_F) | | | |
|-------------------------|--------------|-----------------------------|------------|----------------------------|------------|
| | | Permanent (γ_{gi}) | | Variable (γ_{qi}) | |
| | | Unfavourable | Favourable | Unfavourable | Favourable |
| Equilibrium Limit State | EQU | 1,10 | 0,90 | 1,50 | 0,00 |
| Ultimate Limit State | STR | 1,35 | 1,00 | 1,50 | 0,00 |
| | GEO | 1,00 | 1,00 | 1,30 | 0,00 |

For the combination values, we will consider the actions $F_{res,k}$ and $M_{res,k}$ as variable and unfavourable and the vertical action $F_{z,k}$ as permanent and favourable.

7.3.6.6.2 Equilibrium Limit State

For the equilibrium limit state combination the adopted values are $\gamma_{gi}=0,90$ for $F_{z,k}$ and $\gamma_{qi}=1,50$ for $F_{res,k}$ and $M_{res,k}$. The resulting values are shown in Table 7.15.

Table 7.15 : Equilibrium Limit State design values

| Case | Reference | $M_{res,Ed}$ (kNm) | $F_{res,Ed}$ (kN) | $ F_{z,Ed} $ (kN) |
|------|-------------|-----------------------|----------------------|----------------------|
| G1 | dlc6145352C | 87 346,34 | 1 151,99 | 12 134,59 |
| G2 | dlc6145120E | 97 412,69 | 1 306,40 | 12 333,90 |

The following inequality shall be satisfied for the equilibrium limit state,

$$M_{Rd} \geq M_{Ed}$$

$$|F_{z,Ed}| * B / 2 \geq M_{Ed} \quad (85)$$

where B is the distance between 2 opposite corners (B=17,50m).

Table 7.16 : Equilibrium Limit State verification

| Case | Reference | $M_{res,Ed}$ (kNm) | $ F_{z,Ed} * B/2$ (kNm) |
|------|-------------|-----------------------|-----------------------------|
| G1 | dlc6145352C | 87 346,34 | 106 177,68 |
| G2 | dlc6145120E | 97 412,69 | 107 921,60 |

The Equilibrium Limit State is verified.

7.3.6.6.3 Ultimate Limit State of Bearing Capacity

The bearing capacity has to be verified for the structural (STR) and geotechnical (GEO) cases. The design material properties are presented in Table 7.17.

Table 7.17 : Design soil properties

| | Characteristic values | STR | | GEO | |
|----------------------------------|-----------------------|------------|---------------|------------|---------------|
| | | γ_M | Design values | γ_M | Design values |
| $\phi' (^{\circ})$ | 30 | 1,0 | 30 | 1,25 | 24,8 |
| $c' \text{ (kPa)}$ | 0 | 1,0 | 0 | 1,0 | 0 |
| $\gamma \text{ (kN/m}^3\text{)}$ | 18 | 1,0 | 18 | 1,0 | 18 |

ULS - STR verification

For the ultimate limit state STR combination values the following partial coefficients were used: $\gamma_{gi}=1,00$ for $F_{z,k}$ and $\gamma_{qi}=1,50$ for $F_{res,k}$ and $M_{res,k}$. The resulting values are:

Table 7.18 : Design loads for STR bearing capacity verification

| Case | Reference | $M_{res,Ed}$ (kNm) | $F_{res,Ed}$ (kN) | $ F_{z,Ed} $ (kN) |
|------|-------------|-----------------------|----------------------|----------------------|
| G1 | dlc6145352C | 87 346,34 | 1 151,99 | 13 482,88 |
| G2 | dlc6145120E | 97 412,69 | 1 306,40 | 13 704,33 |

The load combination G2 will be analysed, since it has the largest eccentricity. The bearing capacity equation will be used, with an effective foundation with area A_{eff} , determined with Equ. (82):

$$e = M / N = 7,11m$$

$$\alpha = 2 * \arccos(7,07/8,73) = 1,2$$

$$A_{eff} = 22,36m^2$$

As seen on Figure 7.12, an equivalent rectangular foundation (2,50*8,94 m²) is adopted.

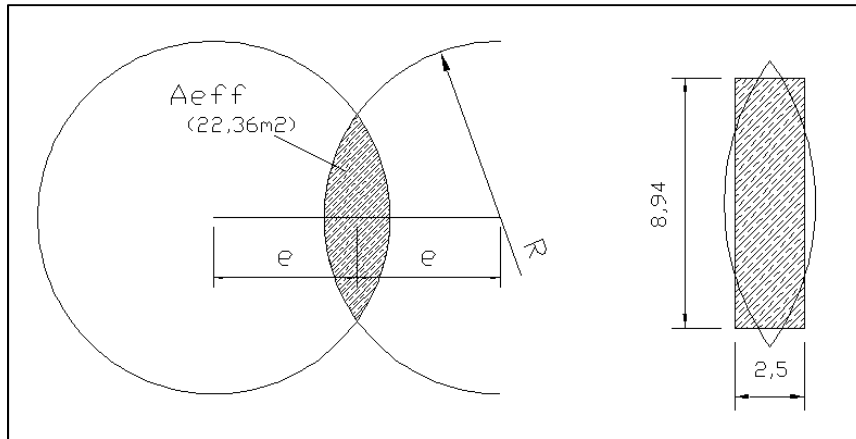


Figure 7.12: Effective area for STR load combination

The bearing capacity value, under drained conditions, is calculated with (EC7 – Annex D),

$$R_d / A_{eff} = c' N_c [s_c i_c f_c] + q' N_q [s_q i_q f_q] + 0,5 B' \gamma' N_\gamma [s_\gamma i_\gamma f_\gamma] \quad (86)$$

Dimensionless bearing resistance factors:

$$\begin{cases} N_q = e^{\pi \cdot \tan \phi'} \cdot \tan^2(45 + \phi' / 2) \\ N_c = (N_q - 1) \cdot \cot \phi' \\ N_\gamma = 2 \cdot (N_q - 1) \cdot \tan \phi'; \delta \geq \phi' / 2 \end{cases} \quad \begin{matrix} N_q = 18,40 \\ N_c = 30,14 \\ N_\gamma = 20,09 \end{matrix} \quad (87)$$

Shape factors:

$$\begin{cases} s_q = 1 + (B' / L') \cdot \sin \phi' \\ s_\gamma = 1 - 0,3(B' / L') \\ s_c = (s_q N_q - 1) / (N_q - 1) \end{cases} \quad \begin{matrix} S_q = 1,14 \\ S_c = 1,15 \\ S_\gamma = 0,92 \end{matrix} \quad (88)$$

Load inclination factors:

H acts in the direction of B' ;

$$\begin{cases} i_q = [1 - 0,7H / (V + A' \cdot c' \cdot \cot \phi')]^3 \\ i_\gamma = [1 - H / (V + A' \cdot c' \cdot \cot \phi')]^3 \\ i_c = (i_q N_q - 1) / (N_q - 1) \end{cases} \quad \begin{matrix} i_q = 0,81 \\ i_c = 0,80 \\ i_\gamma = 0,74 \end{matrix} \quad (89)$$

Using the previous results, the bearing capacity is:

$$R_d / A_{\text{eff}} = 920,43 \text{ kPa}$$

$$R_d = 20\,571,52 \geq 13\,704,33 \text{ kN}$$

Thus, the Bearing Resistance Ultimate Limit State is verified under STR combination.

ULS - GEO verification

For the ultimate limit state GEO combination values the following partial coefficients were used: $\gamma_{gi}=1,00$ for $F_{z,k}$ and $\gamma_{qi}=1,30$ for $F_{res,k}$ and $M_{res,k}$. The resulting values are:

Table 7.19 : Design loads for GEO bearing capacity verification

| Case | Reference | $M_{res,Ed}$ (kNm) | $F_{res,Ed}$ (kN) | $ F_{z,Ed} $ (kN) |
|------|-------------|-----------------------|----------------------|----------------------|
| G1 | dlc6145352C | 75 700,16 | 998,39 | 13 482,88 |
| G2 | dlc6145120E | 84 424,33 | 1 132,21 | 13 704,33 |

The load combination G2 will be analysed, since it has the largest eccentricity ($e=6,16$ m). The bearing capacity equation will be used, with an effective foundation with area A_{eff} , determined with Equ. (86).

The effective area for this load is,

$$e = M / N = 6,16 \text{ m}$$

$$\alpha = 2 * \arccos(7,07 / 8,73) = 1,6$$

$$A_{\text{eff}} = 43,81 \text{ m}^2$$

As seen on Figure 7.13, an equivalent rectangular foundation ($4,0 * 10,95 \text{ m}^2$) is adopted.

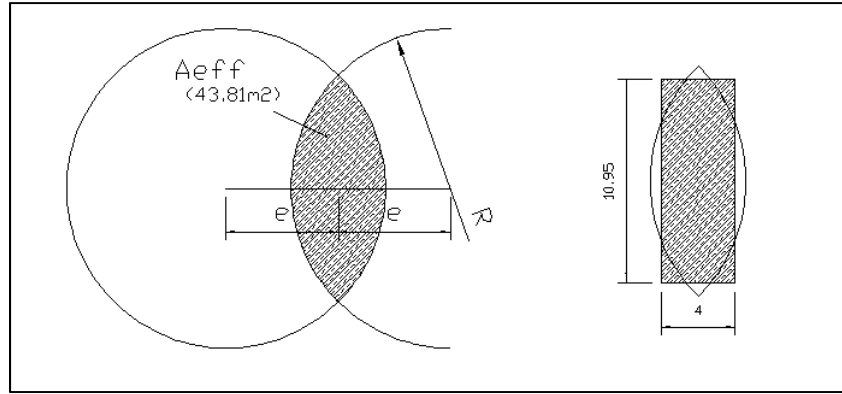


Figure 7.13: Effective area for GEO load combination

The bearing resistance capacity value, under drained conditions, is calculated with Equ. (86). The dimensionless factors:

Table 7.20 : Dimensionless factors for bearing resistance calculation

| | | | | | |
|--------------|-------|--------------|------|--------------|------|
| $N_q =$ | 10,43 | $s_q =$ | 1,15 | $i_q =$ | 0,84 |
| $N_c =$ | 20,42 | $s_c =$ | 1,17 | $i_c =$ | 0,82 |
| $N_\gamma =$ | 8,71 | $s_\gamma =$ | 0,89 | $i_\gamma =$ | 0,77 |

The bearing resistance value is,

$$R_d/A_{eff} = 577,76 \text{ kPa}$$

$$R_d = 25305,84 \text{ kN} \geq 13704,33 \text{ kN}$$

Thus, the Bearing Resistance Ultimate Limit State is verified under GEO combination.

7.3.6.6.4 Ultimate Limit State of Sliding

The following inequality shall be satisfied for the ultimate limit state of failure by sliding:

$$H_d \leq R_d + R_{p,d} \quad (90)$$

where H_d is the design horizontal load, R_d is the base sliding resistance and $R_{p,d}$ is the passive resistance of the ground. The safety against base sliding is guaranteed, on a simplified procedure, by the base friction. The passive impulse is therefore not considered.

The destabilizing force, H_d is equal to

$$H_d = F_{Res,Ed} + F_{h,t} \quad (91)$$

where the force $F_{h,t}$ is the contribution from the torsion, M_z . On a simplified method, this moment is equivalent to eight forces applied around the base centre, at a distance of $2/3R$. Each force is equal to:

$$F_{h,t} = \frac{3 \cdot M_z}{16 \cdot R} \quad (92)$$

and on the most loaded triangular sector:

$$H_d = \frac{1}{8} F_{Res,Ed} + \frac{3M_{z,Ed}}{16R} \quad (93)$$

The design shear resistance for this sector, under drained conditions is equal to:

$$R_d = \frac{|F_{z(b)}|}{8} * tg(\delta_b) \quad (94)$$

where δ_b is the design friction angle for cast-in-situ concrete foundations ($\delta_b = \varphi'$). Simplifying:

$$H_d = F_{Res,Ed} + \frac{3M_{z,Ed}}{2R} \quad (95)$$

The critical load case is G2, due to the highest horizontal force, combined with torsion.

STR Load combination

The design shear resistance, under drained conditions for the assumed soil is:

$$R_d = 13704,33 * tg(30) = 4988,24 \text{ kN}$$

The design shear force (considering $M_{z,Ed}=1,5*1217,58 \text{ kNm}$) is,

$$H_d = F_{Res,Ed} + \frac{3M_{z,Ed}}{2R} = 1306,40 + \frac{3*1826,37}{2*8,75} = 1619,49 \text{ kN} \leq R_d$$

The Ultimate Limit State of Failure Sliding is verified under STR combination

GEO Load combination

$$R_d = 13704,33 * tg(24,8) = 4066,78 \text{ kN}$$

The design shear load (considering $M_{z,Ed}=1,3*1217,58 \text{ kNm}$) is,

$$H_d = F_{Res,Ed} + \frac{3M_{z,Ed}}{2R} = 1132,21 + \frac{3*1582,85}{2*8,75} = 1403,56 \text{ kN} \leq R_d$$

The Ultimate Limit State of Failure Sliding is also verified under GEO combination.

The load case G2 is the only where the torsion has been provided, but since the safety margin is quite large, no problems are foreseen on the other load cases.

7.3.7 Safety verification - Structural design

7.3.7.1 Loads

The safety factors γ_F applied in the structural design were defined by REpower, in agreement with the standard IEC 61400-1:1999(E) (see [8]).

Table 3 – Partial safety factors for loads γ_f

| Source of loading | Unfavourable loads | | | Favourable loads |
|-------------------|--|----------|------------------------|-----------------------|
| | Type of design situation (see table 2) | | | All design situations |
| | Normal and extreme | Abnormal | Transport and erection | |
| Aerodynamic | 1,35 | 1,1 | 1,5 | 0,9 |
| Operational | 1,35 | 1,1 | 1,5 | 0,9 |
| Gravity | 1,1/1,35* | 1,1 | 1,25 | 0,9 |
| Other inertia | 1,25 | 1,1 | 1,3 | 0,9 |

* In the event of the masses not being determined by weighing.

Figure 7.14: Partial safety factors for loads, specified by standard IEC 61400-1:1999(E)

Table 7.21 : Characteristic loads, for structural design, applied 2 m above the ground surface

| Case | Reference | $M_{res,k}$ (kNm) | $ M_{z,k} $ (kNm) | $F_{res,k}$ (kN) | $ F_{z,k} $ (kN) | Safety factors to be applied γ_F |
|------|---------------|----------------------|----------------------|---------------------|---------------------|---|
| S1 | dlc1511_0_gt2 | 51 529,95 | 1 009,73 | 647,11 | 2 351,66 | 1,35 |
| S2 | dlc6145120E | 61 458,07 | 1 217,58 | 870,93 | 2 365,98 | 1,10 |
| S3 | dlc6145300E | 61 000,57 | 948,26 | 885,97 | 2 268,36 | 1,10 |
| S4 | dlc1624352_e | 20 610,43 | 4 797,16 | 204,27 | 2 229,81 | 1,35 |

Table 7.22 : Design loads, for structural design, applied 2 m above the ground surface

| Case | Reference | $M_{res,d}$ (kNm) | $ M_{z,d} $ (kNm) | $F_{res,d}$ (kN) | $ F_{z,d} $ (kN) | Applied safety factors γ_F |
|------|---------------|----------------------|----------------------|---------------------|---------------------|---|
| S1 | dlc1511_0_gt2 | 69 107,28 | 1 363,14 | 873,60 | 3 174,74 | 1,35 |
| S2 | dlc6145120E | 67 472,98 | 1 339,34 | 958,02 | 2 602,58 | 1,10 |
| S3 | dlc6145300E | 66 969,73 | 1 043,09 | 974,57 | 2 495,20 | 1,10 |
| S4 | dlc1624352_e | 27 365,93 | 6 476,17 | 275,76 | 3 010,25 | 1,35 |

Table 7.23 : Design loads, for structural design, applied at the base of the foundation

| Case | Reference | $M_{res(b),d}$ (kNm) | $ M_{z(b),d} $ (kNm) | $F_{res(b),d}$ (kN) | $ F_{z(b),d} $ (kN) | Applied safety factors γ_F |
|------|---------------|-------------------------|-------------------------|------------------------|------------------------|---|
| S1 | dlc1511_0_gt2 | 72 601,68 | 1 363,14 | 873,60 | 18 065,89 | 1,35 |
| S2 | dlc6145120E | 71 305,07 | 1 339,34 | 958,02 | 14 736,10 | 1,10 |
| S3 | dlc6145300E | 70 868,01 | 1 043,09 | 974,57 | 14 628,73 | 1,10 |
| S4 | dlc1624352_e | 28 468,97 | 6 476,17 | 275,76 | 17 901,40 | 1,35 |

7.3.7.2 Materials

The foundation is built with reinforced concrete, with the following characteristics:

- Concrete: C35/45 (on the top part of the foundation)
- Concrete C30/37 (on the bottom of the foundation)
- Steel S500

Exposure class: XC2 (Wet, rarely dry – concrete surfaces subject to long-term water contact. Many foundations).

Nominal cover: $c_{nom} = 50$ mm

7.3.7.3 Structural model

A detailed analysis of model 3 was performed using the finite element method. The code SAP2000 v.10.01 was used in this study and the mesh is depicted in Figure 7.16.

The ground reaction was introduced through bilinear springs, resisting to compression only. The stiffness of these springs was obtained using Vésic's proposal, for two values of the soil modulus ($E_{s,dyn}=40$ MPa e $E_{s,dyn}=200$ MPa). The lower value was selected considering the specified minimum rotational stiffness $K_{\theta,dyn} = 2,5E10$ N*m/rad and taking $\nu = 0,3$. The higher value (200 MPa) corresponds to a stiffer ground and the rotational stiffness is $K_{\theta,dyn}=1,5E11$ N*m/rad.

$$E_{s,dyn} = K_{\theta,dyn} \cdot \frac{3}{4} \cdot \frac{1}{R^3} \cdot \frac{(1+\nu) \cdot (1-\nu)^2}{(1-\nu-2 \cdot \nu^2)} \quad (96)$$

$$E_{s,dyn} \geq 2,5E10 \cdot \frac{3}{4} \cdot \frac{1}{8,73^3} \cdot \frac{(1+0,3) \cdot (1-0,3)^2}{(1-0,3-2 \cdot 0,3^2)} \cdot 1E-6 = 34 \text{ MPa}$$

On a similar procedure, the minimum static modulus $E_{s,stat}$, required to obtain the imposed value of $K_{\theta,stat}=0,8E4$ MN*m/rad can be computed.

$$E_{s,stat} \geq 0,8E10 \cdot \frac{3}{4} \cdot \frac{1}{8,73^3} \cdot \frac{(1+0,3) \cdot (1-0,3)^2}{(1-0,3-2 \cdot 0,3^2)} \cdot 1E-6 = 11 \text{ MPa}$$

Figure 7.15 presents the relationship between $E_{s,dyn}$ and ν for $K_{\theta,dyn} = 2,50E4$ MN*m/rad, octagonal foundation and $R=8,73$ m., and also between $E_{s,stat}$ and ν for $K_{\theta,stat} = 0,80E4$ MN*m/rad.

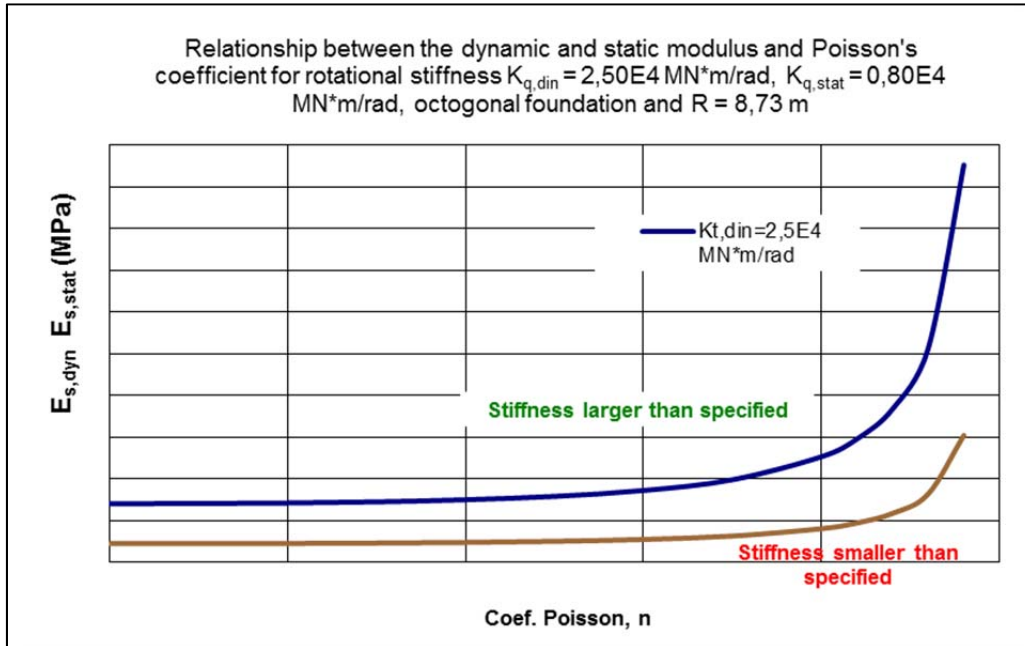


Figure 7.15: Relationship between $E_{s,dyn}$ and ν for $K_{\theta,dyn} = 2,50E4$ MN*m/rad, and $K_{\theta,stat} = 0,80E4$ MN*m/rad, octagonal foundation and $R=8,73$ m

The subgrade reaction coefficient was computed using Vésic's proposal and also the expression to compute elastic settlements of foundations. The two adopted values were $k_z=2,5 \text{ MN/m}^3$ and $k_z=13 \text{ MN/m}^3$, respectively.

$$k_z = \frac{0.65 E_s}{B(1-\nu_s^2)} \sqrt[12]{\frac{E_s B^4}{E_f I_f}} \quad (97)$$

$$k_z = \frac{E_s}{B(1-\nu_s^2) I_s} \quad (98)$$

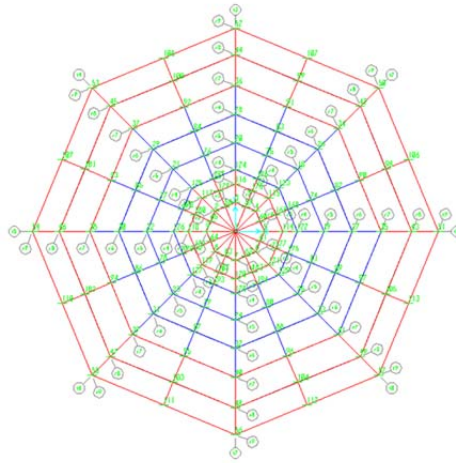


Figure 7.16: Adopted finite element model

Load definition

The most unfavorable load combinations are identified on Table 7.23 as cases S1 and S2. The moment $M_{\text{res(b)}}$ was applied through point loads, on nodes located 2,15 m from the foundation centre, with two possible orientations:

- around the x axis (S2_x);
- around the x' axis, rotated 22,5° in relation to the x axis (S1_x' e S2_x').

The vertical load F_z (Table 7.22) was distributed evenly by the 16 nodes located at 2,15 m from the foundation centre. The weight of the ballast was introduced as uniform loads on each shell element. The self-weight of the element is computed automatically. The point loads applied on each load case are presented on Table 7.24.

Table 7.24: Point loads applied on model 3

| Node | CASE S1_x' $\gamma_F = 1.35$ | | CASE S2_x' $\gamma_F = 1.10$ | | CASE S2_x $\gamma_F = 1.10$ | |
|------|------------------------------|-----------------------------|------------------------------|-----------------------------|-----------------------------|-----------------------------|
| | $F_{3,k}$ (G_S1) (kN) | $F_{3,k}$ (W_S1) (kN) | $F_{3,k}$ (G_S2) (kN) | $F_{3,k}$ (W_S2) (kN) | $F_{3,k}$ (G_S2) (kN) | $F_{3,k}$ (W_S2) (kN) |
| 114 | -146.98 | -1 687.84 | -147.87 | -2 025.39 | -147.87 | |
| 115 | -146.98 | 1 687.84 | -147.87 | 2 025.39 | -147.87 | 2 268.75 |
| 116 | -146.98 | 2 716.53 | -147.87 | 3 259.82 | -147.87 | 6 417.00 |
| 117 | -146.98 | 2 716.53 | -147.87 | 3 259.82 | -147.87 | 2 268.75 |
| 118 | -146.98 | 1 687.84 | -147.87 | 2 025.39 | -147.87 | |

| | | | | | | |
|-----|---------|-----------|---------|-----------|---------|-----------|
| 119 | -146.98 | -1 687.84 | -147.87 | -2 025.39 | -147.87 | -2 268.75 |
| 120 | -146.98 | -2 716.53 | -147.87 | -3 259.82 | -147.87 | -6 417.00 |
| 121 | -146.98 | -2 716.53 | -147.87 | -3 259.82 | -147.87 | -2 268.75 |
| 167 | -146.98 | | -147.87 | | -147.87 | 1 134.38 |
| 177 | -146.98 | -2 881.32 | -147.87 | -3 457.56 | -147.87 | -1 134.38 |
| 178 | -146.98 | 2 881.32 | -147.87 | 3 457.56 | -147.87 | 2 738.62 |
| 179 | -146.98 | 2 716.53 | -147.87 | 3 259.82 | -147.87 | 2 738.62 |
| 180 | -146.98 | 2 881.32 | -147.87 | 3 457.56 | -147.87 | 1 134.38 |
| 181 | -146.98 | | -147.87 | | -147.87 | -1 134.38 |
| 182 | -146.98 | -2 881.32 | -147.87 | -3 457.56 | -147.87 | -2 738.62 |
| 183 | -146.98 | -2 716.53 | -147.87 | -3 259.82 | -147.87 | -2 738.62 |

Analysis method: the analysis was non-linear, static, due to the non-linear springs.

7.3.7.4 Bending reinforcement

The design values of the bending moments are presented in the following figures. The local axis were aligned with the directions of the reinforcement. Thus, axis 1-1 is rotated 22,5° in relation to the x-axis. Similarly, axis 2-2 is rotated 22,5° in relation to the y-axis. The moments are presented according to the local axis (M_{11} is the moment in the direction of axis 1-1, around axis 2-2). A similar reading is valid for M_{22} . The results show that load case S2 causes higher positive M_{22} moments. The inferior face reinforcement was designed based on those values. As for the negative M_{22} moments, load case S1 is critical. Table 7.25 and Table 7.26 display the results for the bending reinforcement.

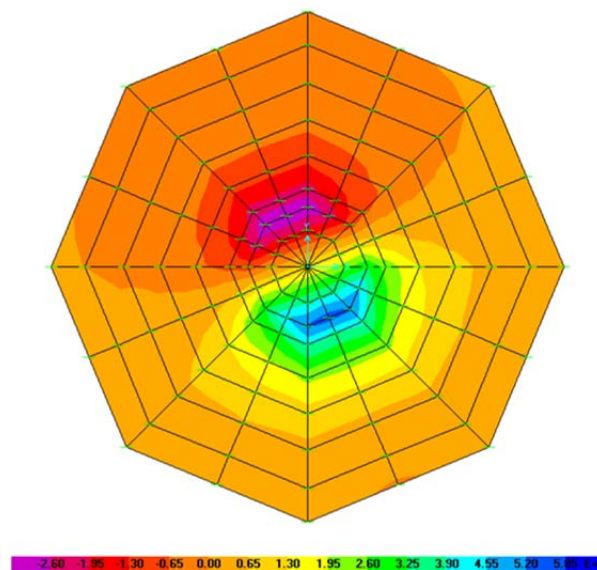


Figure 7.17: Moment M22 – Model 3_200 – S1_x'

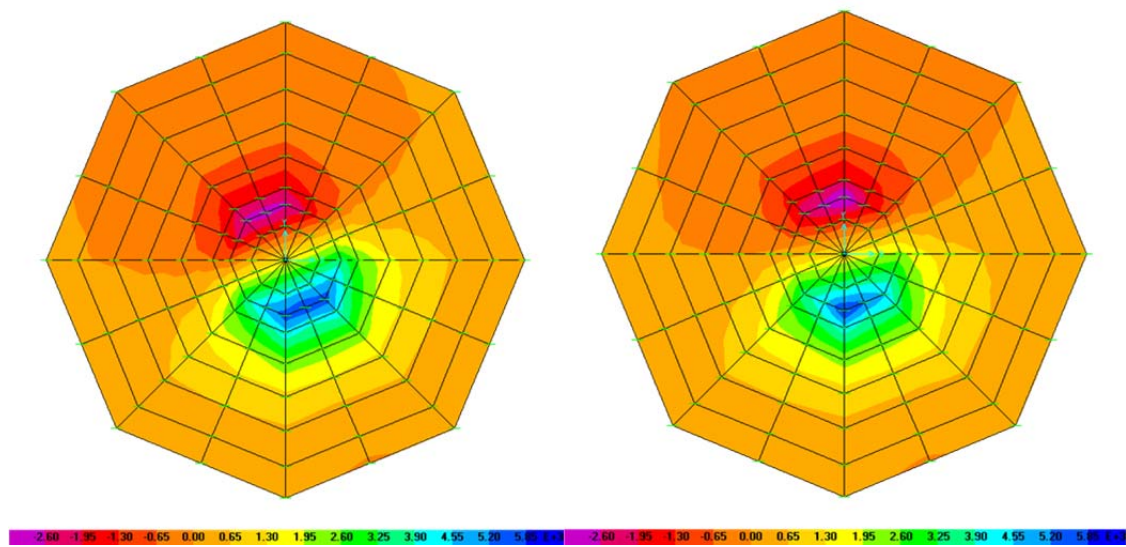


Figure 7.18: Moment M22 – Model 3_200 – S2_x' & Moment M22 – Model 3_200 – S2_x

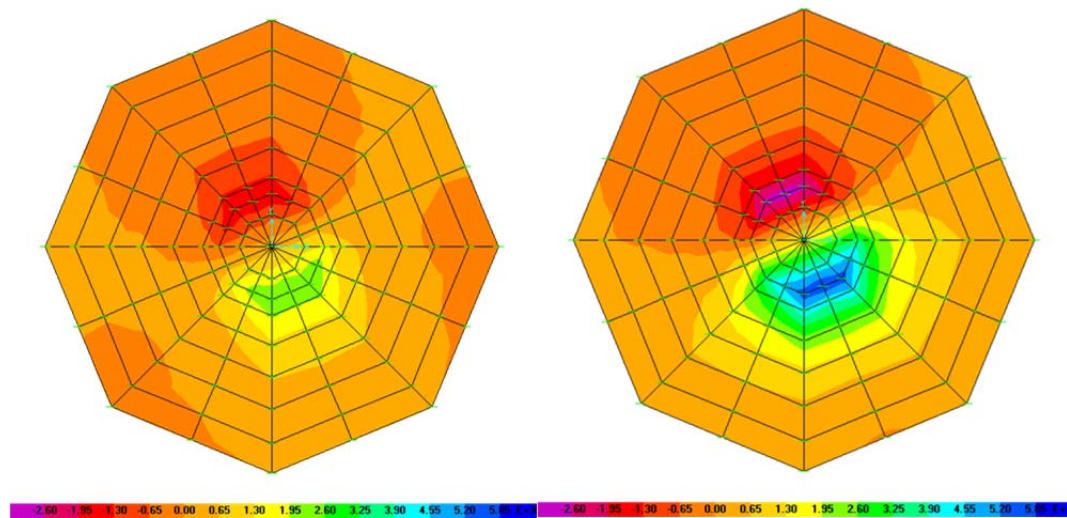


Figure 7.19: Moment M11 – Model 3_200 – S1_x' & Moment M11 – Model 3_200 – S2_x'

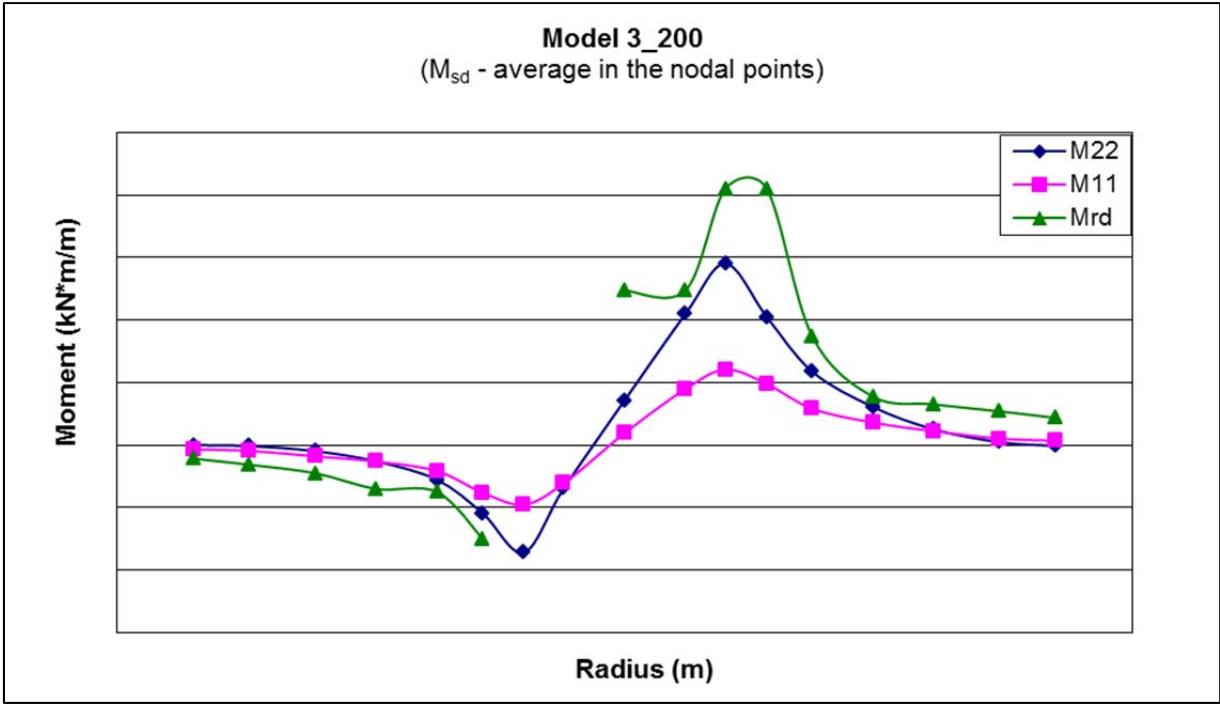


Figure 7.20: Envelope of bending moments along the y axis

Table 7.25: Design of the inferior face bending reinforcement (Model 3_200)

| r (m) | r' (m) | h (m) | M ₂₋₂ (kN*m/m) | M ₁₋₁ (kN*m/m) | A _{s-22} (cm ² /m) | A _{s-22} | A _{s-22} (cm ² /m) | M _{Rd} (kN*m/m) | A _{s-11} (cm ² /m) | A _{s-11} | A _{s-11} (cm ² /m) |
|----------|-----------|----------------|------------------------------|------------------------------|---|-------------------------|---|-----------------------------|---|-------------------|---|
| 0.00 | 0.00 | 2.50 | 1 434 | 383 | 36.66 | Φ25//0.10 | 49.09 | 4 950 | 36.66 | | |
| 1.30 | 1.20 | 2.50 | 4 200 | 1 794 | 41.09 | Φ25//0.10 | 49.09 | 4 950 | 36.66 | | |
| 2.15 | 1.99 | 2.50 | 5 800 | 2 414 | 57.21 | Φ25//0.10+Φ 32//0.24 | 82.60 | 8 200 | 36.66 | | |
| 2.80 | 2.80 | 2.00 e 2.50 | 4 105 | 1 960 | 51.70 | Φ25//0.10+Φ 32//0.24 | 82.60 | 8 200 | 29.13 | | |
| 4.00 | 3.70 | 1.80 | 2 352 | 1 165 | 32.79 | Φ25//0.10 | 49.09 | 3 480 | 25.79 | Φ25//0.10 | 49.09 |
| 5.30 | 4.90 | 1.60 | 1 219 | 721 | 22.78 | Φ25//0.20 | 24.55 | 1 550 | 22.78 | Φ25//0.20 | 24.55 |
| 6.60 | 6.10 | 1.35 | 504 | 444 | 19.02 | Φ25//0.20 | 24.55 | 1 300 | 19.02 | Φ25//0.20 | 24.55 |
| 8.00 | 7.39 | 1.15 | 94 | 209 | 16.00 | Φ25//0.20 | 24.55 | 1 080 | 16.00 | Φ25//0.20 | 24.55 |
| 9.20 | 8.50 | 0.95 | -28 | 137 | 12.99 | Φ25//0.20 | 24.55 | 870 | 12.99 | Φ25//0.20 | 24.55 |

Table 7.26: Design of the superior face bending reinforcement (Model 3_200)

| r (m) | r' (m) | h (m) | M ₂₋₂ (kN*m/m) | M ₁₋₁ (kN*m/m) | A _{s-22} (cm ² /m) | A _{s-22} | A _{s-22} (cm ² /m) | M _{Rd} (kN*m/m) | A _{s-11} (cm ² /m) | A _{s-11} | A _{s-11} (cm ² /m) |
|----------|-----------|----------------|------------------------------|------------------------------|---|-------------------|---|-----------------------------|---|-------------------|---|
| -9.20 | -8.50 | 0.95 | 0 | -134 | 12.99 | Φ25//0.41 | 11.97 | -430 | 12.99 | Φ25//0.30 | 16.36 |
| -8.00 | -7.39 | 1.15 | -34 | -186 | 16.00 | Φ25//0.35 | 14.02 | -630 | 16.00 | Φ25//0.30 | 16.36 |
| -6.60 | -6.10 | 1.35 | -195 | -358 | 19.02 | Φ25//0.30 | 16.36 | -900 | 19.02 | Φ25//0.25 | 19.63 |
| -5.30 | -4.90 | 1.60 | -520 | -526 | 22.78 | Φ25//0.23 | 21.34 | -1 400 | 22.78 | Φ25//0.25 | 19.63 |
| -4.00 | -3.70 | 1.80 | -1 113 | -834 | 25.79 | Φ25//0.19 | 25.84 | -1 500 | 25.79 | Φ25//0.15 | 32.72 |
| -2.80 | -2.80 | 2.00 e 2.50 | -2 180 | -1 523 | 28.81 | Φ25//0.13 | 37.76 | -3 000 | 28.81 | Φ25//0.15 | 32.72 |
| -2.15 | -1.99 | 2.50 | -3 429 | -1 902 | 36.66 | | | | 36.66 | | |
| -1.30 | -1.20 | 2.50 | -1 388 | -1 224 | 36.66 | | | | | | |
| 0.00 | 0.00 | 2.50 | 1 434 | 383 | | | | | | | |

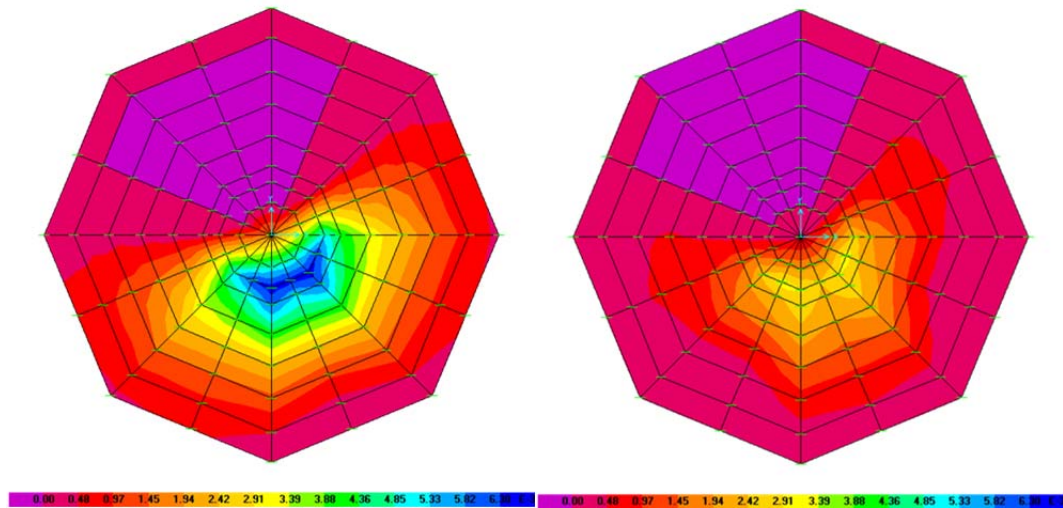


Figure 7.21: Reinforcement at the inferior face, direction y' – Model 3_200 – S2_x' & Reinforcement at the inferior face, direction x' – Model 3_200 – S2_x'

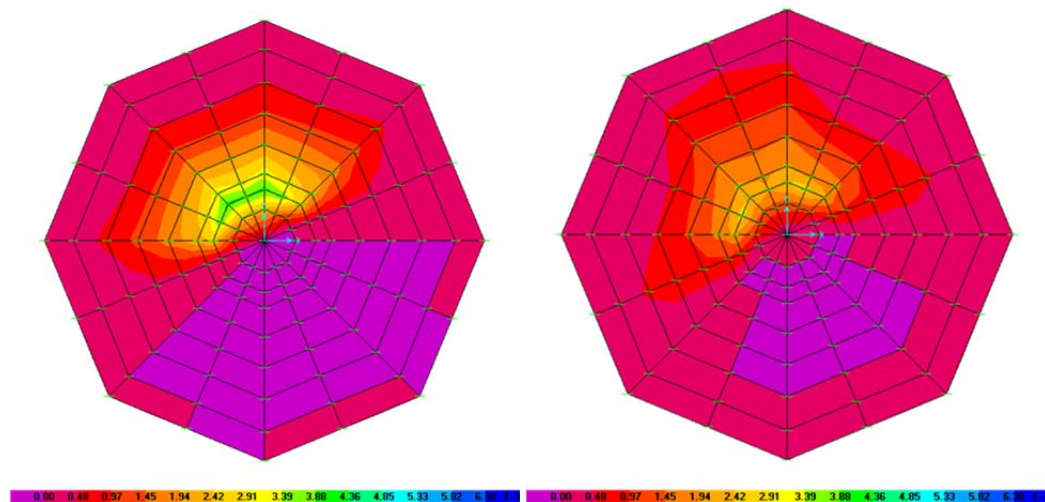


Figure 7.22: Reinforcement at the superior face, direction y' – Model 3_200 – S1_ x' & Reinforcement at the superior face, direction x' – Model 3_200 – S1_ x'

7.3.7.5 Shear reinforcement

The verification of the safety against shear was performed accordingly to Eurocode 2. The critical load case is S2. As may be observed in Table 7.27, the concrete section is not enough to resist to the shear force thus reinforcement is required.

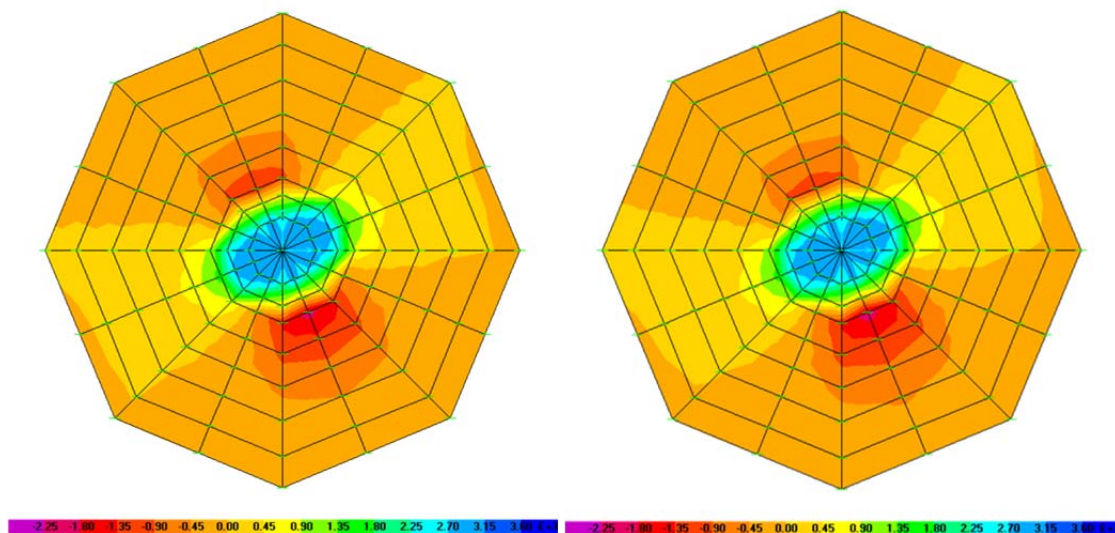


Figure 7.23: Shear force, direction y' – Model 3_200 – S1_ x' & Shear force, direction y' – Model 3_200 – S2_ x'

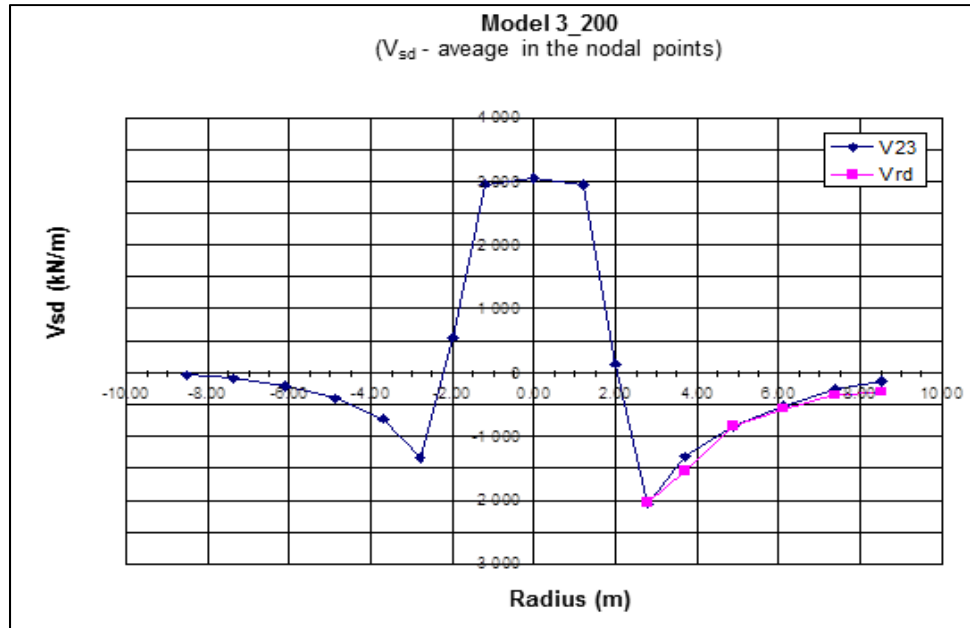


Figure 7.24: Shear force, along y'-axis – Model 3_200 – S2_x'

Table 7.27: Design of the shear reinforcement (Model 3_200-S2)

| r (m) | r' (m) | h (m) | V ₂₋₃ (kN/m) | A _{sl} (cm ² /m) | V _{Rd,c} (kN/m) | A _{sw} (cm ² /m) | V _{Rd,s} (kN/m) |
|----------|-----------|-------------|----------------------------|---|-----------------------------|---|-----------------------------|
| 0.00 | 0.00 | 2.50 | 3 052 | 49.09 | | | |
| 1.30 | 1.20 | 2.50 | 2 942 | 49.09 | | | |
| 2.15 | 1.99 | 2.50 | 133 | 75.89 | | | |
| 2.80 | 2.80 | 2.00 e 2.50 | -2 055 | 75.89 | 692 | Φ32//0.50 m | 2 028 |
| 4.00 | 3.70 | 1.80 | -1 314 | 49.09 | 562 | Φ32//0.50 m | 1 537 |
| 5.30 | 4.90 | 1.60 | -839 | 24.55 | 467 | Φ32//0.60 m | 838 |
| 6.60 | 6.10 | 1.35 | -517 | 24.55 | 405 | Φ32//0.60 m | 571 |
| 8.00 | 7.39 | 1.15 | -256 | 24.55 | 355 | | |
| 9.20 | 8.50 | 0.95 | -134 | 24.55 | 310 | | |

The actual shear reinforcement defined in design is presented in Table 7.28. The minimum shear reinforcement imposed by REpower [50] is on the last column and is respected in the entire foundation.

Table 7.28: Actual shear reinforcement (Model 3_200-S2)

| Ring | r (m) | h (m) | Φ (mm) | A _{sw} (cm ²) | s _r (m) | S ₀ (m) | A _{sw} /m ² (cm ² /m ²) | V _{sd} (kN/m) | (A _{sw} /m ²) _{min} (cm ² /m ²) |
|------|----------|----------|-----------|---------------------------------------|-----------------------|-----------------------|---|---------------------------|---|
| 1 | 3.13 | 1.94 | 32 | 8.04 | 0.39 | 0.61 | 33.54 | 1 783 | 8.07 |
| 2 | 3.58 | 1.86 | 32 | 8.04 | 0.53 | 0.70 | 21.79 | 1 413 | 6.28 |
| 3 | 4.18 | 1.75 | 32 | 8.04 | 0.60 | 0.82 | 16.33 | 1 124 | 5.50 |
| 4 | 4.78 | 1.64 | 32 | 8.04 | 0.63 | 0.94 | 13.71 | 887 | 5.32 |
| 5 | 5.43 | 1.52 | 32 | 8.04 | 0.63 | 1.07 | 12.07 | 697 | 4.00 |
| 6 | 6.03 | 1.41 | 32 | 8.04 | 0.60 | 1.18 | 11.32 | 536 | 3.65 |
| 7 | 6.63 | 1.29 | 32 | 8.04 | 0.70 | 1.30 | 8.82 | 410 | 2.62 |
| 8 | 7.43 | 1.15 | 32 | 8.04 | 0.80 | 1.46 | 6.89 | 252 | 0.00 |

7.3.7.6 Serviceability limit states

7.3.7.6.1 Cracking control

Eurocode 2 specifies a limit value for the crack width of $w_k=0,3$ mm, for quasi-permanent load combinations:

$$S_d = \sum_{j \geq 1} G_{kj} + \sum_{i > 1} \psi_{2i} Q_{ki} \quad (99)$$

Load case G5 was considered to be representative of this case. In the section where $h=2,00$ m, the computed moment was $M_{22}=930$ kN*m/m. The stress in the reinforcement bars may be computed as:

$$\sigma \cong \frac{M}{0,9 \cdot d \cdot A_s} = \frac{0,930}{0,9 \cdot 1,925 \cdot 75,89E-4} = 71 \text{ MPa} \quad (100)$$

The simplified procedure proposed in art. 7.3.3 of EC2 imposes that for $\Phi 25$ bars the maximum stress will not be greater than 200 MPa, which is verified.

7.3.7.6.2 Deflections

The vertical deflections (settlements) along the y' axis are presented in Figure 7.25. As expected, on load case G5, there is no ground gap and the rotational stiffness is equal to $K_{0,dyn}=1,6E+11$ N*m/rad.

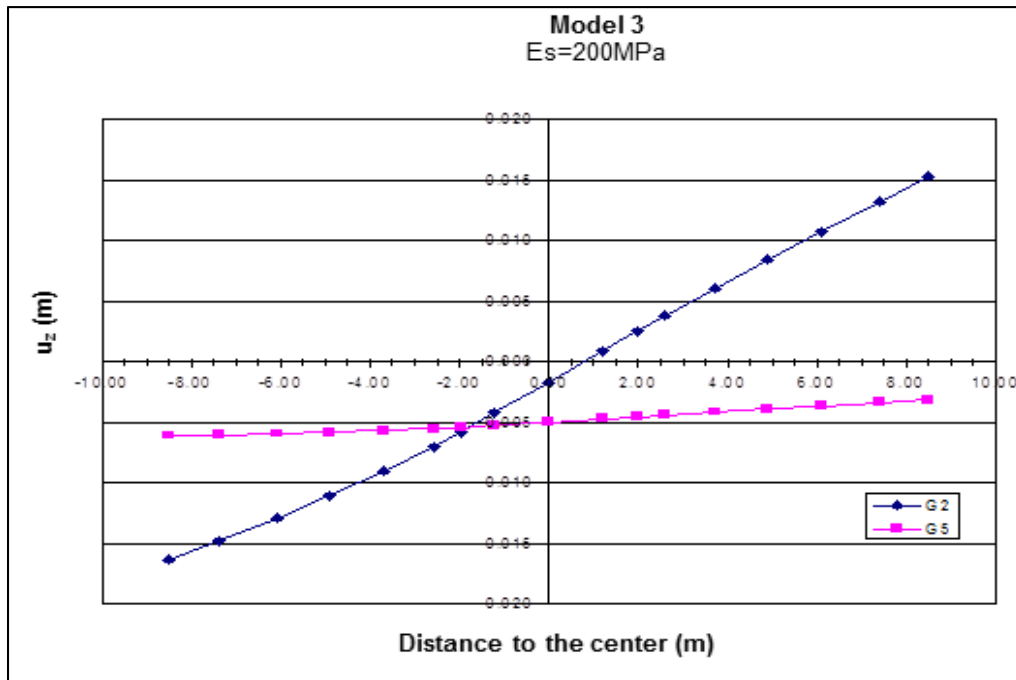


Figure 7.25: Vertical deflections (settlements) along y' axis – Model 3

Table 7.29: Case G5

| | | |
|--------------------|----------------|---------|
| Mres(b) = | 28 035 | kN*m |
| Average rotation = | 0.0001762 | rad |
| K_{θ} = | 1.6E+11 | N*m/rad |

Load case G2 corresponds to the situation where no more that 50% of the foundation is not compressed. That is the case as may be observed on Figure 7.25 and Figure 7.26. Here the maximum bearing pressure is under 250 kPa. On case G5 there is always compression on the foundation base, as imposed.

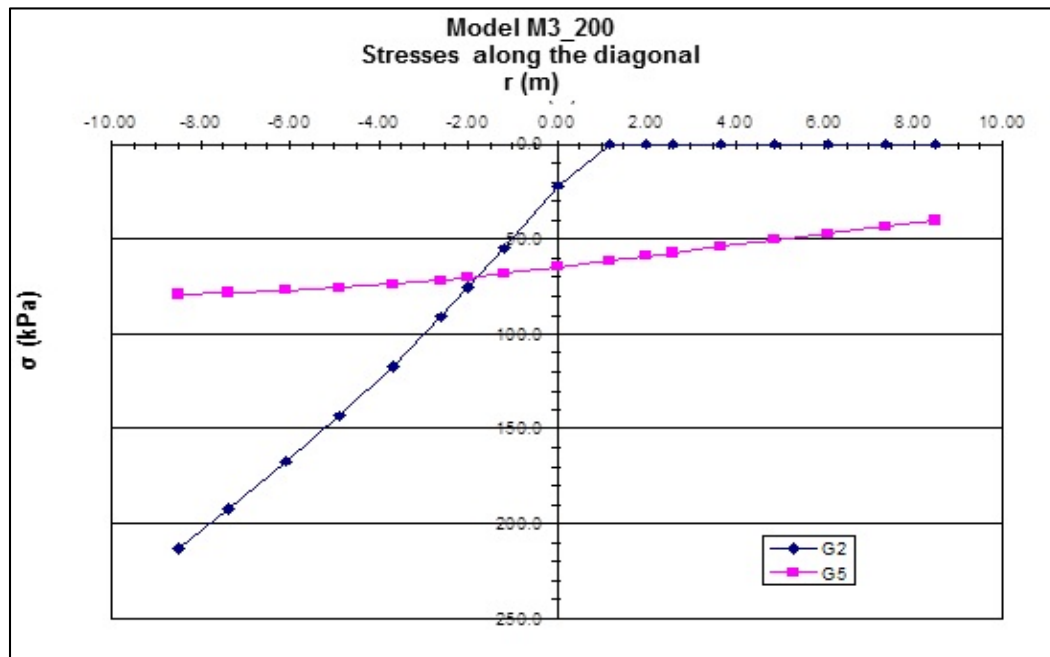


Figure 7.26: Soil bearing pressure along the y' axis – Model 3_200

7.3.8 Connection of the anchor steel ring to the foundation slab

7.3.8.1 Geometric data

The following geometric data is used to perform the safety checks concerning the connection of the steel ring anchored inside the foundation slab as illustrated in Figure 7.27.

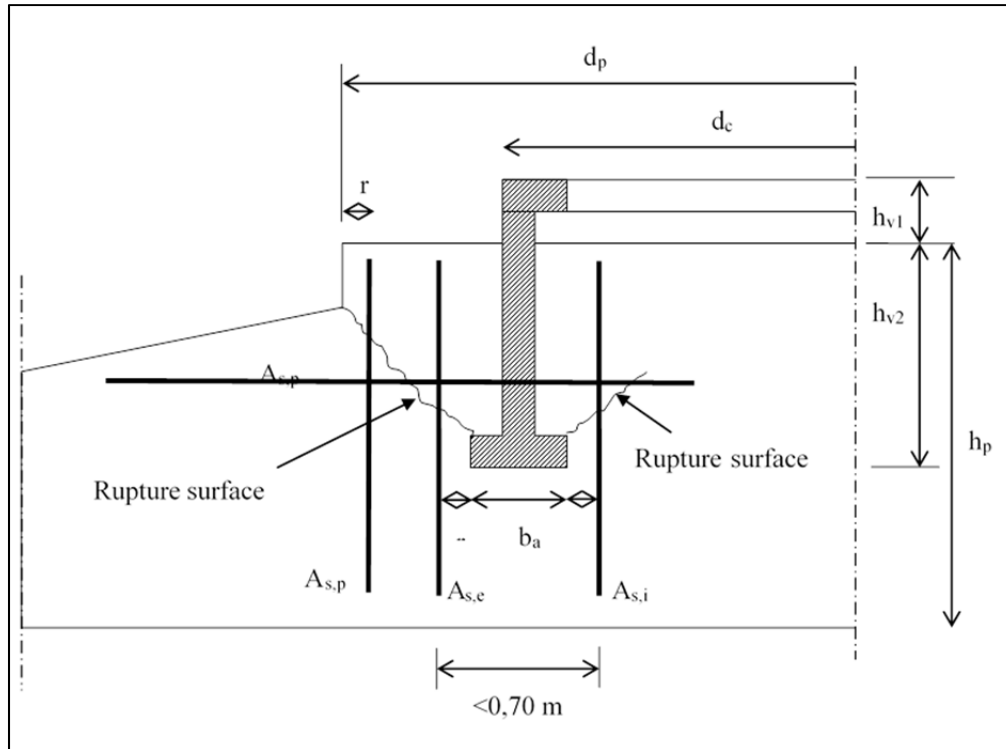


Figure 7.27: Foundation steel ring embedded in the foundation concrete slab

Table 7.30: Geometry of the embedded steel ring

| | | | | |
|---|------------------|----------|-----------|-----------------|
| height | $h_{v1}+h_{v2}=$ | h_v | 1,753E+03 | mm |
| | | h_{v1} | 5,000E+02 | mm |
| | | h_{v2} | 1,253E+03 | mm |
| height of the foundation slab | | h_p | 2,500E+03 | mm |
| distance between bottom of can and bottom of foundation | | | 1,247E+03 | mm |
| diameter exterior | | d_c | 4,300E+03 | mm |
| thickness | | t_c | 3,000E+01 | mm |
| perimeter exterior | | L_c | 1,351E+04 | mm |
| diameter of mean surface | | | 4,270E+03 | mm |
| perimeter mean surface | | | 1,341E+04 | mm |
| steel area | | A_c | 4,024E+05 | mm ² |
| inertia | | I_c | 9,172E+11 | mm ⁴ |
| flexural mudulus | | W_c | 4,266E+08 | mm ³ |

Table 7.31: Ring flange at the bottom of the embedded steel ring

| | | | |
|-------------------|-----------|-----------|-----------------|
| width | b_a | 3,400E+02 | mm |
| thickness | t_a | 6,900E+01 | mm |
| diameter interior | $d_{a,i}$ | 3,930E+03 | mm |
| diameter exterior | $d_{a,e}$ | 4,610E+03 | mm |
| area | A_a | 4,561E+06 | mm ² |
| inertia | I_a | 1,046E+13 | mm ⁴ |
| flexural modulus | W_a | 4,538E+09 | mm ³ |

Table 7.32: Geometry of the steel reinforcement

| | | | |
|---|----------|-----------|----|
| diameter of the circular foundation part | d_p | 5,600E+03 | mm |
| distance between reinforcement and flange | r_s | 5,000E+01 | mm |
| cover | r | 5,000E+01 | mm |
| diameter of inner circular reinforcement | d_{si} | 3,830E+03 | mm |

| | | | |
|---|-----|-----------|----|
| diameter of external circular reinforcement Ase | dse | 4,710E+03 | mm |
| diameter of peripheral circular reinforcement | dsp | 5,500E+03 | mm |
| perimeter of inner reinforcement | | 1,203E+04 | mm |
| perimeter of outer reinforcement | | 1,480E+04 | mm |
| perimeter of peripheral reinforcement | | 1,728E+04 | mm |

7.3.8.2 Material data

Table 7.33: Material parameters

| | | | |
|--------------------------|---------|--------|-------|
| reinforcement steel S500 | fyk | 500,00 | N/mm2 |
| | γs | 1,15 | |
| concrete C35/45 | fyd | 434,78 | N/mm2 |
| | fck | 35,00 | N/mm2 |
| | γc | 1,50 | |
| | fcd | 20,00 | N/mm2 |
| | 0,85fcd | 17,00 | N/mm2 |

7.3.8.3 Design of the anchor reinforcement

7.3.8.3.1 Pull-out Ultimate Limit State

The vertical reinforcement is designed for the tension force developed by the moment and vertical force given by REpower at the top of the foundation steel ring. To perform the pull-out ULS check it is considered that the tension force per unit length of the ring perimeter, developed in the ring vertical wall, is transferred to the concrete and is resisted by vertical reinforcement. Although this reinforcement is considered to be disposed in three layers, as showed in Figure 7.27, and referenced as $A_{s,i}$, $A_{s,e}$ and $A_{s,p}$, only the layers located within a section of 0,70m around the steel flange shall be taken into account. As a consequence only $A_{s,i}$, $A_{s,e}$ will be used for this verification. The peripheral layer is necessary to avoid excessive crack opening near the surface and will be checked for fatigue ULS.

To perform the safety check concerning pull-out ULS following expression is used to compute the force F to be covered by the anchor reinforcement $A_{s,i}+A_{s,e}$ integrated along the perimeter:

$$F = 4 * \frac{M_{res}}{d_c} - 0.9 * |F_z|$$

Loads (according to REpower table 1.1 – Ultimate loads)

Following load cases are considered for the safety check, which include already the safety factor

Table 7.34: Load cases including safety factors applied to the loads (REpower)

| Load case | M_{res} | M_z | F_{res} | F_z |
|-------------------|-----------|----------|-----------|----------|
| Dlc1511_0_gt2.int | 69107,28 | -1363,14 | 873,60 | -3174,74 |
| Dlc6145120E | 67472,98 | 1339,34 | 958,02 | -2602,58 |
| Dlc6145300E | 66969,73 | -1043,09 | 1030,00 | -2495,20 |

7.3.8.3.2 Safety check

Load case *Dlc1511_0_gt2.int* is pertinent for the check of the compression stress in the concrete under the bottom flange of the steel ring and for the design of the reinforcement, as following demonstration:

Table 7.35: Safety check

| | | | | | | |
|---|----------------|----------|-------|--------|-------|-------|
| Maximum Loads at the top of the steel ring | | | | | | |
| Resulting Moment | M_{res} | 69107,28 | kNm | | | |
| Moment zz | M_z | -1363,14 | kNm | | | |
| Resulting Horizontal force | F_{res} | 873,60 | kN | | | |
| Vertical force zz | F_z | -3174,74 | kN | | | |
| Resulting Loads at the bottom of the steel ring | | | | | | |
| Moment Resulting | M_{res} | 70638,70 | kNm | | | |
| Moment zz | M_z | -1363,14 | kNm | | | |
| Resulting Horizontal force | F_{res} | | kN | | | |
| Vertical force zz | F_z | -3174,74 | kN | | | |
| Maximum contact stresses between ring flange and concrete | | | | | | |
| compression | σ_{cd} | -16,26 | N/mm2 | > | -17 | N/mm2 |
| tension | σ_{cd} | 14,87 | N/mm2 | | | |
| Maximum stresses in the steel ring | | | | | | |
| Compression | σ_{min} | -173,46 | N/mm2 | | | |
| Tension | σ_{max} | 157,69 | N/mm2 | | | |
| compression through holes | σ_{min} | -219,22 | N/mm2 | > | -355 | N/mm2 |
| tension through holes | σ_{max} | 199,28 | N/mm2 | | | |
| Steel bars to transfer tension from steel ring to the concrete | | | | | | |
| Tension force per unit length of ring perimeter | $F_{a,total}$ | 5055,39 | kN/m | | | |
| Tension force per unit length of ring perimeter | $F_{a,M}$ | 5292,05 | kN/m | | | |
| Tension force per unit length of ring perimeter | $F_{a,Fz}$ | -236,66 | kN/m | | | |
| Needed area of reinforcement per unit length | A_s | 116,27 | cm2/m | | | |
| Needed area of reinforcement | $A_{s,tot}$ | 1570,73 | cm2 | | | |
| Equivalent reinforcement placed in three layers | | | | | | |
| | | | | Φ | @ cm | n |
| internal layer | $A_{s,i}$ | 93,58 | cm2/m | 32 | 8,59 | 140 |
| external layer | $A_{s,e}$ | 76,09 | cm2/m | 32 | 10,56 | 140 |
| Peripheric layer | $A_{s,p}$ | 26,07 | cm2/m | 32 | 30,86 | 56 |
| Total | | 2702,28 | cm2 | | | |

For the Pull-out safety check following demonstration applies:

Table 7.36: Pull-out safety check

| Repower requirement $F=4*M_{res}/D-0.9* F_z $ | | | |
|---|----------|-----------------|--------------------------|
| $F_z=$ | 3174,74 | KN | |
| $D=$ | 4,30 | m | |
| $M_{res}=$ | 69107,28 | KNm | |
| $F=$ | 35713,18 | KN | |
| $A_{s,tot,needed}=$ | 821,40 | cm ² | < 2251,9 cm ² |

7.3.8.3.3 Stress calculations

Considering that the bottom flange of the ring is stiff enough to remain plane during the deformation imposed by the moment applied on the ring $M_{res,bottom}$, one can obtain the maximum compressive stress under the flange due to moment and normal force with the formula:

$$\sigma_{c,max} = \frac{F_z}{A_a} + \frac{M_{res,bottom}}{I_a} \frac{d_{a,e}}{2} = \frac{F_z}{A_a} + \frac{M_{res,bottom}}{W_a}$$

to be verified as a compressive stress that must be resisted by the concrete, that is,
 $\sigma_{c,max} \leq 0,85 f_{cd}$.

On the opposite side of the flange the same value for the maximum tensile stress would be developed if the concrete could resist tensile stresses. Since it cannot, the reinforcement placed in three layers must resist the total force per unit length of perimeter, as it was shown before. However, for fatigue limit states the tensile stress variation in each reinforcement layer must be checked. Therefore, the tensile stress per unit length of the perimeter corresponding to the reinforcement layer being checked is computed according to the following formulae:

$$\sigma_{si,max} = \left(\frac{F_z}{A_{si} + A_{se} + A_{sp}} \right) + k_{si} \frac{M_{res,bottom}}{W_a} b_a \frac{1}{A_{si}}$$

$$\sigma_{se,max} = \left(\frac{F_z}{A_{si} + A_{se} + A_{sp}} \right) + k_{se} \frac{M_{res,bottom}}{W_a} b_a \frac{1}{A_{se}}$$

$$\sigma_{sp,max} = \left(\frac{F_z}{A_{si} + A_{se} + A_{sp}} \right) + k_{sp} \frac{M_{res,bottom}}{W_a} b_a \frac{1}{A_{sp}}$$

where the coefficients k_{si} , k_{se} and k_{sp} are computed as follows:

$$k_{si} = \frac{1}{1 + \frac{d_{se} A_{se}}{d_{si} A_{si}} + \frac{d_{sp} A_{sp}}{d_{si} A_{si}}}$$

$$k_{se} = \frac{1}{1 + \frac{d_{si} A_{si}}{d_{se} A_{se}} + \frac{d_{sp} A_{sp}}{d_{se} A_{se}}}$$

$$k_{sp} = \frac{1}{1 + \frac{d_{si} A_{si}}{d_{sp} A_{sp}} + \frac{d_{se} A_{se}}{d_{sp} A_{sp}}}$$

Considering unit loads, that is $F_z = -1 \text{ kN}$ and $M_{res, bottom} = 1 \text{ kNm}$ the following stresses are obtained separately for each load.

Table 7.37: Stress calculations

| | | | | | |
|--|-------------------|-----------|------------|------------|-------------------|
| Unit resulting Loads at the bottom of the steel ring | | | | | |
| Moment Resulting | Mres | 1 | kN.m | | |
| Vertical force zz | Fz | -1 | kN | | |
| Safety factors for loads | | | | | |
| Fatigue limite state | $\gamma_{F, fat}$ | 1,00 | | | |
| Maximum contact stresses between ring flange and concrete including safety factor | | | | | |
| Moment | | 2,20E-04 | N/mm2 /kNm | | |
| Axial force | | -2,19E-04 | N/mm2 /kN | | |
| Tension force per unit length of steel ring perimeter | | | | | |
| due to Moment | | 7,49E+01 | N/m /kNm | | |
| due to Axial Force | | -7,45E+01 | N/m /kN | | |
| Tension stress in the reinforcement | | | | | |
| Moment | | | | | %F _{a,M} |
| | internal layer | As,i | 4,00E-03 | N/mm2 /kNm | 0,4 |
| | external layer | As,e | 4,92E-03 | N/mm2 /kNm | 0,4 |
| | peripheric layer | As,p | 5,75E-03 | N/mm2 /kNm | 0,2 |
| Axial Force | | | | | |
| | internal layer | As,i | -4,61E-03 | N/mm2 /kN | |
| | external layer | As,e | -4,61E-03 | N/mm2 /kN | |
| | peripheric layer | As,p | -4,61E-03 | N/mm2 /kN | |

The maximum stresses computed for the three layers in the pull-out ULS using the

Table 7.38: Resulting Loads at the bottom of the steel ring (incl. Safety factor)

| | | | |
|----------------------------|------|----------|-----|
| Moment Resulting | Mres | 70638,70 | kNm |
| Moment zz | Mz | -1363,14 | kNm |
| Resulting Horizontal force | Fres | 873,60 | kN |
| Vertical force zz | Fz | -3174,74 | kN |

are the following

Table 7.39: Tension stress in the reinforcement considering linear-elastic and plane sections behaviour

| | | | | | | |
|-------------------------------------|----------------|--------|-------|---|----------|-------|
| stress in the equivalent steel area | | 252,72 | N/mm2 | < | 434,7826 | N/mm2 |
| internal layer | $\sigma_{s,i}$ | 210,35 | N/mm2 | < | 434,7826 | N/mm2 |
| external layer | $\sigma_{s,e}$ | 258,68 | N/mm2 | < | 434,7826 | N/mm2 |
| peripheric layer | $\sigma_{s,p}$ | 247,59 | N/mm2 | < | 434,7826 | N/mm2 |

7.3.8.3.4 Load cases for fatigue

The load cases for fatigue are given by REpower, separately for the situation of normal production of the turbine and for the vibrations induced by shedding of vortices on the tower.

For the situation of normal production three types of load cases at tower base are given:

- Load spectra, consisting of a load variation interval for each defined number of cycles;
- Damage equivalent loads, which consist of a constant amplitude load variation that would induce fatigue damage equivalent to the cumulative damage induced by the load spectra; the following damage equivalent loads are obtained from REpower table 1.5.2 considering $N^*=2 \times 10^6$ and $m=5$, in accordance with the parameters of the S-N curves given by the Eurocode 2.

Table 7.40: Damage equivalent loads

| Damage equivalent loads (Repower table 1.4) | | | | | |
|---|-------------------|-------------------|-----------------------|-----------------------|-------------------|
| $\Delta F_{x,eq}$ | $\Delta F_{y,eq}$ | $\Delta F_{z,eq}$ | $\Delta M_{x,top,eq}$ | $\Delta M_{y,top,eq}$ | $\Delta M_{z,eq}$ |
| 292,96 | 230,84 | 82,89 | 16293,90 | 18689,24 | 3510,81 |
| Damage equivalent loads bottom of the steel ring | | | | | |
| $\Delta F_{x,eq}$ | $\Delta F_{y,eq}$ | $\Delta F_{z,eq}$ | $\Delta M_{x,bot,eq}$ | $\Delta M_{y,bot,eq}$ | $\Delta M_{z,eq}$ |
| 292,96 | 230,84 | 82,89 | 16698,57 | 19202,80 | 3510,81 |

the following damage equivalent loads are obtained from the load spectra mentioned above considering $N^*=2 \times 10^6$ and $m=5$

Table 7.41: Damage equivalent loads obtained from the load spectra

| $\Delta F_{x,eq}$ | $\Delta F_{z,eq}$ | $\Delta M_{y,top,eq}$ | $\Delta M_{y,bottom,eq}$ | $\Delta M_{z,eq}$ |
|-------------------|-------------------|-----------------------|--------------------------|-------------------|
| 297,60 | 86,40 | 19173,93 | 19320,66 | 3621,24 |

Mean values, around which the fatigue loads vary.

Table 7.42: Fatigue loads mean value

| Fatigue loads mean value (Repower table 1.5) | | | | | |
|--|-----------|-----------|----------------------------|----------------------------|-----------|
| Fx | Fy | Fz | Mx | My | Mz |
| 302,14 | -3,20 | -2401,21 | 1795,01 | 23200,81 | 186,09 |
| Fatigue loads mean value (bottom of steel ring) | | | | | |
| Fx | Fy | Fz | Mx_{bottom} | My_{bottom} | Mz |
| 302,14 | -3,20 | -2401,21 | 1800,62 | 23730,46 | 186,09 |

The safety check is made separately for the reinforcement bars in each layer and for the concrete under the bottom flange of the steel ring using the Eurocode 2 (EN1992-1-1, April 2003) and the REBAP (Portuguese reinforced concrete standard).

Table 7.43: Fatigue loads max/min value

| Fatigue loads maximum value (bottom of steel ring) for N* | | | | | |
|---|------------|------------|----------------------|----------------------|------------|
| Fx | Fy | Fz | Mx _{bottom} | My _{bottom} | Mz |
| 448,62066 | 112,22118 | -2442,6561 | 10149,905 | 33331,861 | 1941,4967 |
| Fatigue loads minimum value (bottom of steel ring) for N* | | | | | |
| Fx | Fy | Fz | Mx _{bottom} | My _{bottom} | Mz |
| 155,65934 | -118,62118 | -2359,7639 | -6548,6657 | 14129,061 | -1569,3167 |
| Fatigue loads maximum value for concrete check | | | | | |
| | | Fz | Mres _{bot} | | |
| | | -2442,6561 | 34842,984 | | |
| Fatigue loads minimum value for concrete check | | | | | |
| | | Fz | Mres _{bot} | | |
| | | -2359,7639 | 15572,906 | | |

7.3.8.3.5 Safety check considering damage equivalent loads

Table 7.44: Verification using damage equivalent stress range (EN 1992-1-1)

| | | | | | | | | | |
|---|------------------|---|-------|-------|-------|---|--------|-------|---|
| Tension in the reinforcement for N*= | | 2,00E+06 | | | | | | | |
| Safety factor for steel | | $\gamma_{s,fat}$ | 1,15 | | | | | | |
| Characteristic fatigue strength curve >>> | | $\Delta\sigma_{Rsk}(N^*)$ | 162,5 | N/mm2 | | | | | |
| Moment | | | | | | | | | $\Delta\sigma_{Rsk}(N^*)\gamma_{s,fat}$ |
| | internal layer | $\gamma_{F,fat} \cdot \Delta\sigma_{s,eq}(N^*)$ | = | 64,45 | N/mm2 | < | 141,30 | N/mm2 | |
| | external layer | $\gamma_{F,fat} \cdot \Delta\sigma_{s,eq}(N^*)$ | = | 79,26 | N/mm2 | < | 141,30 | N/mm2 | |
| | Peripheric layer | $\gamma_{F,fat} \cdot \Delta\sigma_{s,eq}(N^*)$ | = | 92,55 | N/mm2 | < | 141,30 | N/mm2 | |
| Axial Force | | | | | | | | | |
| | internal layer | | | -0,33 | N/mm2 | | | | |
| | external layer | | | -0,33 | N/mm2 | | | | |
| | Peripheric layer | | | -0,33 | N/mm2 | | | | |

Table 7.45: Verification using damage equivalent stress range (REBAP)

| | | | | | |
|---|----------------|------------------------------|-------|-------|---------------|
| Compression in the concrete for N*= | | 2,00E+06 | | | |
| | | fcd | 23,33 | | |
| Characteristic fatigue strength curve >>> | | 0,5fcd | 11,67 | N/mm2 | |
| Moment | | | | | |
| | maximum stress | | 7,68 | N/mm2 | |
| | minimum stress | | 3,43 | N/mm2 | |
| Axial Force | | | | | |
| | maximum stress | | 0,54 | N/mm2 | |
| | minimum stress | | 0,52 | N/mm2 | |
| verification | | | | | |
| | maximum stress | | 8,21 | N/mm2 | |
| | minimum stress | | 3,95 | N/mm2 | |
| | | $\sigma_{max}-\sigma_{min}=$ | 4,26 | N/mm2 | < 11,67 N/mm2 |

7.3.8.3.6 Safety check using load spectra

For multiple cycles with variable amplitudes the damage may be added by using the Palmgren-Miner Rule. In this case a damage index D is obtained as the summation of all the elemental damage indexes calculated for each of the cycle number classes. This index must be less than one.

Table 7.46: Safety check using load spectra

| S-N curve for material | | Stress values for unity loads | |
|------------------------|----------------|---|---------------------|
| reinforcing steel | | reinforcing steel: | As,p |
| N* = | 1,0E+06 cycles | $\Delta\sigma_{s,Fz,unit}$ | 3,808E-03 Mpa / kN |
| k ₁ = | -5,00 | $\Delta\sigma_{s,My,unit}$ | 4,790E-03 Mpa / kNm |
| k ₂ = | -9,00 | | |
| $\Delta\sigma_{Rsk}$ = | 162,50 Mpa | $\gamma_{F,fat}$ = | 1,00 |
| Log $\Delta\sigma_1$ = | 3,41 | $\gamma_{s,fat}$ = | 1,15 |
| Log $\Delta\sigma_2$ = | 2,88 | | |
| | | Damage $D = \sum(n_i/N_i) < 1$ D= 4,25E-02 | |

7.3.9 Quantities

The quantities of Table 7.47 are a rough estimate.

Table 7.47: Quantities

| Item | Unit. |
|-----------------------------------|----------------------------|
| Reinforcement steel (S500) | |
| 1. Diameter 12 mm | kg 393,7 |
| 2. Diameter 16 mm | kg 809,0 |
| 3. Diameter 20 mm | kg 1426,3 |
| 4. Diameter 25 mm | kg 23308,4 |
| 5. Diameter 32 mm | kg 12598,2 |
| Total steel: | kg 38535,6 |
| Concrete of class C30/37 | m³ 227.4 |
| Concrete of class C35/45 | m³ 129.4 |
| Concrete of class C12/15 | m³ 23.9 |
| Ballast | m³ 134.3 |

7.3.10 Conclusions

The foundation designed, guarantees the required safety level for the load and ground conditions specified in the current report.

7.4 Connection of the foundation with partially prestressed anchors

Figure 7.28 shows the connection of a foundation, in which the steel tube is anchored to the reinforced concrete slab with prestressed bolts. The procedure to design this type of foundation is similar to the one presented in the design example of MM92 foundation, whilst for the connection, the design process is described below.

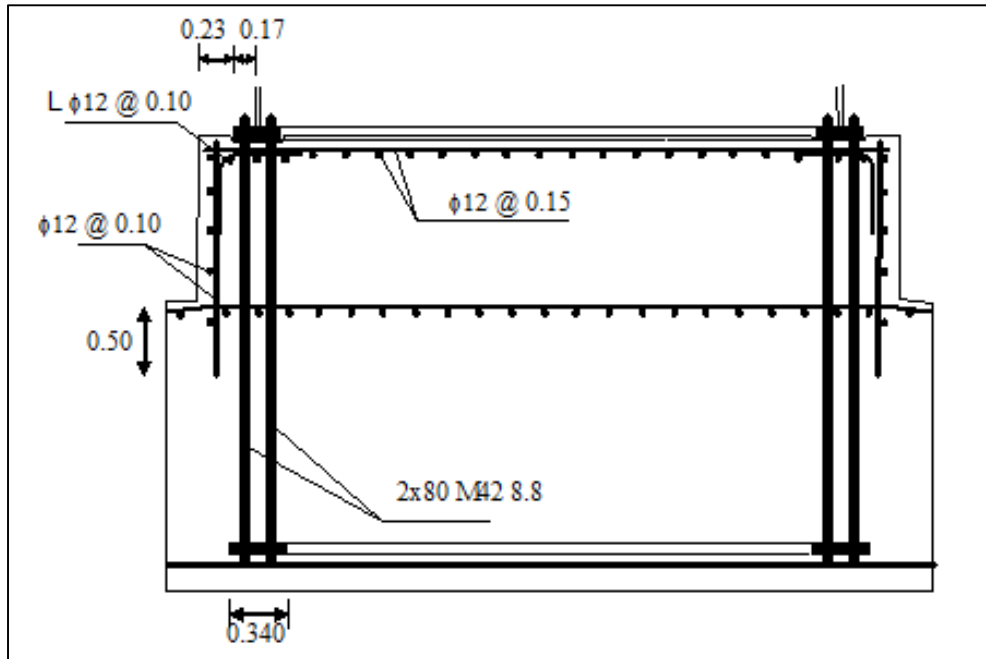


Figure 7.28: Scheme of the anchoring zone

Two limit states concerning the stability of the connection made of prestressed bolt cage need to be analysed:

- Ultimate Limit State (ULS)

The anchor bolts are designed for the tension force imposed by the combination of axial force and bending moment referred to the bottom of the steel tube. To check the ULS, it can be considered that the force per unit length developed along the tube perimeter is transferred to the concrete by compression and to the anchor bolts in tension. A simplified model can be used to check the ULS. This model only takes into account the cross section of the anchor bolts, utilizing an equivalent steel ring with the diameter of the middle surface of both bolt layers and thickness equivalent to the area cross section of both bolt layers.

- Fatigue Limit State (FLS)

For the situation of normal production three load cases can be computed: (a) fatigue spectra which consists on the number of stress cycles experienced by the structure for each level of stress variation, (b) damage equivalent forces, consisting on the amplitude of a steady-state stress variation which would induce the same damage introduced by the application of the fatigue spectra and (c) mean values of the time varying loads.

At a first step, the elastic stresses in steel and concrete for unitary loading need to be computed. The maximum stress introduced in the anchor bolts for unitary value of the normal force ($F_x=1\text{kN}$) and unitary resultant bending moment ($M_{res}=1\text{kNm}$) can be obtained taking into consideration that there is no separation between steel flange and concrete since the connection is prestressed to about 50% of the ultimate strength of the bolts. Accordingly, in the concrete surface below the flange of the steel tube, the maximum compression stress is given by:

$$\sigma_{c\max} = \frac{|M_{res}|}{I_h} r - \frac{|F_x|}{A_h} \quad (101)$$

where I_h and A_h represent respectively the inertia and the area of the homogenized, steel bolts and concrete section below the flange (see Figure 7.29)

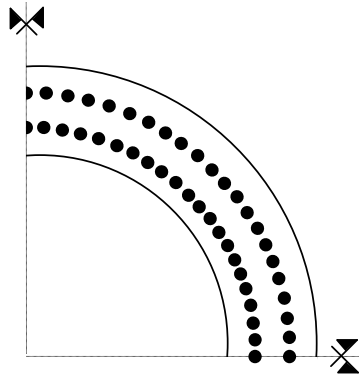


Figure 7.29: 1/4 of the interface cross-section, concrete and steel bolts for a circular foundation

Since there is no adhesion between bolts and concrete, the design model approximates this effect considering low values for the relation between Young's moduli. In this way, the relation between those moduli is considered $E_s/E_c=7$ and the maximum concrete stresses in concrete induced by the unitary axial force and the unitary moment can be computed. If the ratio $E_s/E_c=15$ is considered, the maximum tensile stresses in steel bolts induced by the unitary axial force and the unitary moment are penalized and need to be recomputed.

For the FLS safety check of the anchor bolts, for multiple cycles of variable amplitudes, the damage can be computed using the Palmgren-Miner approach. In this case the damage index D is obtained from the sum of all elementary damage indexes obtained from each of the classes defined by the number of cycles and the stress amplitudes. The index D must be at most equal to 1.0.

For the FLS of the compressed concrete, the maximum and minimum stresses due to the axial force and the bending moment need to be computed and the safety check is based on the maximum and minimum stress for frequent combination of actions.

The load cases for the fatigue limit state are usually given by the manufacturer separately for the situation of normal production of the turbine and for the vibrations induced by shedding of vortices on the tower. The safety check should be made separately for the reinforcement bars in each layer and for the concrete under the bottom

flange of the steel ring, both considering damage equivalent loads and using load spectra (by applying the Palmgren-Miner Rule).

7.5 Other types of foundations

The shallow foundations mentioned in this chapter are the most common types of wind tower foundations located in mountainous terrain, since competent material usually exists at the surface or a few meters deep and also because this is the less technologically demanding solution and therefore suitable to be subcontracted by small local construction companies. In case of poor soil conditions, ground improvements can be implemented to upgrade the soil before the installation of the shallow foundations. The use of rock anchors (e.g. micro-piles) to minimize the slab plane dimensions is also possible, but it requires specialist contractors to carry out the construction works. An example of this foundation is shown in Figure 7.30, where the patented Patrick and Henderson Tensionless Pier and Rock Anchor or Pile Anchor foundations are depicted [53]. This foundation type can be chosen even for poor surficial soil conditions, whilst its use depends on the local drilling requirements.

For offshore WTG applications mono-pile foundations are quite commonly used. Monopile foundations have relatively limited structural dimensions and a restricted interface with their supporting soil, limiting the overall tower stiffness and affecting the dynamic behaviour.

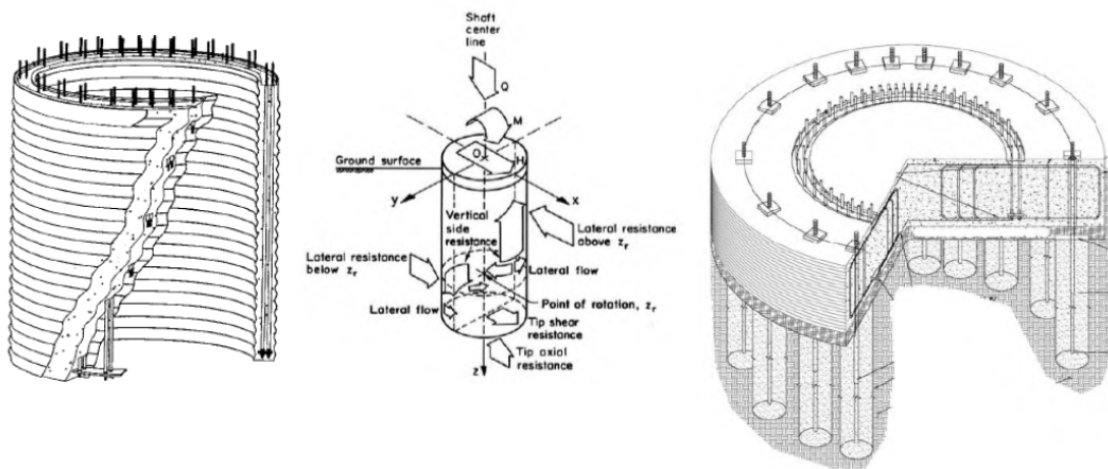


Figure 7.30: The patented Patrick and Henderson Tensionless Pier (left) and Rock Anchor or Pile Anchor foundation (right) [53]

8 ACRONYMS AND ABBREVIATIONS

| | |
|-------|---|
| EC3 | Eurocode for steel structures, in general |
| FE | Finite Element |
| FEA | Finite Element Analysis |
| GMNIA | Geometrically and Materially Nonlinear Analysis with Imperfections included |
| LBA | Linear bifurcation Analysis |
| MNA | Materially Nonlinear Analysis |
| SLS | Serviceability Limit State |
| ULS | Ultimate Limit State |
| WEC | Wind Energy Converter |
| WET | Wind Energy Technology |
| WT | Wind Turbine |

9 REFERENCES

- [1] Hau, E.: Wind Turbines: fundamentals, technologies, application, economics, Springer, Berlin, 2006.
- [2] Engström, S., Lyrner, T. and Hassanzadeh, M.: Tall towers for large wind turbines, Vindforsk project report, Elforsk, Sweden, 2010.
- [3] Hüsermann, K.: Ruukki Wind Towers – High truss towers for wind turbine generators, Ruukki, 2010
- [4] Veljkovic, M. et al.: High-strenght tower in steel for wind turbines (HISTWIN), final report, European Commission, Brussels, Belgium, 2012.
- [5] CEN: EN 45020: Standardization and related activities – General vocabulary, Brussels 2006.
- [6] Germanischer Lloyd WindEnergie GmbH (GL Wind): Guideline for the Certification of Wind Turbines, Hamburg, Germany, 2010.
- [7] Det Norske Veritas & Wind Energy Department at Risø National Laboratory: Guidelines for Design of Wind Turbines, Copenhagen, Denmark, 2002.
- [8] International Electrotechnical Commission: IEC 61400-1 Wind Turbines: Part 1 - Design requirements, Third edition, Geneva, Switzerland, 2005.
- [9] ISO 2394: General principles on reliability for structures. International Organization for Standardization. Geneva, Switzerland, 1998.
- [10] ISO 4354: Wind actions on structures. International Organization for Standardization. Geneva, Switzerland, 2009
- [11] DIBt: Richtlinie für Windenergieanlagen – Einwirkungen und Standsicherheitsnachweise für Turm Gründung, Berlin, Germany, 2012.
- [12] CEN/TC250: EN 1990: Eurocode - Basis of structural design, Brussels, 2002.
- [13] CEN/TC250: Eurocode 7 – Geotechnical design – EN 1997 Part 1: General rules. European Committee for Standardization. Brussels, 2004.
- [14] CEN/TC250: EN 1998-1: Eurocode 8: Design of structures for earthquake resistance – Part 1: General rules, seismic actions and rules for buildings, Brussels, 2004.
- [15] CEN/TC250: Eurocode 2 – Design of concrete structures – EN 1992 Part 1-1: General rules and rules for buildings. European Committee for Standardization. Brussels, 2004.
- [16] CEN/TC250: Eurocode 3 – Design of steel structures – EN 1993 Part 1-1: General rules and rules for buildings. European Committee for Standardization. Brussels, 2005.
- [17] CEN/TC250: EN 1993-1-9: Eurocode 3: Design of steel structures - Part 1-9: Fatigue, Brussels, 2005.
- [18] CEN/TC250: EN 1998-6: Eurocode 8: Design of structures for earthquake resistance – Part 6: Towers, masts and chimneys, Brussels, 2005.

-
- [19] SIMIS AG: User Manual ASHES 2.1, Aero-Servo-Hydro-Elastic-Simulation, www.simis.no, 2013.
 - [20] Schijve, J.: Fatigue of Structures and Materials, Springer, Netherlands, 2009
 - [21] Jesus, A., Matos, R., Fontoura, B., Rebelo, C., Simões da Silva, L. and Veljkovic, M.: A comparison of the fatigue behavior between S355 and S690 steel grades, Journal of Constructional Steel Research, 79, 140–150, 2012
 - [22] Veljkovic, M. et al.: High-strength tower in steel for wind turbines (HISTWIN), final report, European Commission, Brussels, Belgium, 2012.
 - [23] Heistermann, C.: Resistance to Friction Connections with Open Slotted Holes in Towers for Wind Turbines, doctoral thesis, Luleå University of Technology, Sweden, 2014.
 - [24] International Electrotechnical Commission: IEC 61400-1 Wind Turbines: Part 1 - Design requirements, Third edition, Geneva, Switzerland, 2005.
 - [25] European Committee for Standardization: EN 1990: Eurocode - Basis of structural design, Brussels, Belgium, 2002.
 - [26] Germanischer Lloyd Wind Energie GmbH (GL Wind): Guideline for the Certification of Wind Turbines, Renewables Certification, Hamburg, Germany, 2010.
 - [27] Kammel, Ch., Sedlacek, G.: Dauerverhalten von GV-Verbindungen bei verzinkten Konstruktionen im Freileitungs-, Mast- und Kaminbau. Research Report P409, Stahl-Zentrum, Studiengesellschaft Stahlanwendung e.V., Düsseldorf. January 2001.
 - [28] VDI Guideline 2230 – Part 1: Systematic calculation of high duty bolted joints – Joints with one cylindrical bolt. VDI-Handbuch Konstruktion. Beuth Verlag GmbH, Berlin. February 2003.
 - [29] Jakubowski, A.: Ermüdungssichere Bemessung geschraubter Ringflanschstöße in turmartigen Stahlbauten unter besonderer Berücksichtigung von Flanschimperfectionen, doctoral thesis, Essen University, Germany, 2003.
 - [30] Faulhaber, A & Thomala, W 1987, 'Erläuterungen zur Richtlinie VDI 2230 Blatt 1: Der nichtlineare Berechnungsansatz', *VDI-Z – Zeitschrift des Vereins Deutscher Ingenieure*, 1986, vol. 129, no. 9, p. 79 - 84.
 - [31] Matzner, I.: "Stabilitäts- und Wirtschaftlichkeitsuntersuchungen kaltgeformter und kreisförmiger Hohlprofile für den Windenergieanlagenbau" Lehrstuhl für Stahlbau RWTH Aachen, Study 2007
 - [32] Kulak, G. L., Fisher, J. W., Struik, J. H. A.: Guide to Design Criteria for Bolted and Riveted Joints Second, 2001.
 - [33] Petersen, C.: Stahlbau. 4. Edition, Wiesbaden: Springer Vieweg, 2013.
 - [34] Research Council on Structural Connections (RCSC): Specification for Structural Joints Using High-Strength Bolts, Chicago, Illinois, USA, 2009.
 - [35] European Committee for Standardization: EN 1993-1-8: Eurocode 3 - Design of steel structures, Part 1-8: Design of joints, Brussels, Belgium, 2005.
-

-
- [36] European Committee for Standardization: EN 1090-2: Execution of steel structures and aluminium structures, Part 2: Brussels, Belgium, 2008.
 - [37] Veljkovic, M., Heistermann, C., Tran, A. T., Feldmann, M., Möller, F., Richter, C. et al.: High steel tubular towers for wind turbines (HISTWIN2). Brussels, Belgium, to be published.
 - [38] European Committee for Standardization: EN 1993-1-6: Eurocode 3 – Design of Steel Structures, Part 1-6: Strength and Stability of Shell Structures, Brussels, Belgium, 1993.
 - [39] Tran, A.T., Veljkovic, M., Rebelo, C., Simões da Silva, L.: Influence of geometrical imperfections on analyses of door openings in tubular steel towers for wind turbines, 7th European conference on Steel and Composite Structures, Napoli, Italy, 2014.
 - [40] Richter, C. : Zur Segmentierung von Türmen für Windenergieanlagen, diploma thesis, Aachen, Germany, 2011.
 - [41] Möller, F., Richter, C.: Design recommendation for modular steel towers, Deliverable D12, High steel tubular towers for wind turbines (HISTWIN2). Brussels, Belgium, 2013.
 - [42] CEN/TC250 (2007) EN 1993-1-6: Eurocode 3 - Design of steel structures, Part 1-6: Strength and Stability of Shell Structures, Brussels, Belgium.
 - [43] Seidel, M., Schaumann, P. (2001) Measuring fatigue loads of bolts in ring flange connections. Proc. Eur. Wind Energy Conf. Exhib, EWEC 2001, Copenhagen.
 - [44] Kulak, G. L., Fisher, J. W., Struik, J. H. A. (2001) Guide to Design Criteria for Bolted and Riveted Joints Second.
 - [45] Veljkovic, M., Heistermann, C., Husson, W., Limam, M., Feldmann, M., Naumes, J. et al. (2012) High-strength tower in steel for wind turbines (HISTWIN), Brussels, Belgium.
 - [46] Veljkovic, M., Heistermann, C., Tran, A. T., Feldmann, M., Möller, F., Richter, C. et al. (2014) High steel tubular towers for wind turbines (HISTWIN2). Brussels, Belgium.
 - [47] European Committee for Standardization: EN 1997-1, Eurocode 7 – Geotechnical design, Part 1: General rules, Brussels, Belgium, 2004.
 - [48] European Committee for Standardization: EN 1998-5, Eurocode 8 – Design of structures for earthquake resistance, Part 5: Foundations, retaining structures and geotechnical aspects, Brussels, Belgium, 2004.
 - [49] DNV and Risø, Guidelines for Design of Wind Turbines. 2nd Edition. Norway, 2002.
 - [50] European Committee for Standardization: EN 1992-1-1, Eurocode 2 – Design of concrete structures, Part 1: General rules and rules for buildings, Brussels, Belgium, 2004.
 - [51] T-2.9-TT.00.26-A-E – REpower MM92 – Specifications for foundation design. Tower with 80.00 m Hub Height. Rotor Blades LM45.3p RE45.2. Wind Zone III DIBt (2004) and class 2a, IEC, 07.09.2007.
-

-
- [52] V-1.1-FG.00.00-A-(F) – “General Specifications for the Design of Onshore-Foundations”, REpower Systems AG, 14.10.2008
- [53] Patrick and Henderson, P&H Foundation for wind turbine support, http://earthsys.com/Library/P%20and%20H%20Presentations/Patrick_Henderson_Foundations_Pamphlet.pdf